

# POLITECNICO DI TORINO

Master's Degree in Aerospace Engineering



Master's Degree Thesis

## Structural analysis and optimization of wind turbine blade for offshore applications

Supervisors

Prof. Giovanni BRACCO

Prof. Bruno PADUANO

Prof. Massimo SIRIGU

Prof. Gabriele MANGIA

Candidate

Gabriele CASO

DECEMBER 2024



## Abstract

This master's thesis work stems from a combined interest in complex structures and renewable energy production. In the context of the energy transition, the need for a shift to cleaner energy sources is evident, and countries all over the world are facing this challenge along with its related issues. Wind energy is a key player in this transition and is expected to be one of the largest components of the energy mix in the coming decades. Additionally, offshore wind energy is of significant interest to researchers and investors due to its clear advantages over onshore wind energy, primarily greater wind availability and reduced impact on land environments. With this premise, this thesis focuses on the structural aspects of offshore wind turbine blades.

The thesis begins with an introduction that contextualizes the problem by presenting the current state of wind energy in terms of installed gigawatts and highlighting the countries most involved in the development of this technology. Following this, an overview of offshore wind energy is provided, outlining its advantages and disadvantages compared to onshore wind energy.

After the introduction, key theoretical concepts are discussed to understand the aerodynamic parameters involved in blade design that most significantly affect turbine performance.

Next, a description of the loads acting on the turbine rotor is presented, followed by a review of the state-of-the-art in wind turbine blade structures. This section explains the load distribution among various structural components, with a focus on composite materials that have replaced metals, following trends in the aerospace industry.

A simplified finite element model of a reference 15 MW wind turbine blade is created using ANSYS Mechanical. The model is automated with a Python script using PyMechanical. With the model established, several analyses are conducted to verify both the model and the structural properties of the blade.

Finally, using the introduced FEM model, an optimization process is performed on the blade with the objective of reducing its cost by minimizing material usage while respecting certain structural constraints.



# Table of Contents

<b>List of Tables</b>	VI
<b>List of Figures</b>	VII
<b>1 Introduction</b>	1
1.1 Background . . . . .	1
1.1.1 History . . . . .	1
1.1.2 Energy transition . . . . .	2
1.2 Offshore wind energy . . . . .	8
1.3 Thesis objective . . . . .	10
<b>2 Aerodynamics</b>	13
2.1 Wind turbine . . . . .	13
2.1.1 Wind turbine types . . . . .	14
2.2 Horizontal-Axis Wind Turbine . . . . .	17
2.3 Rotor . . . . .	19
2.3.1 Rotor using aerodynamic lift . . . . .	19
2.3.2 Number of rotor blades . . . . .	23
2.3.3 Rotor blade planform . . . . .	24
2.3.4 Blade airfoil . . . . .	27
2.3.5 Blade twist . . . . .	27
<b>3 Load</b>	29
3.1 Load sources . . . . .	29
3.1.1 Aerodynamic load . . . . .	32
3.1.2 Gravity and Inertial loads . . . . .	34
3.2 Blade load condition . . . . .	35
3.2.1 Flapwise bending moment . . . . .	35
3.2.2 Edgewise bending . . . . .	37
3.3 Structural blade regions . . . . .	39
3.4 Blade structure . . . . .	40

3.4.1	Materials	41
<b>4</b>	<b>Reference Turbine</b>	<b>45</b>
4.1	IEA Wind 15-MW	46
4.1.1	Blade	46
4.2	Model	50
4.2.1	CAD Model	50
4.2.2	Materials	51
4.2.3	Layers	53
4.2.4	Puck failure criteria	57
4.3	Modal analysis	58
4.4	Static structural analysis	60
4.4.1	Loads	60
4.4.2	Results	65
4.5	Modified 15 MW IEA Wind Turbine	73
4.5.1	Modified blade structure	73
4.5.2	Analysis results	73
<b>5</b>	<b>Structural optimization</b>	<b>79</b>
5.1	Literature review	79
5.2	Objective	80
5.3	Optimization process	81
5.3.1	Model definition	81
5.3.2	Objective function	84
5.4	Case 1: Carbon optimization	85
5.5	Case 2: Blade optimization	89
<b>6</b>	<b>Conclusions</b>	<b>99</b>
	<b>Bibliography</b>	<b>102</b>

# List of Tables

4.1	IEA Wind 15-MW Turbine data [23]. . . . .	46
4.2	Blade main properties [23]. . . . .	48
4.3	Fiber reinforced materials properties. . . . .	52
4.4	Core properties. . . . .	52
4.5	Natural frequencies. . . . .	58
4.6	Operating condition of the 7 load cases selected. . . . .	62
4.7	Data for tower clearance calculation. . . . .	66
4.8	Tower clearance. . . . .	66
4.9	Maximum Puck's failure index. . . . .	71
4.10	Buckling analysis results. . . . .	72
4.11	Maximum Puck's Failure Index. . . . .	75
4.12	Buckling analysis results . . . . .	78
5.1	Materials unit costs. . . . .	81
5.2	Optimization data. . . . .	85
6.1	Optimization results. . . . .	101

# List of Figures

1.1	Wind energy technologies from early stages to outbreak of California [3]. . . . .	2
1.2	Temperature vs Solar activity [source: nasa.gov]. . . . .	3
1.3	Global primary energy consumption by source [source: ourworldindata.org]. . . . .	4
1.4	EU energy consumption by source [7]. . . . .	5
1.5	The capacity for different energy sources of EU for 2022 [8]. . . . .	6
1.6	The renewable energy installed capacity of the EU (2010 - 2022) [source: windeurope.org]. . . . .	6
1.7	The global wind energy production [6]. . . . .	6
1.8	Wind energy installation capacity [6]. . . . .	7
1.9	Cumulative installed capacity of offshore wind energy worldwide [source: GWEC]. . . . .	9
1.10	Cumulative and annual installed capacity of offshore wind energy in Europe [source: windeurope.org]. . . . .	9
1.11	PyMechanical logo [pyansys.com]. . . . .	10
1.12	PyMechanical interface. . . . .	11
2.1	Power Coefficients of wind turbine rotors of different type [15]. . . . .	15
2.2	Wind turbine concepts [16]. . . . .	16
2.3	Components of a wind turbine [17]. . . . .	17
2.4	Power and rotor diameters of existing and planned onshore wind farms [source: IRENA]. . . . .	18
2.5	Power and rotor diameters of existing and planned offshore wind farms [source: IRENA]. . . . .	18
2.6	Aerodynamic forces acting on an airfoil exposed to an airstream [15]. . . . .	19
2.7	Flow velocities and aerodynamic forces acting on a propeller-like rotor [15]. . . . .	20
2.8	HAWTs aerodynamic forces distribution [15]. . . . .	21
2.9	Power coefficient map example [15]. . . . .	23
2.10	Power coefficients by varying the number of blades [15]. . . . .	24



2.11	Theoretical shape of rotor blades considering the effect of different tip speed ratios and different number of rotor blades [15]. . . . .	25
2.12	Power losses due to deviations from the aerodynamically optimal shape [15]. . . . .	26
2.13	Rotor blade twist effect on rotor performances [15]. . . . .	28
3.1	Aerodynamics, gravity and inertia acting on the rotor of a horizontal-axis wind turbine [15]. . . . .	31
3.2	Tangential load distribution over the blade length [15]. . . . .	32
3.3	Thrust load distribution over the blade length [15]. . . . .	32
3.4	Cantilever beam model - flapwise bending [19]. . . . .	36
3.5	Flapwise bending [19]. . . . .	37
3.6	Cantilever beam model - edgewise bending [19]. . . . .	38
3.7	Edgewise bending [19]. . . . .	39
3.8	The three blade regions [19]. . . . .	40
3.9	The three blade regions [22]. . . . .	40
4.1	IEA Wind 15-MW [23]. . . . .	47
4.2	Blade top and edge view [23]. . . . .	47
4.3	DTU FFA-W3 airfoils series [23]. . . . .	48
4.4	Chord (on the left) and relative thickness (on the right) along the relative blade span [23]. . . . .	49
4.5	Schematic of IEA Wind Turbine Ontology composite definition, from root to tip [23]. . . . .	49
4.6	CAD model - front view. . . . .	50
4.7	CAD model - top view. . . . .	51
4.8	CAD model - side view. . . . .	51
4.9	Blade materials. . . . .	51
4.10	Section 0% . . . . .	53
4.11	Section 25% . . . . .	53
4.12	Section 50% . . . . .	53
4.13	Section 75% . . . . .	53
4.14	Section 100% . . . . .	53
4.15	Material thickness along blade span (shell). . . . .	54
4.16	Material thickness along blade span (shear web). . . . .	54
4.17	Leading edge reinforcement. . . . .	55
4.18	Trailing edge reinforcement. . . . .	55
4.19	Spar cap. . . . .	55
4.20	Panels. . . . .	55
4.21	Shear web. . . . .	55
4.22	Thickness plot - trailing edge view (mm). . . . .	56

4.23	Thickness plot - leading edge view (mm).	56
4.24	1st Flapwise.	58
4.25	1st Edgewise.	58
4.26	2nd Flapwise.	59
4.27	2nd Edgewise.	59
4.28	Modal analysis - comparison with literature.	59
4.29	Normal pressure.	61
4.30	Tangential pressure.	61
4.31	FX.	61
4.32	FY.	61
4.33	FX (case 1).	62
4.34	FY (case 1).	62
4.35	FX (case 2).	63
4.36	FY (case 2).	63
4.37	FX (case 3).	63
4.38	FY (case 3).	63
4.39	FX (case 4).	63
4.40	FY (case 4).	63
4.41	FX (case 5).	64
4.42	FY (case 5).	64
4.43	FX (case 6).	64
4.44	FY (case 6).	64
4.45	FX (case 7).	64
4.46	FY (case 7).	64
4.47	Mesh convergence.	65
4.48	Tip deflection.	67
4.49	Deformed shape (load case 3).	67
4.50	Tip deflection load case 1 (front view).	68
4.51	Tip deflection load case 3 (front view).	68
4.52	FRX.	69
4.53	FRY.	69
4.54	FRZ.	69
4.55	Flapwise (MY).	69
4.56	Edgewise (MX).	69
4.57	Equivalent (Von Mises) stress in load case 3.	70
4.58	Puck's failure indices (tensile fiber failure).	70
4.59	Tip damage (load case 3).	71
4.60	Buckling occurring at blade tip.	72
4.61	Tip deflection.	74
4.62	Deformed shape load case 3.	74
4.63	Equivalent Stress (Von Mises): load case 3.	75

4.64	Maximum Puck's failure index - left view. . . . .	76
4.65	Maximum Puck's failure index - right view. . . . .	76
4.66	Maximum Puck's failure index - Fiber Tensile. . . . .	76
4.67	Maximum Puck's failure index - Matrix Tensile. . . . .	76
4.68	Maximum Puck's failure index - Shear Web. . . . .	77
4.69	Maximum Puck's failure index - Shear Web tensile. . . . .	77
4.70	Maximum Puck's failure index - Shear Web compression. . . . .	78
5.1	Floating offshore wind turbine component cost breakdown [34]. . . . .	80
5.2	Simplification from 49 to 10 sections. . . . .	82
5.3	Key points. . . . .	82
5.4	Glass Triax - first set. . . . .	82
5.5	Carbon - first set. . . . .	82
5.6	Glass uni te - first set. . . . .	83
5.7	Glass uni te - first set. . . . .	83
5.8	Foam skin - first set. . . . .	83
5.9	Foam web - first set. . . . .	83
5.10	Glass Biax - first set. . . . .	83
5.11	Objective function: case 1. . . . .	85
5.12	Tip deflection: case 1. . . . .	86
5.13	Maximum Puck Failure Index: case 1. . . . .	86
5.14	Mass evolution: case 1. . . . .	87
5.15	Blade cost: case 1. . . . .	87
5.16	Carbon thickness: case 1. . . . .	88
5.17	Spar cap optimized (case 1). . . . .	88
5.18	Objective function: case 2. . . . .	89
5.19	Tip deflection: case 2. . . . .	90
5.20	Maximum Puck Failure Index: case 2. . . . .	90
5.21	Mass evolution: case 2. . . . .	91
5.22	Glass Triax Mass evolution: case 2. . . . .	91
5.23	Blade cost: case 2. . . . .	92
5.24	Carbon thickness: case 2. . . . .	92
5.25	Glass UNI (LE) thickness: case 2. . . . .	93
5.26	Glass UNI (TE) thickness: case 2. . . . .	93
5.27	Glass TRIAX (skin) thickness: case 2. . . . .	94
5.28	Glass Biax (web) thickness: case 2. . . . .	94
5.29	Foam (skin) thickness: case 2. . . . .	95
5.30	Foam (web) thickness: case 2. . . . .	95
5.31	Leading edge reinforcement optimized. . . . .	96
5.32	Trailing edge reinforcement optimized. . . . .	96
5.33	Spar cap optimized. . . . .	96

5.34	Panels optimized. . . . .	96
5.35	Shear web optimized. . . . .	96
5.36	Leading edge reinforcement optimized (zoom). . . . .	97
5.37	Trailing edge reinforcement optimized (zoom). . . . .	97
5.38	Spar cap optimized (zoom). . . . .	97
5.39	Panels optimized (zoom). . . . .	97
5.40	Maximum displacement (optimized blade). . . . .	98
5.41	Maximum Puck failure index (optimized blade). . . . .	98

# Chapter 1

## Introduction

This chapter introduces the author's Master's Degree thesis, the work which represents the culmination of a Master's Degree in Aerospace Engineering at *Politecnico di Torino*.

The chapter begins by outlining the wind power generation history, from ancient devices to the newest wind turbines, then analyzing its role in the context of energy transition and the expectations for the future.

A brief introduction to offshore wind energy is given in Section 1.2. Offshore wind turbines have several advantages with respect to onshore turbines, such as a lot more available space and fewer complaints about noise and visual intrusion. Plus, wind over the water is generally stronger, more consistent and much smoother than wind over land.

Lately, the thesis objective is presented in Section 1.3.

### 1.1 Background

Wind energy is a way to produce electricity by converting the kinetic energy of air in motion. In modern wind turbines, wind causes the rotation of the rotor blades and then this rotational energy is transferred to a generator by a shaft, thereby producing electricity.

#### 1.1.1 History

People have been using wind energy since ancient times. The ancient Egyptians used wind to move boats along the Nile River as early as 5000 BC. By 200 BC, other wind-powered devices had appeared, such as water pumps in China or windmills in Persia and the Middle East for grain grinding. By the 11<sup>th</sup> century, wind pumps and windmills were used in the Middle East for food production.

Windmills were brought to Europe by immigrants, merchants and Crusaders. Dutch people developed large wind pumps to drain lakes and marshes in the Rhine River Delta. In the period 1300-1875, windmills were developed and used in the Netherlands and the Mediterranean [1, 2]. Further improvements were made in the USA during the 19<sup>th</sup> century. Over 6 million small water pumps were used between 1850 and 1970. The first large wind turbine to generate electricity was installed in Cleveland, Ohio, in 1888. In Europe, 25 kW machines were used in Denmark during World War I. Wind energy technology continued to develop in the USA and Europe. The oil crisis of 1973 led the USA government to invest in wind energy research. As a result, the wind turbine market grew from small to large-scale between 1973 and 1986. In California, over 16,000 wind turbines were installed between 1981 and 1990. They ranged from 20 to 350 kW, with a total capacity of 1.7 GW. In northern Europe, wind farms grew steadily through the 80s and 90s. The higher cost of electricity and excellent wind resources led to a small but stable market [3].

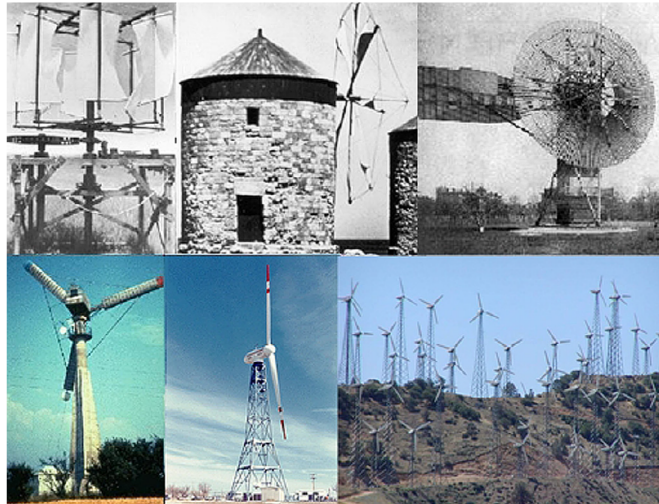


**Figure 1.1:** Wind energy technologies from early stages to outbreak of California [3].

### 1.1.2 Energy transition

Today, countries must keep investing in wind energy to face climate change. *Climate change* is the name for long-term changes in weather and temperature. These changes can be natural or human-made. The graph in Figure 1.2 compares global temperature changes with the Sun's energy received by the Earth since 1880. The thinner lines show yearly levels, while the thicker lines show 11-year trends. Averaging over 11 years reduces natural fluctuations in the data, making trends

more obvious.

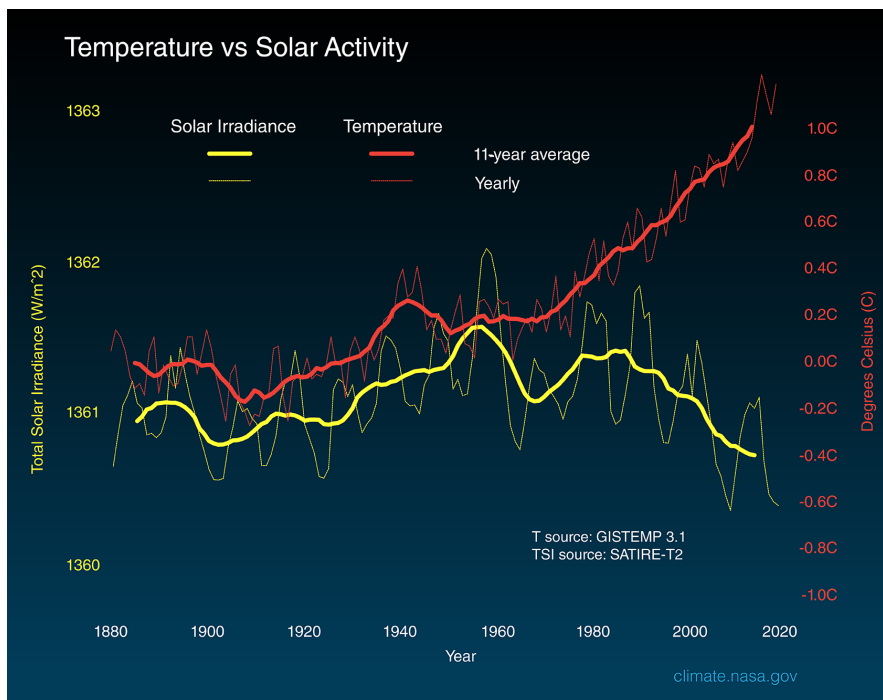


**Figure 1.2:** Temperature vs Solar activity [source: nasa.gov].

The amount of solar energy Earth gets has changed over time. Since the 1950s, there has been no overall increase. Global temperatures, instead, continued to rise. It is unlikely that the Sun has caused global temperatures to rise over the past 50 years. It is more likely that human activities have caused climate change since the Industrial Revolution, mainly because of burning fossil fuels like coal, oil and gas.

Fossil fuels usage causes the release of greenhouse gases that trap heat and cause global warming. The main greenhouse gases are carbon dioxide and methane. The main sources of greenhouse gases are energy, industry, transport, buildings, agriculture and land use [4].

The Earth's surface has warmed by about 1.2°C since the late 1800s, reaching a level not seen in 100,000 years. The scientific community agrees that limiting the temperature rise to 1.5°C would help to stop climate change. The main problem is that current policies mean the scientific community agrees a 3°C temperature rise by the end of the century is likely. To avoid this, it is necessary to switch to cleaner energy. Some ways to tackle climate change can also help the economy, people's lives and the environment. There are already some global plans to help the world making progress. These include the *Sustainable Development Goals*, the *UN Framework Convention on Climate Change* and the *Paris Agreement*.

Basically, there are three main ways to tackle climate change: cutting emissions, adapting to climate change and paying for the changes needed. While more countries are aiming for net zero emissions by 2050, emissions must be cut by 50% by 2030 to avoid global warming of over 1.5°C. This means using less coal, oil and gas. Humans must keep over two-thirds of current fossil fuel reserves in the ground by 2050 to avoid catastrophic climate change.

Using more renewable energy can also have other benefits. Most of the world’s people import fossil fuels from other countries. This makes them vulnerable to political crises. Renewable energy sources, instead, are available in all countries. This can help reduce import dependency and create jobs, as well as help fight poverty. The cost of renewable energy is falling. Wind energy costs have fallen by 56% and 48% respectively between 2010 and 2020 [5]. Another thing to think about is the chance of creating jobs. The *International Energy Agency (IEA)* says that moving towards net-zero emissions will create more jobs in the energy sector. Fossil fuel jobs could be lost, but clean energy jobs will be created, resulting in a net gain of 9 million jobs. Also, 16 million more workers will be needed in energy-related industries. This includes manufacturing electric vehicles, highly efficient appliances, and pioneering technologies like hydrogen. This could create over 30 million jobs in clean energy, efficiency, and low-emissions technologies by 2030 [6]. The shift trend to a cleaner energy mix is shown in the chart in Figure 1.3.

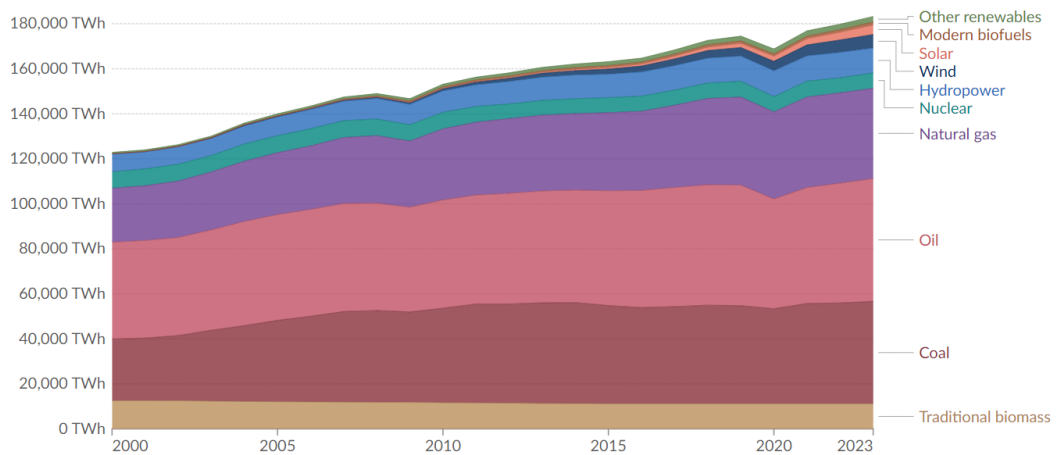


**Figure 1.3:** Global primary energy consumption by source [source: ourworldindata.org].

Since 2015, coal usage has slowed as people worry about the environment and more renewable energy becomes available. Oil is still an important energy source globally, mainly because it is used a lot in transport. People are trying to use different types of energy in transport to reduce their reliance on oil. This is being



done by encouraging electric vehicles and making cars more efficient. Research is also being done into alternative fuels. Natural gas is growing in use because it is found abundant in nature and it is the cleanest fossil fuel. It produces fewer pollutants and greenhouse gases than other fossil fuels, such as coal and oil. Nuclear energy has grown slowly because people are worried about safety. However, it represents a safe and low-carbon option. Many countries are investing in renewable energy to reduce their carbon footprint. Solar, wind and hydro sources are growing fast. However, this is not happening at the same rate in all countries. Some countries with big energy needs are making different policies. The USA and China use the most energy in the world. These countries still use a lot of fossil fuels, despite evidence that both countries are moving towards renewable energy. Russia and Saudi Arabia does not have the same objective, yet. Norway and New Zealand, on the other hand, are leading the way in renewable energy. The EU is changing its energy mix, moving from fossil fuels to renewables [7]. The following graphs show energy consumption in the EU.

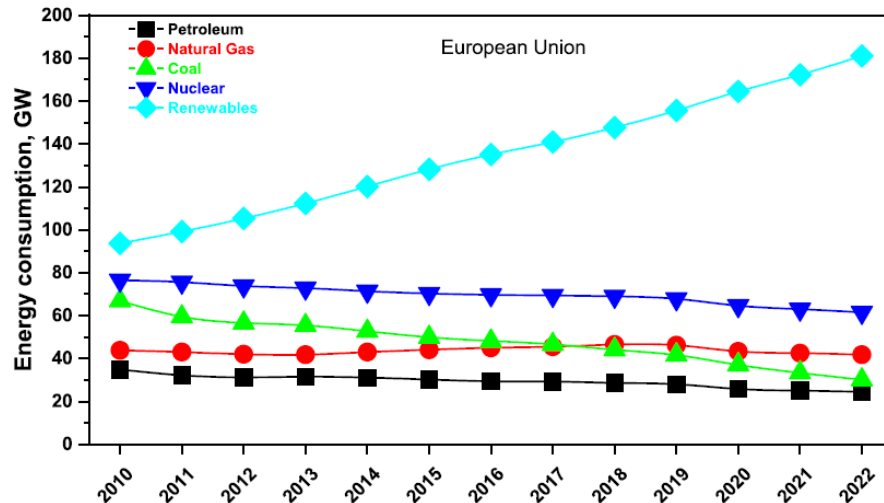
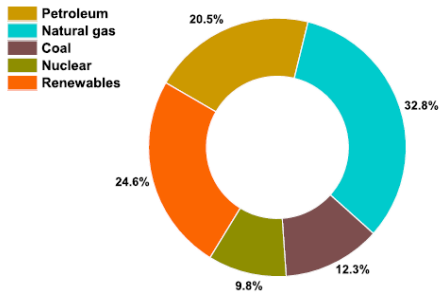


Figure 1.4: EU energy consumption by source [7].

Petroleum consumption in the EU fell gradually over time as countries tried to rely less on fossil fuels. Petroleum consumption dropped by between  $-2\%$  and  $-4\%$ . Natural gas consumption was stable, with a growth rate of  $0 - 2\%$  [7]. Coal consumption fell, showing a shift towards greener energy. Coal consumption dropped by between  $-5\%$  and  $-8\%$ . Nuclear energy consumption stayed the same, with a growth rate of between  $-1\%$  and  $1\%$ . Renewable energy consumption grew a lot thanks to policies and investments. Renewable energy grew by  $6 - 10\%$ . By 2022, 600 GW of renewable energy was installed, representing  $24.6\%$  of all energy sources [source: [iea.org](http://iea.org)] (see Figures 1.5 and 1.6). This is due to increased

investments and policies that support renewable energy.



**Figure 1.5:** The capacity for different energy sources of EU for 2022 [8].

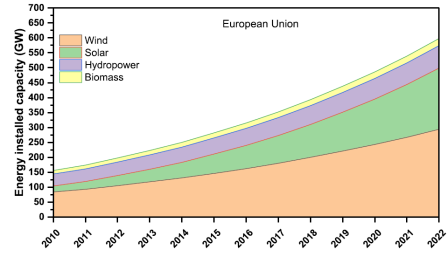


**Figure 1.6:** The renewable energy installed capacity of the EU (2010 - 2022) [source: windeurope.org].

As the world’s energy mix changes and more focus is placed on renewable sources, wind and solar power are becoming the main sources of renewable energy. Wind and solar energy are important parts of the global renewable energy sector because they have a lot of potential, can be adapted easily, and are good for the environment. They are a green alternative to fossil fuels, which helps to reduce greenhouse gases and slow climate change. Wind and solar energy are becoming more popular because they are cheaper, more advanced, and governments are supporting them [9, 10]. Wind and solar energy have helped many countries around the world to use different types of energy and use less oil and gas. Further investment in research, development and infrastructure will make wind and solar energy more efficient and competitive, helping them to grow further. The wind power industry has grown quickly in recent years. Figure 1.7 shows global wind energy production data.

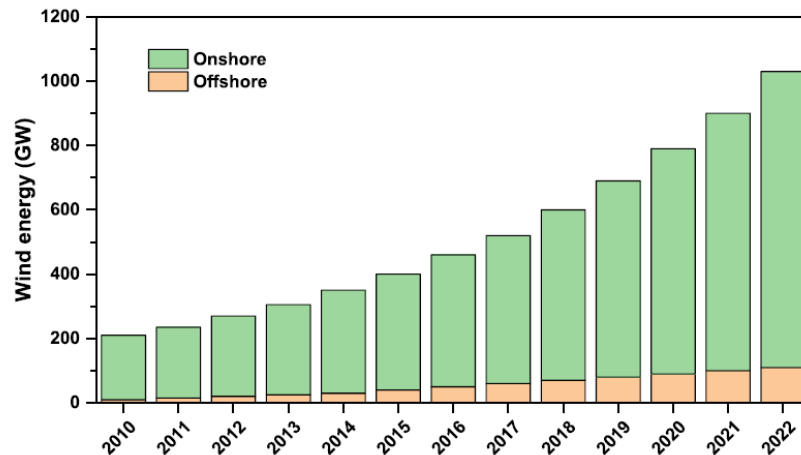


**Figure 1.7:** The global wind energy production [6].

Wind energy is expected to become more competitive in the coming decades, depending on various factors such as new technologies implementation. These include larger and more efficient turbines and better energy storage. These developments will make wind energy more affordable and reliable, making it a better choice than traditional fossil fuels [6]. By 2040, wind power would probably be an important part of the global energy mix. Newer, better turbines will make wind power cheaper. Wind power will be one of the cheapest ways to make electricity, beating other types of energy. By 2050, wind power could be the main type of electricity production. New technology, environmental awareness and government policy will make wind power more popular. By 2050, it will be the most popular source of new energy because it is affordable, sustainable and helps to reduce carbon emissions. Figure 1.8 shows the countries with the most wind energy installed capacity in 2021 and 2022.

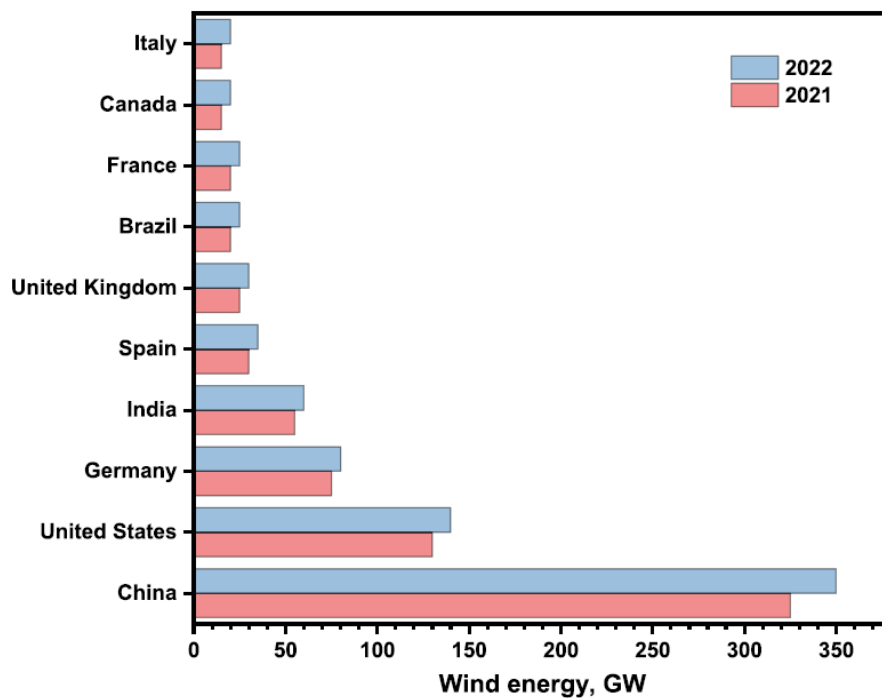


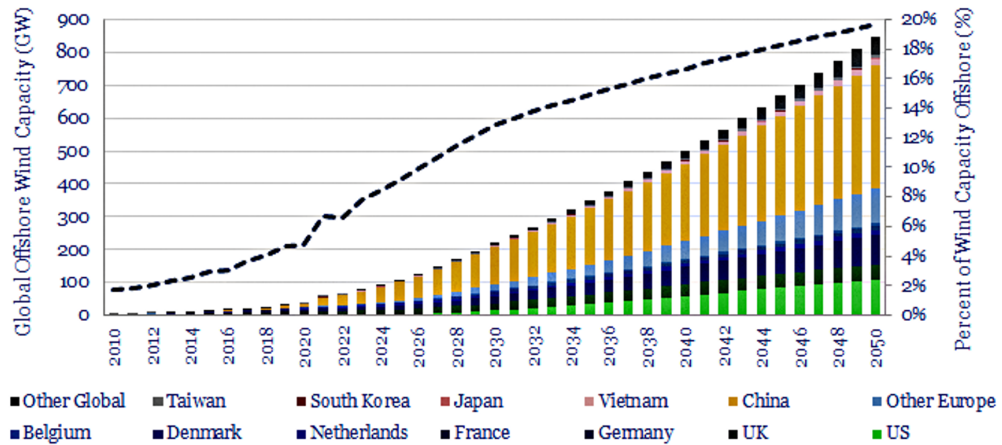
Figure 1.8: Wind energy installation capacity [6].

Figure 1.7 shows data on onshore and offshore wind power. By the end of 2022, China had installed over 350 GW of onshore wind power, making it the world's largest onshore wind capacity. The United States has seen a big increase in wind energy capacity because of the good wind resources in many states. By 2022, the United States had over 120 GW of onshore wind capacity. Germany, India and Spain have also helped develop onshore wind power. By 2022, Germany had

over 60 GW of onshore wind energy. India and Spain had reached 40 GW and 27 GW of onshore wind capacity, respectively. Other countries have also expanded their onshore wind power capacity, including the United Kingdom, France, Brazil, Canada, and Sweden. There are many reasons for the rapid growth of onshore wind power. New technology, better turbines and economies of scale have made onshore wind power cheaper [11, 12]. Offshore wind power grew a lot in 2022. Many countries have contributed to the growth of offshore wind energy. The UK is leading the way in offshore wind power, with a steady increase in capacity. By the end of 2022, the UK had installed over 11 GW of offshore wind power, making it the global leader. By 2022, Germany had over 7 GW of offshore wind capacity, making it one of the top countries in offshore wind development. China is now a major player in offshore wind power, thanks to a rapid increase of its offshore wind capacity. Its coastline and commitment to renewable energy have helped. By the end of 2022, China had over 7 GW of offshore wind power. The efforts of countries including the UK, Germany, Denmark, the Netherlands, Belgium, Sweden and China have helped the industry grow. They have set new records for how much energy can be produced and are helping the world move towards cleaner energy. This shows that offshore wind energy is becoming more important in meeting energy needs and helping to stop climate change.

## 1.2 Offshore wind energy

Onshore wind farms are usually limited by the availability of suitable land. People are worried about the noise and look of wind turbines near homes. Offshore wind turbines are similar to onshore ones, but there are many advantages to installing them at sea. There is more space and fewer complaints about noise and visual intrusion. Wind speeds over water are stronger, more consistent and smoother than over land. Coastal regions are usually the most developed and use more electricity. So, using offshore wind energy can help with the power supply and reduce greenhouse gases. Offshore wind power is growing fast and is set to become a major focus of development in many countries. On the other hand, the main problem with using offshore wind energy is that it is expensive. Offshore wind turbines are more expensive and difficult to install and maintain than onshore ones because of the sea conditions [13]. However, costs could be reduced by using new technology to improve each stage of offshore wind energy production. The benefits of offshore wind energy are shown by the growth in global offshore installation capacity, which has increased every year since the last decade, as evidenced by data from the *Global Wind Energy Council (GWEC)* presented in Figure 1.9.



**Figure 1.9:** Cumulative installed capacity of offshore wind energy worldwide [source: GWEC].

The European situation is reported in Figure 1.10, with UK as leader both in cumulative and new offshore wind installations.

### Cumulative and annual offshore wind installations 2010-2021

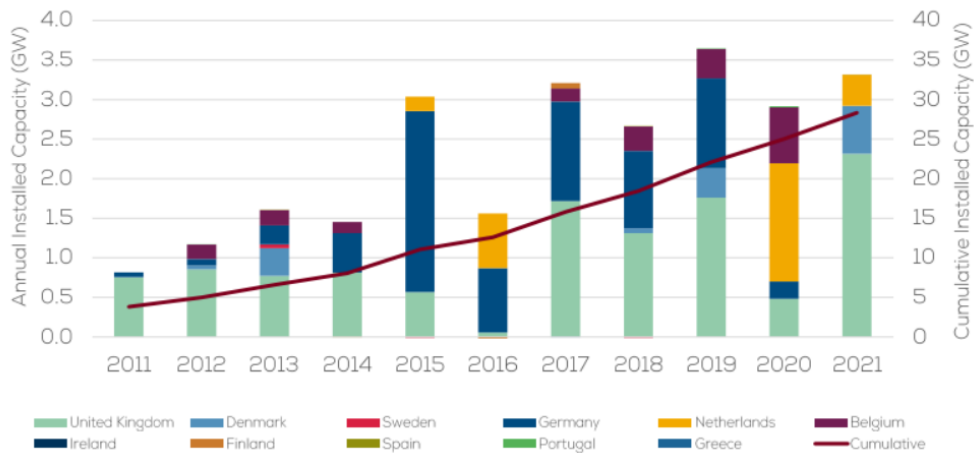


**Figure 1.10:** Cumulative and annual installed capacity of offshore wind energy in Europe [source: windeurope.org].

Onshore and offshore wind installations are different because of where they are situated. The marine environment is more complex at every stage of the installation process. There are several things that can affect these processes. Wind speeds are usually higher in the sea, and get faster the further you go out to sea. The height of a wind turbine depends on its diameter, with the optimal height being the

maximum height above the waves. The wind is also more regular, which means less wear and tear on the turbines. An advantage is that the air near the sea surface is less turbulent than on ground, so offshore turbines can be mounted lower than onshore ones. A second advantage is that offshore wind farms can be bigger because there is more space in the sea. The wind turbine is placed far from people to reduce noise pollution. The distance between offshore turbines and the coastline can also reduce the visual impact. The factors and constraints allow larger wind turbine units to be installed, which improves production per unit. The initial disadvantage is the cost of permits, engineering, construction and operation. Offshore wind farms cost about 75% more than onshore ones. This is mainly because marine operations are expensive. Also, unlike onshore wind farms, there are usually no power lines connecting the best wind areas with consumer centers. This means building longer electrical networks and sometimes strengthening existing ones. Offshore wind farms require more sophisticated technology. This is important for the wind turbine generators, which are usually the same as onshore ones. Some research projects are looking at the best type of wind turbine generator for offshore wind farms, especially those with floating foundations. These generators will be under a lot of pressure and must be able to cope with the marine environment and corrosion. The same is true for the foundations. Access is restricted and it is difficult to work in this environment during construction and operation. Wind turbine generators also affect the wind around them, which can damage the turbines. To avoid this, there should be a minimum distance between wind turbines. It is also more expensive and difficult to assess wind resources offshore [14]. Despite the cost difference, there is a need to speed up the development of offshore wind technology. This means understanding more about things like wind turbine design, foundations, building techniques and how they work.

### 1.3 Thesis objective

After a global background presented in the first introductory chapter on the current situation regarding wind power generation, this thesis focuses on offshore wind turbine blade. In particular, the objective of the thesis is to develop a Python code based on *Ansys PyMechanical* (Figure 1.11), which is a Python application programming interface (API) enabling the interaction with *Ansys Mechanical* directly from Python code.



Figure 1.11: PyMechanical logo [pyansys.com].

The code is thought to generate an automated and fast Finite Element Model which permits to perform FEM analysis and optimization on several blade geometries and in several load scenarios (see Figure 1.12).

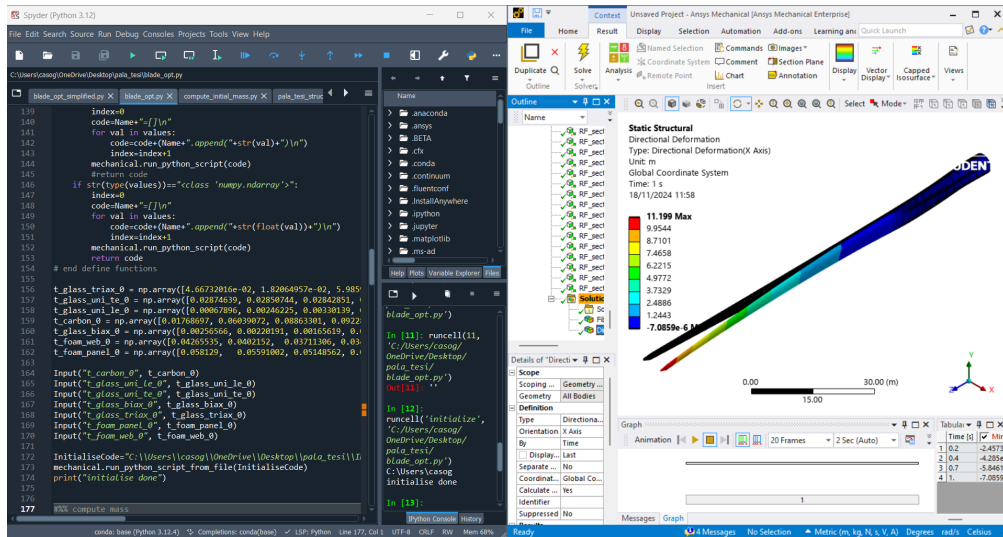


Figure 1.12: PyMechanical interface.

Chapters 2 and 3 report some useful theoretical concepts coming from literature review. In particular, chapter 2 is focused on the functioning and the aerodynamics parameters which influences the blade design while chapter 3 analyzes the possible load sources and their effects on the current state-of-the-art blade structural design. These theoretical concepts are the basis to explain the reference wind turbine blade considered (a 15 MW wind turbine blade) for the developing of the FEM model and the analysis. Offshore wind turbine blades are getting bigger in order to produce more electricity at lower prices so the engineering behind them is challenging. With bigger dimensions it is necessary to reduce the blade weight in order to reduce gravity and inertial loads: as a consequence, the usage of composites materials has become essential. The definition of the composite laminates and layers is the main part of the FEM model. Once the model is complete, in chapter 4 some FEM analysis are performed in order to verify the blade structural behavior. A modal analysis is performed to calculate the first natural frequencies and to compare them with literature data. A static structural analysis is performed along with a buckling analysis in order to check if the blade structure is well designed to address some basic structural requirements such as maximum tip deflection to avoid tower collision and strength resistance. In the end, a first optimization attempt on the blade is performed. The objective of the optimization is to minimize the blade cost by optimizing the material usage and thickness distribution. The

optimization process performed in this thesis enables to define an optimized blade with a considerable savings of material mass and costs. However, some possible algorithms problem are noted making the optimization technique to be further investigated.



# Chapter 2

## Aerodynamics

This chapter introduces the basic principles of how a wind turbine works. In the first part, the different types of wind turbines are briefly described. The architecture of a Horizontal Axis Wind Turbine (HAWT) is then presented, with a final focus on rotor blade aerodynamic design and a description of the main parameters which affect the blade performances.

### 2.1 Wind turbine

A wind turbine is a machine that transforms the kinetic energy of the wind into electrical energy. The conversion process occurs through the use of aerodynamic forces acting on blades due to the wind flow. These forces are analogous to those observed in airplane wings and helicopter rotor blades, which cause the turbine rotor to rotate. The rotor is mechanically connected to a generator that produces electricity. While the fundamental process of electricity generation remains consistent, there are various wind turbine designs that differ in their architectural configuration.

The **power coefficient** ( $C_P$ ) is used to measure the efficiency of a wind turbine. The power coefficient is defined as the ratio between the electrical power produced by a wind turbine and the total energy available in the wind at a given wind speed

$$C_P = \frac{\text{Electricity produced by the wind turbine}}{\text{Total energy available in the wind}}.$$

In *Blade Element Theory*, another important ratio, named **tip speed ratio** ( $\lambda$ ), is defined as

$$\lambda = \frac{\text{Tangential velocity of the rotor blade tip}}{\text{Wind velocity}} = \frac{u}{v_W}.$$

The ratio is determined by the tangential velocity of the rotor blades ( $u$ ) in relation to the undisturbed axial airflow and the wind velocity ( $v_W$ ), and it represents the ratio between the energy components derived from the rotary motion and the translational motion of the air stream. Power coefficient varies significantly with the tip speed ratio [15].

A wind turbine extracts energy from the wind by slowing it down, a process known as wind energy conversion. In order for a wind turbine to be 100% efficient, it would be necessary for it to halt the wind's movement. However, this would necessitate the rotor to be a solid disk, which would preclude its ability to rotate and, consequently, the conversion of kinetic energy. At the opposite end of the spectrum, a wind turbine with a single rotor blade would permit the majority of the wind to traverse the area encompassed by the turbine blade, thereby preventing blade rotation and thereby retaining the kinetic energy of the wind. The optimal efficiency for wind power generation is situated between the two aforementioned extremes. This was calculated by Albert Betz and is known as the **Betz limit**, which states that no wind turbine can convert more than 59.3% of the kinetic energy of the wind into mechanical energy turning a rotor [15]. The Betz limit represents the theoretical maximum power coefficient for any wind turbine.

### 2.1.1 Wind turbine types

The majority of wind turbines can be classified into two principal categories: **Horizontal-Axis Wind Turbines** (HAWTs) and **Vertical-Axis Wind Turbines** (VAWTs). The horizontal-axis wind turbines (HAWTs) are the most prevalent type of wind turbine utilized in the energy sector. These turbines feature a rotor with a shaft aligned with the ground and blades oriented in the direction of the prevailing wind. In contrast, VAWTs have a rotor shaft that is perpendicular to the ground, thereby enabling the blades to capture wind from any direction. Both types of wind turbine have their own advantages and disadvantages. Horizontal-axis turbines are more efficient and reliable than vertical-axis turbines, as they are able to harness more wind energy and operate at higher wind speeds. Nevertheless, data concerning the performance of actual wind turbines can be found in Figure 2.1.

It is evident that HAWTs reach the highest power coefficient achievable. In addition, HAWTs are more readily available, having been subjected to more extensive testing given their longer history of use and deployment on larger scales. However, there are also some disadvantages associated with HAWTs, including higher installation and maintenance costs, noise and visual impacts. In contrast, VAWTs are more cost-effective and straightforward to install and maintain, as they have fewer moving parts and do not necessitate the inclusion of a tower or a yaw mechanism. Furthermore, they are quieter and less conspicuous, and are capable of functioning effectively in turbulent and low-wind conditions. However, there

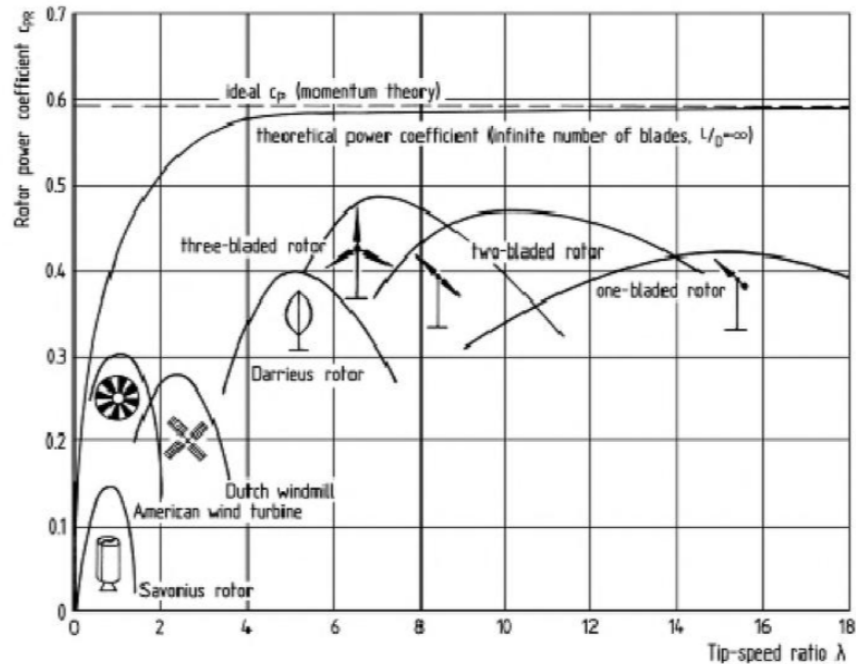


**Figure 2.1:** Power Coefficients of wind turbine rotors of different type [15].

are also certain other limitations associated with VAWTs, including a reduced reliability compared to HAWTs. This is due to the fact that they experience greater drag and torque variations, and operate at lower wind speeds. Furthermore, they are less prevalent and have not been subjected to the same degree of testing as other turbine types. An additional method of categorizing rotor types is based on the aerodynamic forces used to generate power. It can happen exclusively using the aerodynamic drag or it is possible to utilize also the aerodynamic lift created by the flow against suitably shaped surfaces. Consequently, there are two principal categories of rotor: those that rely on **aerodynamic drag** (the so called *drag-type rotors*) and those that utilize the **aerodynamic lift**.

The first documented wind turbine were equipped with a vertical axis of rotation. In the beginning, vertical-axis rotors were pure drag-type rotors. The **Savonius rotor**, which is commonly used for ventilation system or cup anemometer to measure wind velocity, are well-known examples of rotors with a vertical axis of rotation. Vertical-axis designs capable of utilize aerodynamic lift are quite recent achievements. The **Darrius rotor** represents a promising design, in which the blades are shaped and rotate in the pattern of a surface line on a geometric solid of revolution with a vertical axis of rotation. The resulting geometric complexity of the rotor blades presents a significant challenge in their manufacture. As with horizontal-axis rotors, the optimal configuration for Darrius rotors is two or three

rotor blades. **H-rotor** is a valid design, which aim to avoid the complexities of the Darrieus rotor. In fact, in contrast to the curved blades typically employed in Darrieus rotors, straight blades connected to the rotor shaft by struts are utilized. However, the production costs of these systems remain prohibitively high, rendering them unable to compete with horizontal-axis rotors [15]. Figure 2.2 shows a representation of the wind turbine typologies cited in the paragraph.

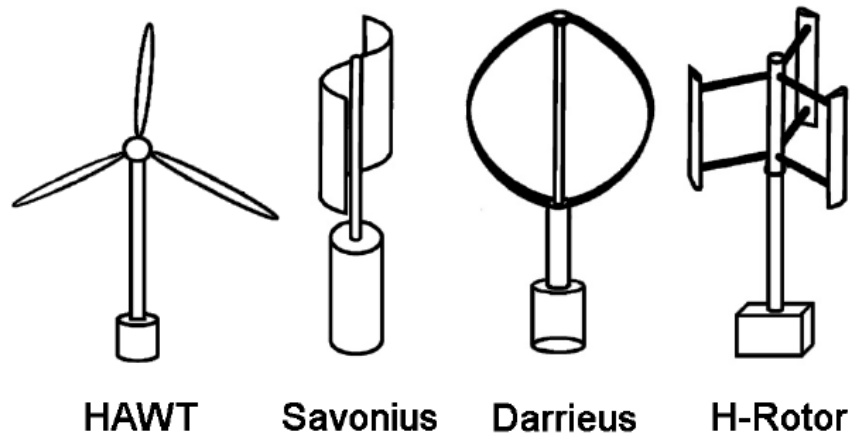


**Figure 2.2:** Wind turbine concepts [16].

As previously stated, the majority of wind turbines constructed for the purpose of electricity generation are horizontal axis wind turbines (HAWTs). Consequently, the following section will focus on the characteristics of this particular wind turbine type.

## 2.2 Horizontal-Axis Wind Turbine

A schematic view of a typical modern HAWT is shown in Figure 2.3.

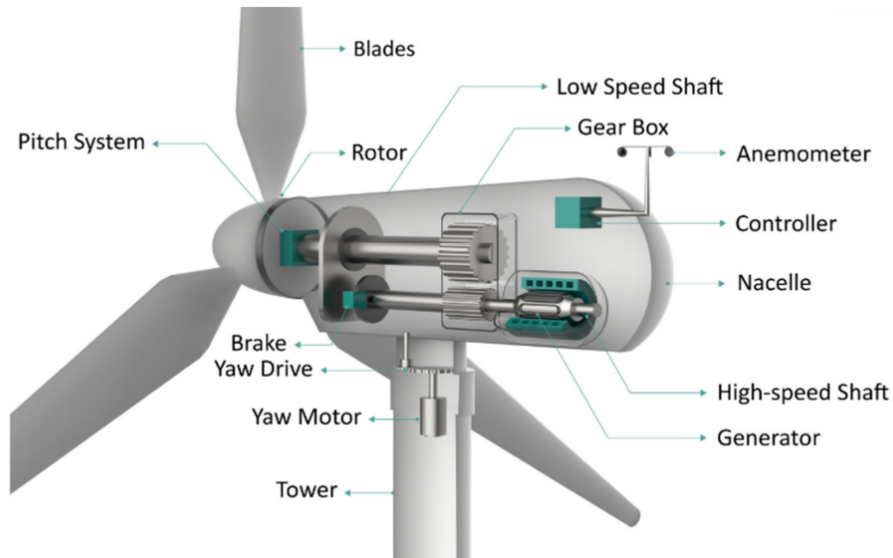


**Figure 2.3:** Components of a wind turbine [17].

The main component of a wind turbine is the **rotor**. In a HAWT, typically 3 **rotor blades**, thanks to an aerodynamic profile, are put into rotational motion by the wind airflow which invests the rotor. The rotor is connected to a **low-speed shaft** which rotates at the same angular velocity of the rotor. This angular velocity is not enough to produce a good quantity of electricity so a **gearbox** is needed to increase the angular velocity and connect the low-speed shaft to an **high-speed shaft**. The high-speed shaft transfers the mechanical motion to a **generator** which generates electricity.

Horizontal-axis wind turbines are equipped with several control systems, with the function to optimize the functioning and the performances of the turbine. The most important control systems are the **blade pitch control system** and the **yaw system**. The first one acts by changing the pitch angle of the blade, consequently changing the blade angle of attack, optimizing turbine performances at different wind speed. The yaw system is necessary to adjust the turbine orientation when the wind direction changes.

The **nacelle** is the box structure mounted behind the rotor on top of the **tower** which protects all the electricity generations components.

The **tower** is connected to the ground through the use of **foundations**. In the case of offshore wind turbines, the foundation is submerged and may be either

**fixed** to the seabed or comprise a **floating structure**. Since the early 2000s, there has been a notable increase in the size of wind turbines, both in hub height and blade length, with the objective of enhancing energy generation. The rationale behind the construction of taller towers is that they are able to capture more energy, given that wind speeds typically increase with altitude. The change in wind speed with altitude is referred to as *wind shear*. At elevated altitudes, wind can flow with greater freedom, experiencing reduced friction from obstacles on the Earth's surface, including trees, other vegetation, buildings, and mountains. Similarly, larger rotor diameters permit wind turbines to sweep a greater area, capture more wind, and produce more electricity. Longer blades allow the turbine to capture more of the available wind than shorter blades, even in areas with relatively less wind. The ability to harvest more wind at lower wind speeds can increase the number of areas available for wind development. This trend is illustrated in Figures 2.4 and 2.5.

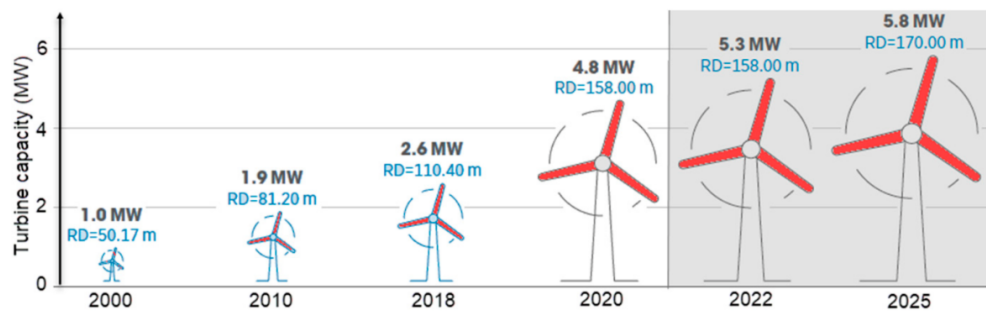


**Figure 2.4:** Power and rotor diameters of existing and planned onshore wind farms [source: IRENA].



**Figure 2.5:** Power and rotor diameters of existing and planned offshore wind farms [source: IRENA].

## 2.3 Rotor

The rotor represents the initial component within the operational sequence of a wind turbine. The aerodynamic characteristics of the rotor blades are responsible for the amount of energy production and the rotor efficiency, so the aerodynamics is fundamental for the rotor performances. Betz's limit is the theoretical best possible efficiency of mechanical power extraction from a free-stream airflow but it does not consider the energy converter design. Nevertheless, the power that can be generated under real-world conditions is contingent upon the characteristics of the energy converter in question. The main difference in power generation comes from the aerodynamic forces involved to create mechanical power. All bodies exposed to an airflow are subjected to aerodynamic forces, the **aerodynamic drag** in the direction of flow and the **aerodynamic lift** at a right angle to the direction of flow. The real power coefficients obtained vary greatly depending on whether aerodynamic drag or aerodynamic lift is used (Figure 2.1). This thesis considers a rotor using aerodynamic lift, which is the most common type of rotor adopted in modern wind turbines.

### 2.3.1 Rotor using aerodynamic lift

In order to utilize the aerodynamic lift, the rotor must be furnished with an appropriate blade configuration, analogous to that observed in the case of an airplane wing (see Figure 2.6). When the blade shape of the rotor permits the utilization of aerodynamic lift, the power coefficient is significantly higher. Similarly, as is the case with an aircraft airfoil, the utilization of aerodynamic lift markedly enhances efficiency.

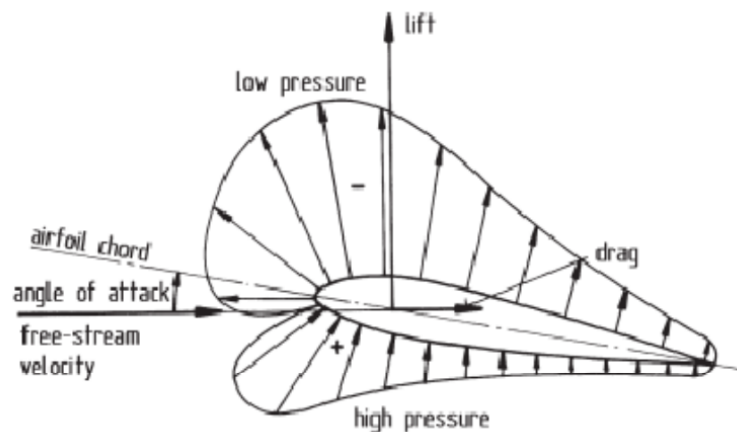


**Figure 2.6:** Aerodynamic forces acting on an airfoil exposed to an airstream [15].

All contemporary wind rotor designs are configured to harness this phenomenon, with the optimal choice being the propeller type with a horizontal rotational axis (Figure 2.7). The wind velocity ( $v_W$ ) is combined vectorically with the peripheral velocity ( $u$ ) of the rotor blade. When the rotor blade is in motion, this represents the peripheral velocity at a specific blade cross-section distance from the axis of rotation. In conjunction with the airfoil chord, the resultant free-stream velocity ( $v_r$ ) constitutes the aerodynamic angle of attack. The aerodynamic force thus created is resolved into two components: a component in the direction of the free-stream velocity, named the **drag**,  $D$ , and a component perpendicular to the free-stream velocity, named the **lift**,  $L$ . The latter can itself be resolved into two further components: a component, named  $L_{torque}$ , in the plane of rotation of the rotor, and a second component, named  $L_{thrust}$ , perpendicular to its plane of rotation. The tangential component,  $L_{torque}$ , constitutes the **driving torque** of the rotor, whereas  $L_{thrust}$  is responsible for the **rotor thrust**. Modern airfoils, which have been developed for use in aircraft wings and have also been employed in wind rotors, exhibit an exceptionally favorable **lift-to-drag ratio** ( $E$ ). This ratio can attain values of up to 200. This fact demonstrates, at the qualitative level, the extent to which the utilization of aerodynamic lift as a driving force must be more effective.

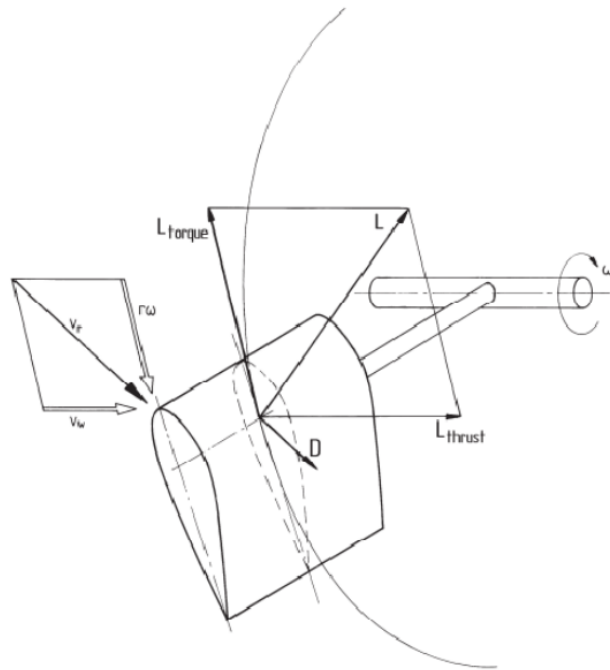


**Figure 2.7:** Flow velocities and aerodynamic forces acting on a propeller-like rotor [15].



The Blade Element Theory [15] allows for the calculation of the local aerodynamic lift and drag coefficients, from which the distribution of the aerodynamic forces along the blade span can be calculated (Figure 2.8). This is typically divided into two components: the **tangential force distribution** in the plane of rotation of the rotor and the **thrust distribution** in the plane of the rotor shaft. Integration of the tangential force distribution over the rotor radius provides the **driving torque** of the rotor, which, in conjunction with the rotational speed of the rotor, yields the **rotor power**. Integration of the **thrust distribution** yields the total **rotor thrust**, for instance to the tower.

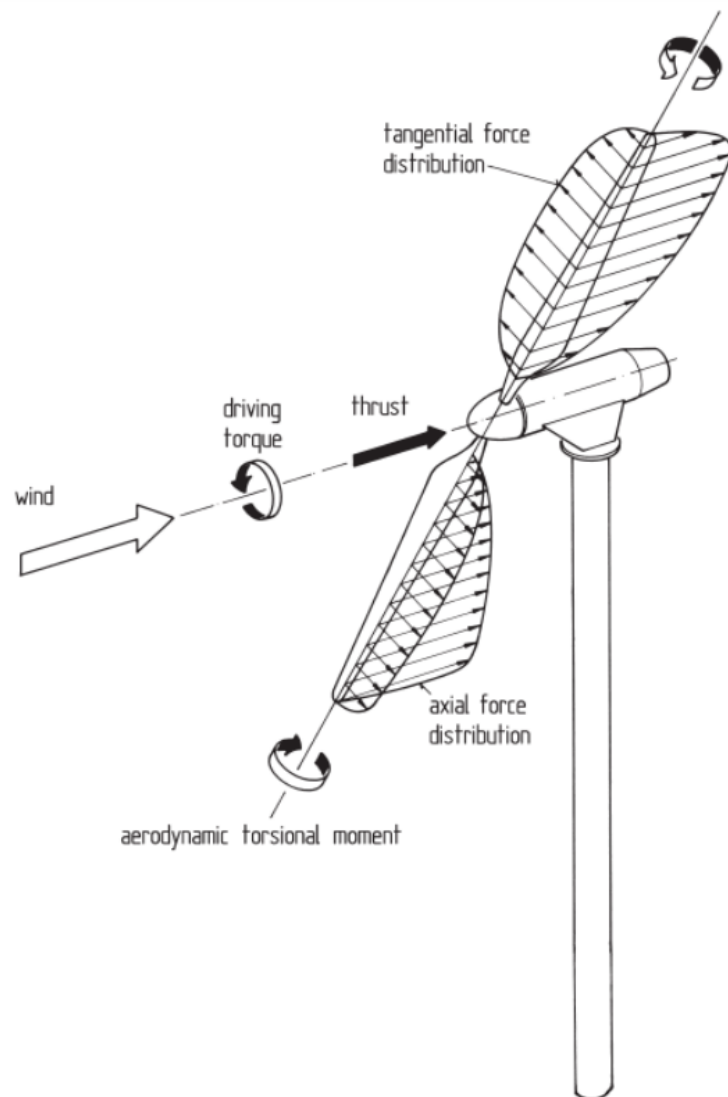


**Figure 2.8:** HAWTs aerodynamic forces distribution [15].

The **rotor power** ( $P_R$ ) can be calculated as follows

$$P_R = \frac{1}{2} \rho c_{PR} v_W^3 A$$

where:

- $\rho$  is the **air density** in  $kg/m^3$ ;
- $c_{PR}$  is the **rotor power coefficient**;
- $v_W$  is the **wind speed** in  $m/s$ ;
- $A$  is the **swept area** in  $m^2$ ;
- $P_R$  is the **rotor power** in  $W$ .

Analogously to the power, the **rotor torque** ( $M$ ) can also be calculated by using a **torque coefficient**  $c_{MR}$ , as follows

$$M = \frac{1}{2} \rho c_{MR} v_W^2 A \cdot R$$

where the rotor radius  $R$  is the reference parameter. Since the torque can be calculated by dividing the power by the rotational speed, a simple relationship between the power and torque coefficient can be derived

$$c_{PR} = \lambda \cdot c_{MR}.$$

Using the blade element theory, it is possible to calculate power and torque coefficients for each tip speed ratio. By doing that, coefficients map can be built. Figure 2.9 shows an example of power coefficients map.

The rotor power and torque curves are specific for each rotor configuration. The main parameters dominating the  $c_{PR}$  map are:

- number of rotor blades;
- chord length distribution of the blades (planform);
- aerodynamic airfoil characteristics;
- twist variation of the blades.

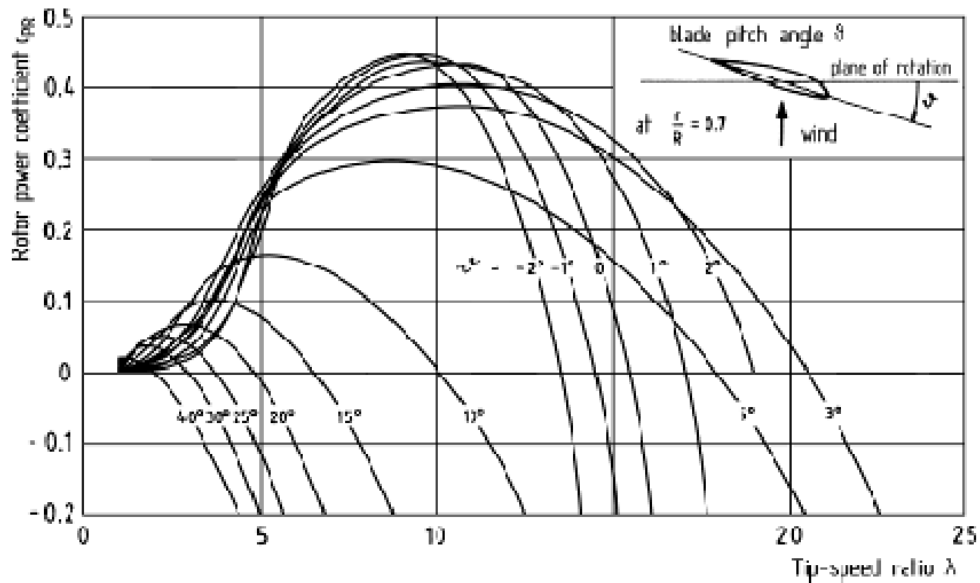
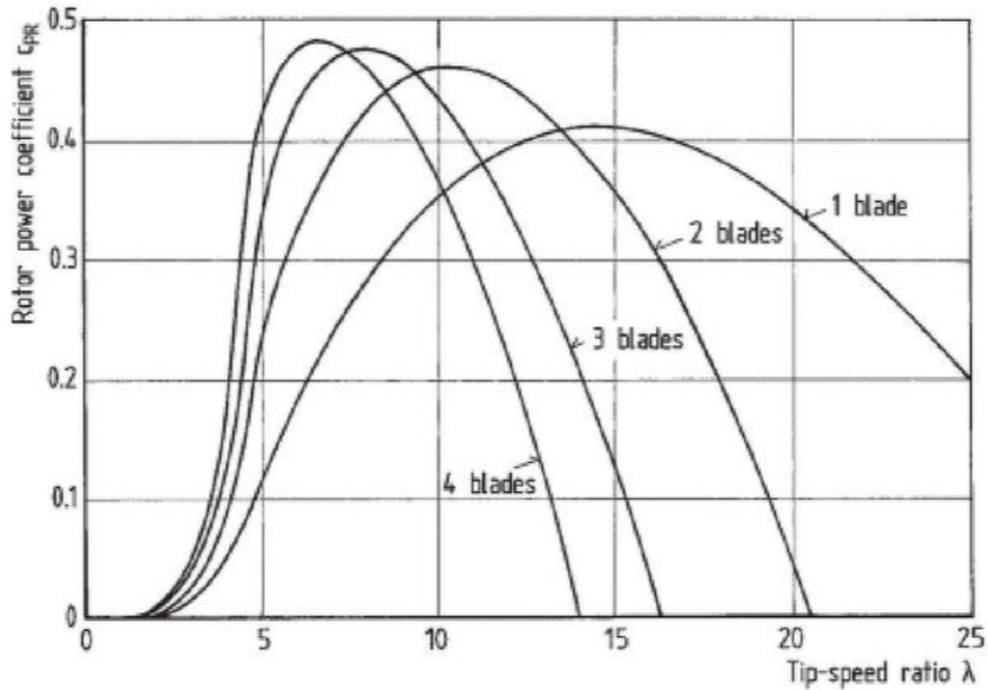


Figure 2.9: Power coefficient map example [15].

### 2.3.2 Number of rotor blades

Figure 2.10 illustrates how the number of rotor blades affects the power coefficient, and so the rotor performances. By switching from 1 to three blade, the power coefficient increases considerably. Then, the increase continues but always with a smaller percentage. This suggests that a maximum number of 3-4 blades is sufficient to reach an high power coefficients without adding excessive weight and costs.

The variation of the  $c_{PR}$  curves as a function of the tip-speed ratio also demonstrates the range within which the optimal tip speed ratio for rotors with different numbers of blades must fall. The three-bladed rotor exhibits optimal performance at a design tip speed ratio of between 7 and 8, whereas a two-bladed rotor attains its maximum  $c_{PR}$  value at a tip speed ratio of approximately 10. The optimal tip speed ratio for a single-bladed rotor is approximately 15. The optimal tip-speed ratio also exhibits a slight dependence on the selected airfoil. However, it should be noted that only the maximum values of the  $c_{PR}$  curves are primarily influenced by the airfoil characteristics, with the correlations between the number of blades, power coefficient and optimum tip-speed ratio remaining largely consistent. It must be noted that a reduction in the number of blades results in an increasingly unfavorable dynamic behavior of the wind rotor [15]. The discrepancy between the aerodynamic characteristics of a three-bladed rotor and those of a two-bladed or single-bladed rotor is particularly pronounced. The elevated dynamic loads



**Figure 2.10:** Power coefficients by varying the number of blades [15].

resulting from an aerodynamically asymmetrical rotor necessitate the incorporation of enhanced complexity in the remaining components of the wind turbine. As a consequence of these developments, the three-bladed rotor has become the standard configuration for commercial wind turbines.

### 2.3.3 Rotor blade planform

The *Blade Element Theory* allows for the calculation of an optimal shape for rotor blades. The optimal shape enables the capture of maximum mechanical power from the wind by the rotor. The pivotal criterion in this calculation is the stipulation that at each blade radius, the wind speed in the rotor plane must be reduced to two-thirds of its undisturbed value [15]. Without reporting all the assumptions, an optimum chord distribution along the blade span can be derived, which is described by the following law [18]

$$c_{opt} = \frac{2\pi r}{N} \frac{8}{9 \cdot c_L} \frac{v_{WD}^2}{\lambda \cdot v_{res}}$$

where

- $c_{opt}$  is the optimum local blade chord (m);

- $N$  is the number of rotor blades;
- $c_L$  is the local lift coefficient;
- $v_{WD}$  is the design wind speed ( $m/s$ );
- $\lambda$  is the local tip speed ratio;
- $v_{res} = \sqrt{v_W^2 + u^2}$  is the local effective flow velocity;
- $r$  is the local rotor radius ( $m$ ).

Figure 2.11 illustrates the theoretical shape of rotor blades considering the effect of different tip speed ratios and different number of rotor blades.

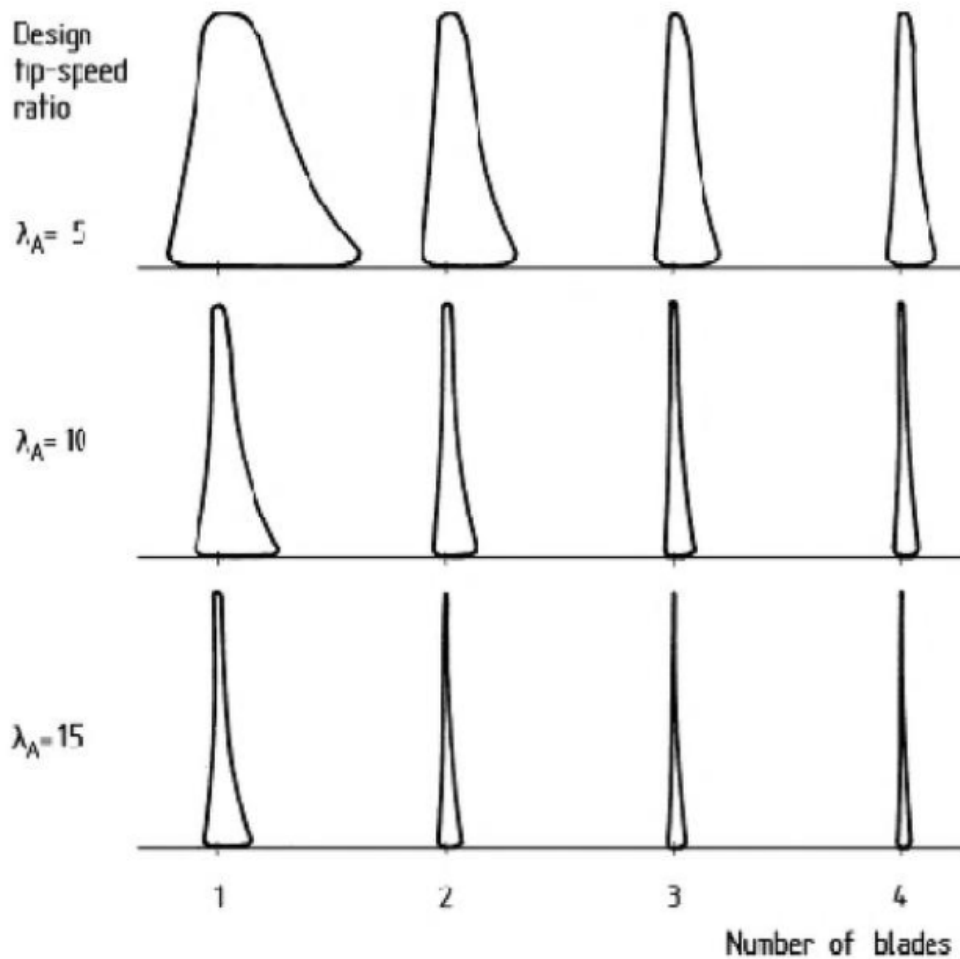


**Figure 2.11:** Theoretical shape of rotor blades considering the effect of different tip speed ratios and different number of rotor blades [15].

Rotor blades become slender at high tip speed ratios. If the blade is too slender, it cannot respect strength and stiffness requirements.

The optimal contour is difficult to manufacture. The actual blades have a simplified planform to help manufacturing. Figure 2.12 illustrates the extent of the power losses incurred due to deviations from the aerodynamically optimal shape. The **trapezoidal planform** with straight leading and trailing edges is a highly effective approximation [15]. The maximum power coefficient is only marginally below that of the optimal hyperbolically delimited shape.

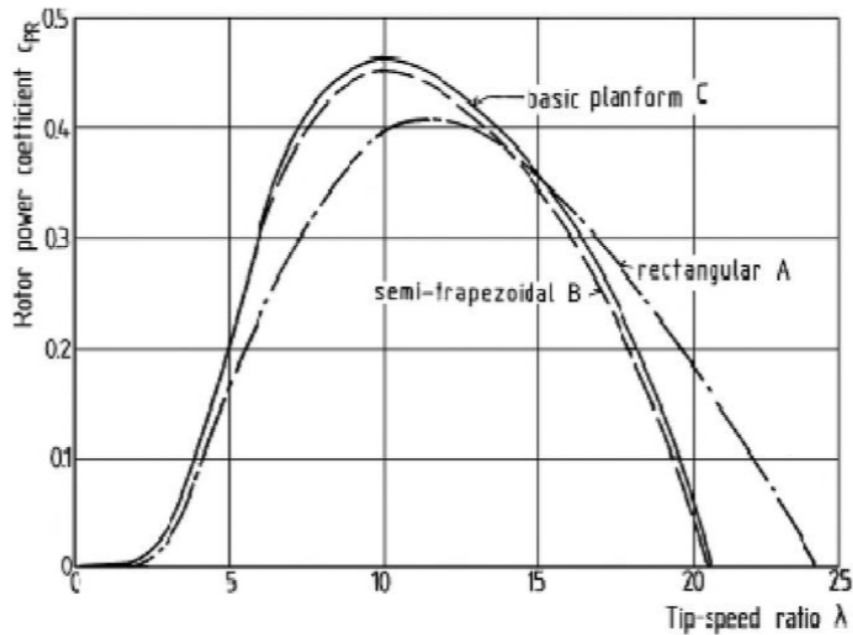


**Figure 2.12:** Power losses due to deviations from the aerodynamically optimal shape [15].

For characterizing the geometrical rotor blade shape, some parameters coming from aircraft technology are used and which are defined as follows

$$\text{Rotor solidity} = \frac{\text{Total blade planform area}}{\text{Rotor swept area}}$$

$$\text{Aspect ratio} = \frac{(\text{Rotor radius})^2}{\text{Planform area of a rotor blade}}$$

$$\text{Taper} = \frac{\text{Chord length at the blade tip}}{\text{Chord length at the blade root}}$$

### 2.3.4 Blade airfoil

From an aerodynamic perspective, all airfoils currently employed for high-speed wind rotors can be classified as *laminar airfoils*. The airfoils are distinguished by a markedly **low drag coefficient** over a specific range of angles of attack. However, their high performance is contingent upon specific prerequisites, particularly the presence of a geometrically precise and extremely smooth airfoil surface. In the event that these conditions are not satisfied, the performance of the airfoil is inferior to that of a conventional airfoil. However, airfoils that do not exhibit extreme laminar characteristics are employed, which demonstrate consistent aerodynamic performance across a broad range of angles of attack in turbulent airflows. In light of these considerations, the demands placed on the aerodynamic design by wind power technology remain distinct from those observed in aircraft construction, where the reduction of drag represents a pivotal objective. The NACA series of standard airfoils continues to be the predominant choice. In contrast to the decline in usage of the earlier NACA 44 and 230 series airfoils, the 63 and 64 series continue to be widely employed. It is anticipated that the utilization of bespoke aerodynamic airfoils for wind rotors will become increasingly prevalent in the future [15].

### 2.3.5 Blade twist

The velocity relative to the blade is responsible for the generation of aerodynamic forces. The relative velocity is a combination of the absolute velocity of the incoming wind, normal to the rotor plane, and the rotational velocity of the rotor. The rotational velocity is the same for all blade sections, but the absolute velocity of each blade section is different. In particular, each blade section has an absolute velocity given by the product of the rotational velocity and the section radius. This means that the absolute velocity of the blade section increases from the hub to the tip. Consequently, the angle of attack increases from hub to tip. This means that a blade twist is necessary, in order to maintain a constant angle of attack to maximize rotor performances. The effect of a blade twist is clearly shown in Figure 2.13.

However, in order to simplify the manufacturing process of rotor blades, the blade twist is typically limited. The absence of twist results in a notable decline in power output. For large turbines, this represents an excessive compromise in favor of simplified blade manufacture.

In order to determine the optimum blade twist, it is necessary to consider a number of factors, including the type of power control (pitch or stall) and certain operational characteristics of the rotor. Furthermore, the selection of airfoil has an impact on the outcome.

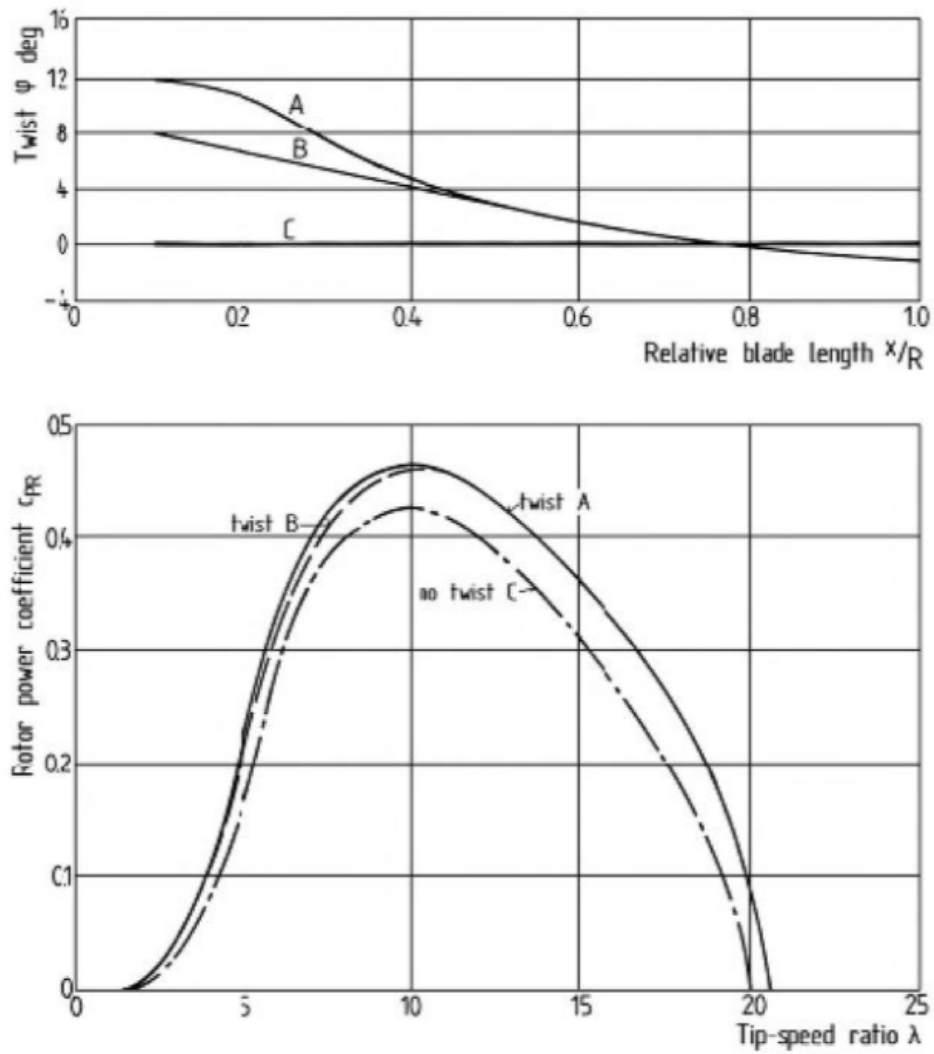


Figure 2.13: Rotor blade twist effect on rotor performances [15].



# Chapter 3

## Load

Wind turbines are subjected to a range of specific loads and stresses. This chapter describes the potential sources of significant load for a wind turbine rotor blades, focusing on aerodynamic and mass loads, which are always present and will be object of analysis in the next chapter. After presenting the load sources, the functioning of a blade structure is presented in order to explain the current state-of-the-art of wind turbine blade in terms of structural components and materials.

### 3.1 Load sources

On initial observation, the primary challenge appears to be the stability of the structure in the presence of heavy storms and hurricanes. However, the continuous alternating loads, even under normal wind conditions, present a significant challenge. The challenge of alternating loads is that they are more difficult to cope with than static loads. This is because the material becomes fatigued. The dimensions of the components present an additional challenge.



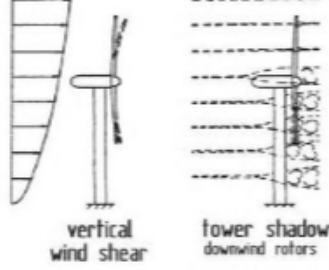
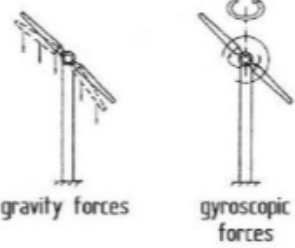
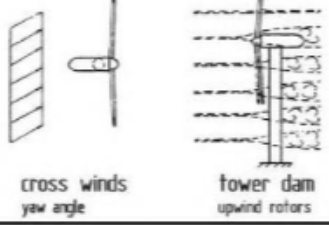

The air is a low density working medium, so it is necessary to use large aerodynamic surfaces to convert enough energy. Large structures have always an elastic behavior so, under changing loads, dynamic loads are expected, so vibrations and resonances must be studied. It is inevitable that dynamic loading will occur on the wind turbine due to the fluctuating external loads. However, it is crucial to ensure that this does not result in a critical vibrational behavior of the components.

Following these considerations, the three main aspects that must be checked in a wind turbine structural dimensioning are:

- extreme load endurance;
- fatigue life;
- vibration and resonances.

A significant challenge arises even before the structural design loads are calculated. This concerns the loads to be stipulated and the situations in which the loads occur, which determine the dimensions of the structure. This necessitates a comprehensive examination of all external operational conditions and potential malfunctions of the turbine. In light of the aforementioned considerations, the load cases can be defined. However, it is not possible to account for the full complexity of the actual loads that a wind turbine will experience. As a result, the loads that are specified in the design process must necessarily be approximated and idealized. The load assumptions, that is to say the load cases with the associated loads, constitute an essential element of the design process. The starting point for the entire load spectrum of a wind turbine is the analysis of the loads acting on the rotor. The loads on the rotor blades are transferred to the other components, and to a significant extent, they determine their loading. In comparison, the loads originating directly from downstream components are of lesser significance. Consequently, discussions of the loads acting on a wind turbine can be focused on the rotor, which can be considered representative of all other components. A local rotor coordinate system is defined for forces and moments definition. In the direction of the airfoil chord, the "edgewise" component is obtained, while perpendicularly to the airfoil chord it is the "flapwise" component. The main forces acting on the rotor, always present, are those due to **aerodynamics**, **gravity** and **inertia** (see Figure 3.1).

In order to conduct an investigation of structural stresses, it is essential to consider the effects of load variations over time. It is essential to acknowledge the impact of fluctuating and alternating loads, particularly in relation to the fatigue life of the structure. It is essential to be aware of the potential for extreme loads in specific situations in order to ensure the survival of the structure with respect to ultimate stress. It is not feasible to ascertain in advance which of the loads within the entire range of loads will exert the dominant influence. As is the case in all structures, the larger the turbine, the greater is the significance of the gravitational loads. Furthermore, the elasticity of the structure assumes greater significance with respect to the extent to which external loads are transformed into structural stresses. To illustrate, the variability of rotor speed and the elasticity of rotor blades are of consequence with respect to the conversion of external loads into structural stresses. In other words, the load level is also determined by the design of the wind turbine, in addition to the external loads. In general, it can be stated that the greater the elasticity of a structure, the more effectively alternating loads can be absorbed, thereby reducing the likelihood of material fatigue. However, at the opposite end of the spectrum, excessive flexibility can lead to the onset of vibration problems. Furthermore, the mathematical complexity of a structure's dimensional design increases in proportion to its elasticity.

	Aerodynamic forces	Inertial and gravity forces
steady loads	 <p>steady mean wind speed</p>	 <p>centrifugal forces</p>
unsteady loads	 <p>vertical wind shear tower shadow downwind rotors</p>	 <p>gravity forces gyroscopic forces</p>
	 <p>cross winds yaw angle tower dam upwind rotors</p>	
non-cyclic loads	 <p>wind turbulence</p>	

**Figure 3.1:** Aerodynamics, gravity and inertia acting on the rotor of a horizontal-axis wind turbine [15].

### 3.1.1 Aerodynamic load

Aerodynamic loads is strongly dependent upon the airflow conditions which cross the rotor. Three main cases could be possible: *uniform and steady-state airflow*, *vertical wind shear and cross winds* and *wind turbulence and gusts*. In this paragraph all the three situations are briefly presented, then the focus of the thesis is on a uniform and steady-state airflow case.

#### Uniform and Steady-State airflow

It is important to note that the assumption of a uniform and steady wind flow is an idealization that does not reflect the actual conditions observed in the open atmosphere. In practice, this concept is beneficial for determining the average load level experienced over an extended duration. Assuming a consistent and symmetrical flow enters the region covered by the rotor, the blades of a horizontal-axis rotor encounter stable aerodynamic forces. The wind loads on the blades during steady and symmetrical stream are largely determined by the effective wind speed, which varies from the blade root to the tip. Additionally, the geometrical shape of the rotor blades influences the load distribution over the length of the blade. Figures 3.2 and 3.3 provide an impression of the aerodynamic load distribution on a typical rotor blade.

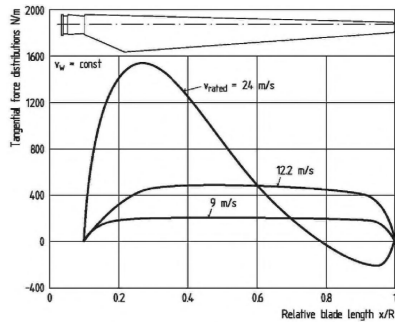


**Figure 3.2:** Tangential load distribution over the blade length [15].

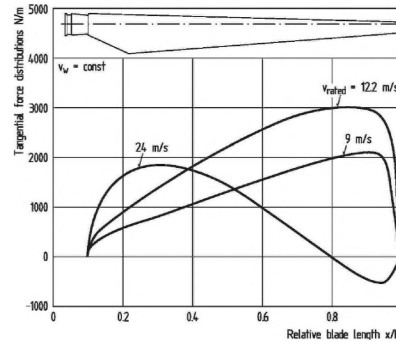


**Figure 3.3:** Thrust load distribution over the blade length [15].

The bending moments experienced by the rotor blades in the edgewise direction are a consequence of the distribution of tangential forces, whereas the thrust distribution is responsible for the blade bending moments in the flapwise direction [15]. As a consequence of the rotor blade twist, in particular, the distribution profile undergoes a notable change from the start-up wind speed to the shut-down wind speed. The twist is optimized for a nominal wind speed only, such that the distribution of aerodynamic loads corresponds approximately to the theoretical

optimum for this wind speed. At other wind speeds, particularly those above the nominal value, the flow separates in the blade sections situated in the vicinity of the hub. This results in a notable alteration to the distribution of aerodynamic loads. The integration of load distributions across the length of the rotor blade provides the overall rotor loads and moments. The tangential loading provides the rotor torque, while the thrust load distribution provides the total rotor thrust. These two parameters are, in essence, responsible for determining the static load level for the entire turbine. The aforementioned examination of rotor blade loads pertains solely to the distribution of loads in the direction of the blade. The two-dimensional representation of the loads in reality conceals a significant variation in the loads, which also extend in the direction of the blade chord. Information regarding load distribution along the blade chord is typically of limited consequence.

### **Vertical wind shear and cross winds**

The wind flow generates fluctuating, cyclically varying loads as soon as it strikes the rotor asymmetrically. One unavoidable asymmetry of the oncoming wind flow is caused by the increase in wind speed with height, which is an inherent characteristic of atmospheric conditions. During each rotation, the rotor blades experience higher wind velocities in the upper part of their movement, leading to increased loads when compared to the lower sector closer to the ground. This flow asymmetry at the rotor is similarly influenced by the unavoidable crosswinds that accompany rapid shifts in wind direction. The presence of vertical wind shear and crosswinds on the rotor results in a cyclical variation in the distribution of aerodynamic loads across the blades. When contrasted with the basic loading conditions of a steady, symmetrical wind, significant differences in load distribution become evident. The fluctuating aerodynamic forces acting on the rotor blades throughout their revolution also lead to variations in total rotor loads, which subsequently affect the loads experienced by other components of the turbine.

A similar asymmetry in rotor crosswinds arises from the increase in wind speeds with altitude, further exacerbated by the rapid changes in wind direction. The relatively slow yaw drive is only able to respond to these changes with a significant time lag, which can lead to the airflow striking the rotor at a yaw angle at certain times. Additionally, asymmetrical inflow conditions for the rotor may occur due to the redirection of wind streams caused by complex topographical features or as a result of rotor design, particularly when the rotor axis is inclined. This underscores the importance of keeping the rotor axis inclination to a minimum. However, with highly flexible rotor blades, this inclination is necessary to ensure that adequate clearance is maintained between the blade tips and the tower during maximum deflection.

## Wind turbulence and gusts

The power output and energy yield of a wind turbine are contingent upon the long-term variations in mean wind speed. Conversely, the non-cyclic fluctuating loads on the wind turbine are determined by the short-term fluctuations in wind speed, wind turbulence, and gusts. The constant presence of wind turbulence plays a significant role in the development of material fatigue, particularly in the case of rotor blades. It is also necessary to consider the effects of extreme wind speeds, which are far less common, when designing components to withstand fatigue. Furthermore, they can elevate loads to the point of fracture. The most significant issues with regard to loading are posed by stochastic fluctuations in wind speed. There are numerous "turbulence models," which can be traced back to two fundamental approaches: the *spectral model of turbulence* and the *gust model*. As this thesis does not investigate the impact of wind turbulence on rotor blade structure, it will not elaborate further on this topic.

### 3.1.2 Gravity and Inertial loads

Gravity and inertial loads are easier to calculate with respect to aerodynamic loads. The main difficulty is due to the fact that the mass of the blade is not definitive at the beginning of the design process so several iterations are needed.

#### Gravitational loads

It is essential to consider the loads resulting from the dead weight of the components for all components of the turbine, in particular the blades. The blade mass generates cyclic loads along the blade span, both in edgewise and flapwise direction, during rotor revolutions. The significance of this gravitational loading increases from the blade tip to the root, in opposition to the influence of the aerodynamic loads. It can be reasonably deduced that the larger the rotors, the greater these influences will be. As is the case with any other structure, as dimensions increase, the primary challenge with respect to strength is the structure's weight. The situation is further compounded for horizontal-axis rotors due to the presence of dead weight, which introduces alternating loads. Those who advocate the vertical-axis concept rightly highlight that this configuration is more suitable for extreme dimensions due to the avoidance of alternating loads caused by blades weight. The optimal approach, or indeed the only viable approach, is to reduce the natural weight of the rotor blades. The use of lightweight construction is almost mandatory for very large rotor blades, even when expensive materials such as carbon fiber are employed.

## Centrifugal loads

Centrifugal forces are of minimal consequence in wind rotors, largely due to their comparatively low rotational velocity. This is in contrast to helicopter rotors, where the strength of the blades and their dynamic behavior are determined by the centrifugal forces. There are some technique which uses the centrifugal loads to mitigate the load on the rotor blades. Introducing a **cone angle** induces a bending moment distribution along the blade span, which counters the bending moments created by the aerodynamic thrust. This is in addition to the centrifugal forces, which also act to bend the blades. Nevertheless, complete compensation can only be achieved for a single combination of rotor speed and wind speed. However, to establish if a cone angle of the rotor blade is a technically viable solution, a comprehensive assessment of the relevant factors must be taken. In more recent turbine designs, there is a growing tendency to eschew the use of a rotor cone angle.

## Gyroscopic loads

Gyroscopic effects result in loads when the rotor, which is rotating, is yawed into the wind. A rapid yawing rate gives rise to considerable gyroscopic moments, which are manifested as pitching moments on the rotor axis. However, since yawing rates are typically low, the practical effects are minimal and gyroscopic loads are usually not taken into account in the design process, at least during first steps.

## 3.2 Blade load condition

Once the load sources have been described, this section presents a simplified analysis of the rotor blade in order to understand how the blade is loaded and how the blade structure is expected to carry the load. According to [19], for this scope, the blade is initially modelled as a **cantilever beam**, which permits to easily calculate an approximation of the flapwise and edgewise bending moments.

### 3.2.1 Flapwise bending moment

Aerodynamic loads are responsible for the flapwise bending moment. To calculate an approximation of the flapwise bending moment, the blade can be modelled as a cantilever beam and the resultant aerodynamic load is represented by a uniformly distributed load [20]. A representation of the model is given in Figure 3.4.

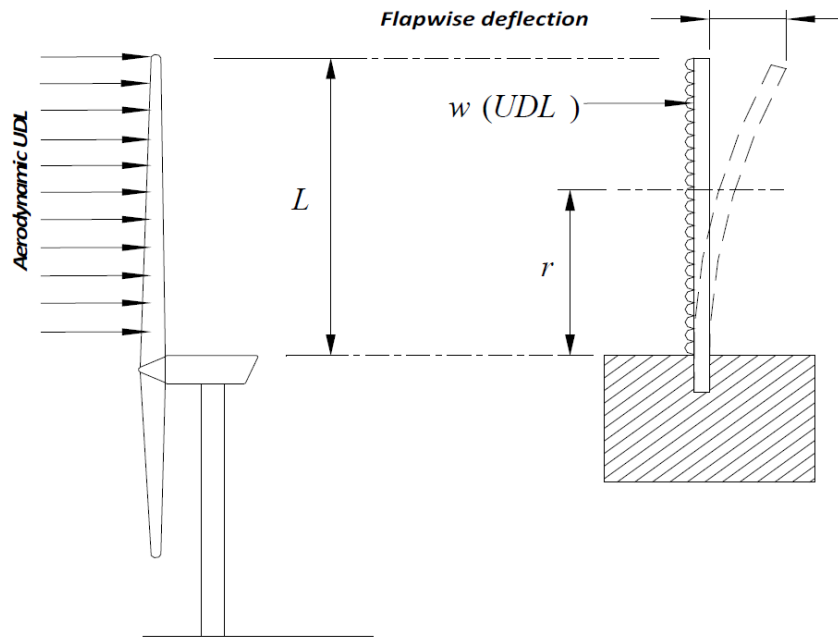


**Figure 3.4:** Cantilever beam model - flapwise bending [19].

According to the *beam theory*, flapwise bending moment can be calculated as

$$M = -\frac{1}{2}w(L - r)^2$$

L = Total blade length  
 M = Bending moment  
 w = UDL  
 r = radial distance from the hub.

Flapwise moment bends the beam around the chord axis. In the blade, this means that the flapwise bending moment stress principally the spar caps (see Figure 3.5).



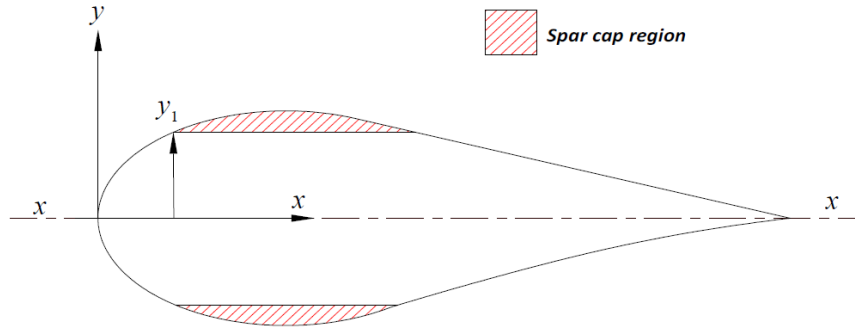


**Figure 3.5:** Flapwise bending [19].

Material stresses can be calculated as

$$\sigma = \frac{M}{I} \cdot y$$

$\sigma$  = Stress  
 $y$  = Distance from the chord  
 $M$  = Bending moment  
 $I$  = Second moment of area.

where the second moment of area  $I_{xx}$  can be calculated as

$$I_{xx} = \iint (y - y_1)^2 dx dy.$$

This simplified analysis shows that is convenient to put load-bearing material far from the neutral axis. In fact, causes an increase in moment of area and a consequently decrease in the stress. In the case of flapwise bending moment, this is done by putting load-bearing material in the spar caps. From a structural point of view, thicker airfoils can help reducing stresses. Reducing stresses by using thicker airfoil can save material usage and weight [21]. However, the airfoil choice is always a compromise between structures and aerodynamics. Near the root, structural requirements are more urgent as the stresses are higher, in fact the root airfoils tend to be circular.

### 3.2.2 Edgewise bending

The edgewise bending moment is a result of blade mass and gravity. Therefore this loading condition can be considered negligible for smaller blades with negligible blade mass. Simple scaling laws dictate a cubic rise in blade mass with increasing turbine size. Therefore for increasing turbine sizes in excess of 70 m diameter, this loading case is said to be increasingly critical [20].

Using a simplified model, the blade is modelled as a cantilever beam subjected to a distributed load which has its maximum at the beam root and tends to zero

towards the tip. The representative moment is when the blade is horizontal, as the load is maximum. the model is represented in Figure 3.6.

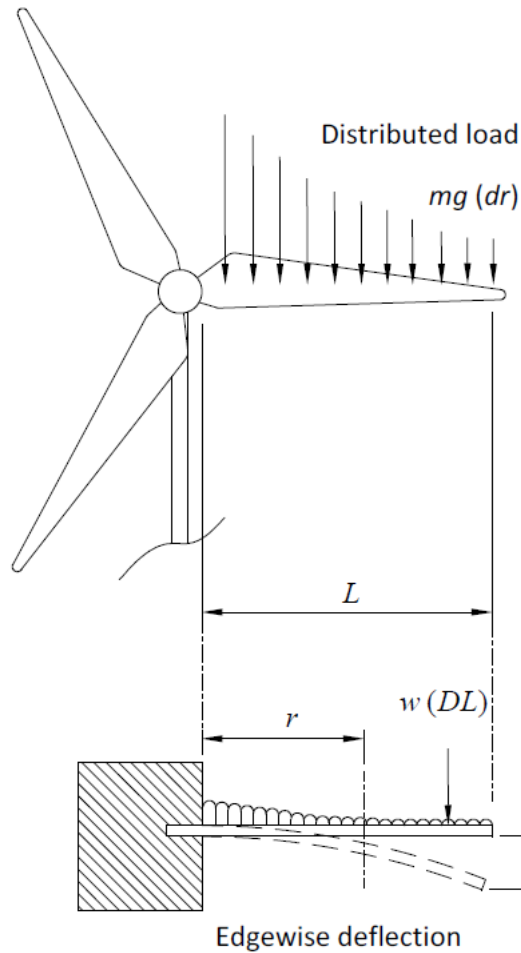


**Figure 3.6:** Cantilever beam model - edgewise bending [19].

The analytical formulas are the same as the flapwise bending moment, with the right variables, so it is omitted in this section. Figure 3.7 shows that the edgewise bending moment acts normally to the flapwise moment so the spar caps do not carry the edgewise load.

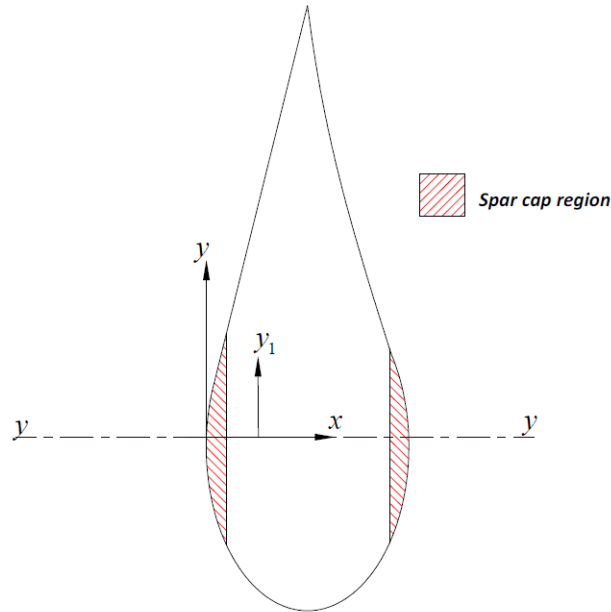


**Figure 3.7:** Edgewise bending [19].

Following the considerations made for flapwise bending moment, it is evident that to carry the edgewise loads, reinforcement material is useful in the zone of leading and trailing edge.

### 3.3 Structural blade regions

The modern blade can be split into three main areas based on aerodynamic and structural function [19] (Figure 3.8):

- the **blade root**. In the root region the structural requirements drive the airfoil choice, due to the high stresses. Thicker airfoils are selected in order to ensure the structural integrity;
- the **mid span**. The aerodynamic significance of this design feature is that the lift-to-drag ratio will be optimized. Accordingly, the thinnest feasible airfoil section should be employed, in accordance with the structural constraints;
- the **tip**. The objective is to achieve optimal aerodynamic performance, which will be reflected in the maximum lift-to-drag ratio. Consequently, the utilization of slender airfoils and meticulously crafted tip geometries serves to diminish noise and losses. The efficacy of such tip geometries remains untested in the field. Nevertheless, they are still employed by some manufacturers.

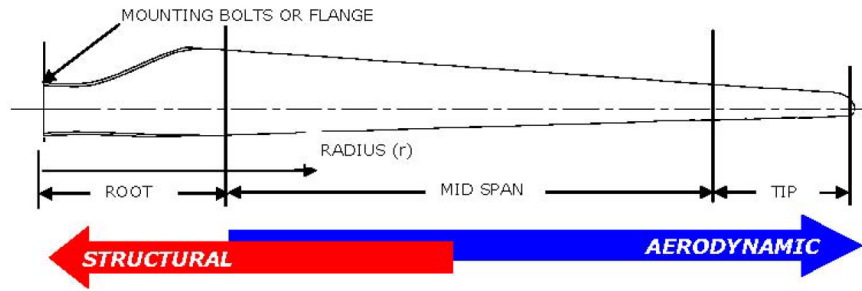


Figure 3.8: The three blade regions [19].

### 3.4 Blade structure

It is a common practice to manufacture the rotor blades of modern wind turbines from **fiber composites**. The principal fiber material is glass fiber; carbon fiber is being employed with increasing frequency as a reinforcement at critical locations. The structural design of today's rotor blades is largely based on the principles of aircraft construction. In the most basic configuration, the blade cross-section is a **hollow shell** comprising an upper and lower half-shell (*suction* and *pressure side*, respectively). The shape of the shell is determined by the requisite aerodynamic properties. A hollow shell structure is capable of resisting significant torsional loads; however, it lacks the requisite strength to withstand out-of-plane loads. Accordingly, rotor blades are equipped with one or more **shear spar webs**, which are designed to accommodate these specific loads. The configuration of the webs varies, from a single web to two or three distributed along the length of the blade chord. Additionally, box-like structures are employed (see Figure 3.9). The webs are composed of laminated composite materials.

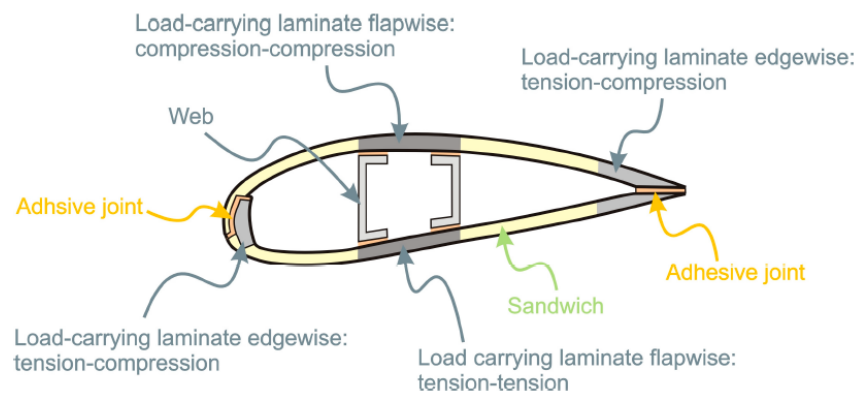


Figure 3.9: The three blade regions [22].

The shells are manufactured using a sandwich construction methodology, whereby only the outer layers consist of "hard" fiber composites, while a softer support material is used on the inside. This methodology represents the sole viable approach for attaining the desired minimal weight. The spar webs or spar boxes are manufactured separately and, subsequent to the molding of the lower shell, are inserted into and bonded to it. In the outer, thinner sections of the blade, foam material or balsa wood is employed in lieu of webs. The webs and spar boxes are subjected to the greatest proportion of the load, particularly in terms of bending moments. It is therefore imperative that particular care is exercised during the manufacturing and bonding processes with the rotor blade shells. The majority of rotor blades are currently manufactured using glass fiber composites. In the majority of cases, carbon fiber is employed as a reinforcement material for blades of considerable dimensions. The production of rotor blades comprising entirely carbon fiber composite material remains financially infeasible for the manufacture of commercial wind turbines. Consequently, carbon fiber is employed in only minimal quantities at the points on the rotor blades that are subjected to the greatest loads. To illustrate, the spar flanges in numerous blades are reinforced with carbon fiber in the principal stress direction. The use of carbon fiber is almost inevitable for extremely large rotor blades with a rotor diameter of more than 120 meters.

### 3.4.1 Materials

From a technological standpoint, **fiber-reinforced composite material** (GFRP) is a composite of synthetic resin and fibers. The fibers serve to absorb the stresses within the material, while the resin is responsible for embedding the fibers and shaping the material. In principle, there is a vast array of resins and fibers that can be combined. However, each combination has different mechanical properties so the acceptable combinations are limited for each specific application.

#### **Fiber material**

Fibers are the primarily responsible for mechanical properties of the composite material. Three different fiber materials are currently available:

- glass fiber;
- carbon fiber;
- organic aramid fiber (KEVLAR).

The properties of the fiber material determine the strength and the stiffness of the components, whereas the type of resin is important for the manufacturing process.

The fibers are available in a wide range of qualities, from those of the highest quality suitable for use in aerospace applications to those of a lower grade that are only fit for use in simple fairing structures. This is reflected in the pricing structure. Although organic fibers such as Kevlar possess comparable strength properties to carbon fiber, their other properties present certain challenges with regard to their utilization in rotor blades. One disadvantage of these fibers is that they are hygroscopic, meaning that they absorb moisture. Conversely, the fatigue strength of organic aramid fiber has yet to be sufficiently field-tested. Glass fiber is the most widely utilized fiber. It has high strength properties, even if its modulus of elasticity is not so high. This involves that the stiffness of glass fiber components is not particularly high, which is one of the reasons why large rotor blades need reinforcements. Carbon fiber is distinguished by its exceptional tensile strength and modulus of elasticity. Carbon-fiber components have a stiffness similar to that of steel structures. Furthermore, they have favorable fatigue strength properties. The continued high price of carbon fiber represents a significant drawback. Consequently, carbon fiber is often employed in conjunction with glass fiber materials in regions that are particularly susceptible to stress.

### **Matrix material**

Matrix materials are basically **polyester resins** or **epoxy resins**. Polyester resins are employed in a variety of applications, particularly in the field of boat building. They are relatively inexpensive and demonstrate satisfactory performance under moderate stress conditions. The majority of earlier rotor blades, particularly those produced in Denmark, were manufactured using polyester resins. Furthermore, polyester resin cures at room temperature, which facilitates processing. The primary disadvantages of polyester resin when compared to epoxy resin are its comparatively lower strength and the relatively high degree of shrinkage that occurs during the drying process, which can reach up to 8%. An increasing number of rotor blade manufacturers now opt to utilize the expensive, high-quality epoxy resins that are exclusively employed in aircraft construction. Epoxy resin shows better mechanical properties and does not experience shrinkage. In addition, the blade weight is reduced. Apart from the higher costs associated with the material itself, the inability of epoxy resins to be cured at room temperature also presents a disadvantage. They must be dried at a higher temperature of approximately 150°C, and the overall processing is considerably more complex.

### **Surface protection**

**Gelcoats**, which are also based on synthetic resins, are widely utilized as a protection surface, particularly for rotor blades. These are inserted as the top layer in the production mold, resulting in the formation of a smooth and permanent

surface that does not require further painting. They protect the blade from external agents and UV rays.





## Chapter 4

# Reference Turbine

In the context of the wind energy sector, reference wind turbines fulfill a number of roles, and as a result, they have become increasingly significant in recent years. Primarily, they serve as open benchmarks, defined with publicly available design parameters, which are used as baselines for studies exploring new technologies or design methodologies. It has been customary to construct reference wind turbines with realistic designs that are not fully optimized. This enables them to be updated and enhanced by the active wind energy community. Secondly, as open designs, reference wind turbines facilitate collaboration between industry and external researchers. The utilization of a reference turbine enables the safeguarding of intellectual property on the part of the industry, while simultaneously facilitating the exploration of advanced technology development in collaboration with external parties. Additionally, reference wind turbines serve as an entry point and educational platform for those new to wind energy, facilitating comprehension of fundamental design elements and system trade-offs. In order to retain its relevance in the present era and in the years to come, a new reference wind turbine must surpass the current generation of industry wind turbines. Nevertheless, the enhancement in performance should not be so considerable that it requires the incorporation of revolutionary new technologies. The extant range of reference wind turbine designs is insufficient to meet the requirements of the research community and industry in advancing the state of the art in a number of areas, including blade scaling, floating foundation design, wind farm control, logistics studies, and many others. It is therefore evident that a reference wind turbine with a capacity above 10 MW but below 20 MW is required, which continues on the same growth trend as the previous industrial conceptual designs. The current reference turbine used by the wind energy community is the *IEA Wind 15-MW*, a Class IB direct-drive machine which was jointly designed by the *National Renewable Energy Laboratory*, the *Technical University of Denmark*, and the *University of Maine* [23].

## 4.1 IEA Wind 15-MW

The IEA Wind 15-MW is designed to be an offshore wind turbine with a fixed-bottom monopile support structure. The **blade** design ended selecting a rotor diameter of 240 meters and a maximum tip speed of 95 meters per second (m/s). The structural design provides two principal load-bearing, carbon fibers-reinforced spars, linked by two sandwich shear webs, with laminate reinforcement on trailing and leading edges and foam fillers.

Some of key parameters are reported in Table 4.1.

Parameter	Units	Value
Power rating	MW	15
Turbine class	-	IEC Class 1B
Rotor orientation	-	Upwind
Number of blades	-	3
Control	-	Variable speed Collective pitch
Design tip-speed ratio	-	90
Minimum rotor speed	rpm	5.0
Maximum rotor speed	rpm	7.56
Maximum tip speed	m/s	95
Rotor diameter	m	240
Airfoil series	-	FFA-W3
Hub height	m	150
Hub diameter	m	7.94

**Table 4.1:** IEA Wind 15-MW Turbine data [23].

An overview of the IEA Wind 15-MW reference turbine is given in Figure 4.1.

### 4.1.1 Blade

The blade of the IEA Wind 15-MW reference turbine is 117 m long and starts with a root diameter of 5.2 m. The maximum chord is 5.77 m large at approximately 20% of the span. Figure 4.2 shows the reference blade geometry while Table 4.2 summarizes the main properties of the blade.

### Aerodynamics

For the IEA Wind 15-MW turbine, the DTU FFA-W3 series of airfoils were used. These are publicly available and well-documented airfoils. The airfoils shapes are

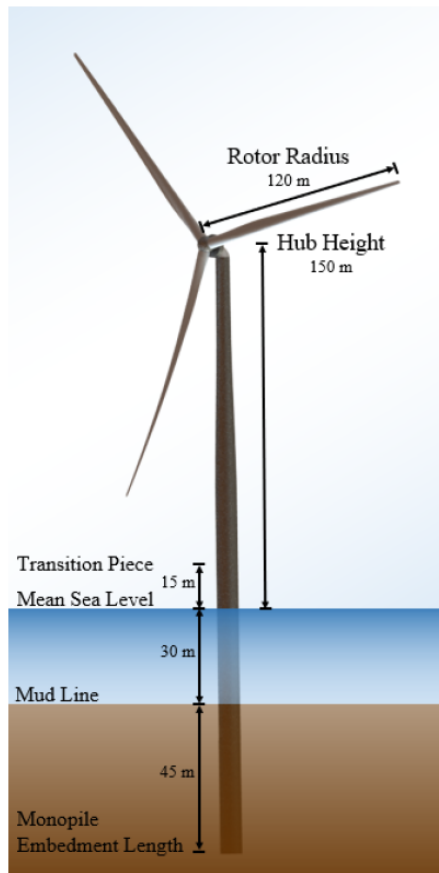


**Figure 4.1:** IEA Wind 15-MW [23].



**Figure 4.2:** Blade top and edge view [23].

reported in Figure 4.3.

Figure 4.4 shows the chord distribution (on the left) and the relative thickness (on the right) along the blade span. It is evident that the transition from a cylinder cross section to the thickest 50% airfoil occurs between 2.34 m to 17.55 m or 2% to 15% of the span, with the maximum chord of 5.77 m at 27.2 m of span (23.3%).

Description	Value	Units
Blade length	117	m
Root diameter	5.20	m
Root cylinder length	2.34	m
Max chord	5.77	m
Max chord spanwise position	27.2	m
Tip prebend	4.00	m
Precone	4.00	deg
Design tip-speed ratio	9.00	-
Design $C_P$	0.489	-
Design $C_T$	0.799	-

**Table 4.2:** Blade main properties [23].

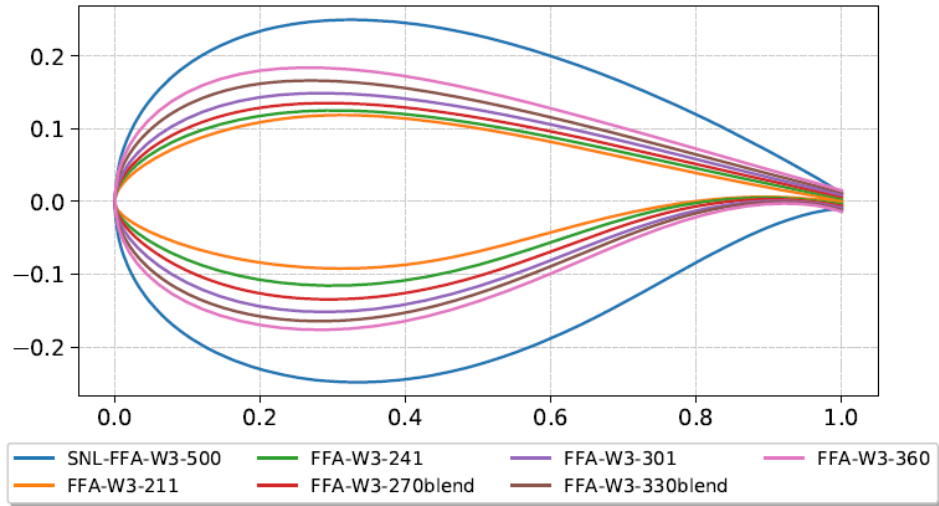


**Figure 4.3:** DTU FFA-W3 airfoils series [23].

### Blade structure

The structural layout of the blade is based on a traditional design, comprising two main load-carrying spars positioned on a straight line connecting the root and the tip. Reinforcement is provided along the trailing and leading edges. One of the spars is positioned on the airfoil pressure side, while the other is located on the suction side. The spars are constructed from carbon fiber in order to provide the requisite stiffness with the minimum weight. The blade is equipped with two shear webs, which connect the pressure and suction sides and are attached to the main spars. These webs extend from a span of 10% to 95%. Additionally,

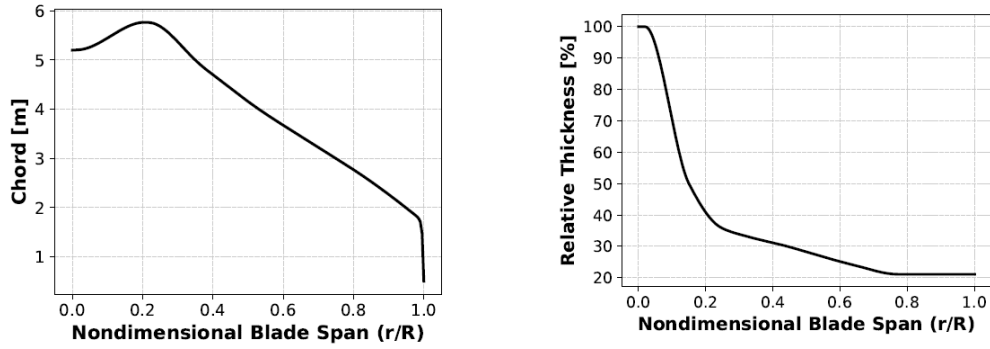


**Figure 4.4:** Chord (on the left) and relative thickness (on the right) along the relative blade span [23].

uniaxial glass fiber is employed to reinforce the leading and trailing edges, thereby augmenting the edgewise stiffness. Foam filler panels were incorporated into the design between the leading-edge and trailing-edge reinforcement and the spar caps, on both the pressure side and suction side. The internal structure and composite layup of the blade are defined in accordance with the IEA Wind Turbine Ontology. The composite layers are defined as spanwise elements that are superimposed on the blade shell or shear webs, in alignment with the curved blade reference axis. The wind turbine ontology permits the definition of elements in multiple ways, both dimensionally and non dimensionally. The dimensional definition is based on the layer width (arc length), offset, and rotation relative to a reference position. The non-dimensional definition is based on the normalized arc length positions. The coordinate ( $s$ ) of the normalized arc length position is defined as zero at the suction-side trailing edge and as one at the pressure-side trailing edge. These concepts are illustrated in Figure 4.5.

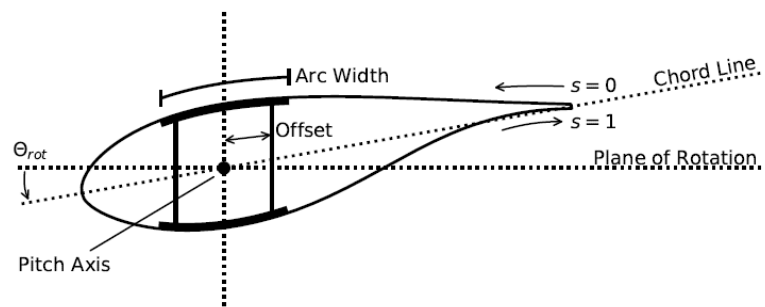


**Figure 4.5:** Schematic of IEA Wind Turbine Ontology composite definition, from root to tip [23].

## 4.2 Model

Once the reference wind turbine is established, the aim of this thesis is to create a model of its blade in order to perform FEM analysis and conduct further optimizations. In this section, the creation of the model is presented. Firstly, the CAD model used is described, followed by the material definition. The blades are made of composite materials, so the material definition involves creating layers that vary along the blade's cross-section and span, both in terms of material plies and thickness. After defining the model, a modal analysis is performed, and the results are compared with reference literature. A structural and buckling analysis is conducted to verify essential requirements such as tip clearance, material damage, and the buckling load multiplier. All steps are performed using "Ansys Mechanical 2024R2" and are automated by writing a PyMechanical script, which is part of the broader PyAnsys initiative, enabling the use of Ansys technologies directly from Python. PyMechanical provides a Python-friendly interface to drive the software, facilitating the use of Mechanical scripting commands.

### 4.2.1 CAD Model

The reference geometry used for the analysis is a CAD model obtained through a script developed at Politecnico di Torino, built using the open-source software for 3D CAD modeling, "Salome". As shown in Figures 4.6 to 4.8, the model is constructed as a shell and divided into several surfaces. This design allows for an efficient definition of the material layup, as described in the next section. In particular, the blade is divided into 49 sections in the direction of the blade span in order to discretize the variable thickness of materials and each sections is divided into other surfaces to define the different layers stackups. Before the analysis, the CAD model is imported into "Ansys SpaceClaim" to unify the topologies, enabling the FEM solver to treat the various surfaces as a single body (a shell, in this case).

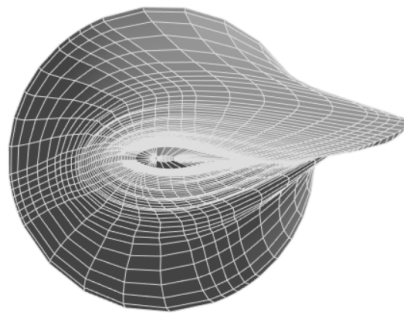


**Figure 4.6:** CAD model - front view.



**Figure 4.7:** CAD model - top view.



**Figure 4.8:** CAD model - side view.

## 4.2.2 Materials

The reference blade selected, as all large wind turbine blades currently used in industry, is composed of fiber composite materials so that a stiff, lightweight design with a high fatigue life is achieved. In the case of 15 MW reference turbine, the fibers which compose the blades are **Carbon UD** with a unidirectional carbon fiber orientation of  $0^\circ$ , **Glass UNI** with a unidirectional glass fiber orientation of  $0^\circ$ , **Glass Biax** with glass fibers orientation of  $+45^\circ$  and  $-45^\circ$  and **Glass Triax** with glass fibers orientation of  $+45^\circ$ ,  $0^\circ$  and  $-45^\circ$ . Plies with  $0^\circ$  fibers are used for resisting bending while plies with  $45^\circ$  fibers are implemented for torsional stiffness and buckling resistance. The material properties used in this study are presented in Table 4.3. In addition to fiber reinforced materials, an homogeneous isotropic core is used. Implementing a core material into a composite layup is a light-weight method to increase buckling resistance. Figure 4.9 offers a visualization of materials used in the blade.

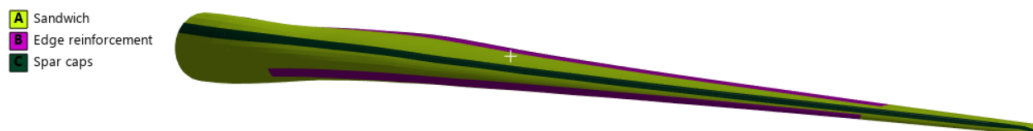


**Figure 4.9:** Blade materials.

Material	Carbon UD	Glass Uni	Glass Biax	Glass Triax
Density (kg/m <sup>3</sup> )	1220	1940	1940	1940
Longitudinal E (MPa)	$1.15 \cdot 10^5$	$4.46 \cdot 10^4$	$1.11 \cdot 10^4$	$2.87 \cdot 10^4$
Transverse E (MPa)	$8.39 \cdot 10^3$	$1.70 \cdot 10^4$	$1.11 \cdot 10^4$	$1.66 \cdot 10^4$
Longitudinal G (MPa)	$5.99 \cdot 10^3$	$3.27 \cdot 10^3$	$1.35 \cdot 10^4$	$8.40 \cdot 10^3$
Transverse G (MPa)	$5.99 \cdot 10^3$	$3.48 \cdot 10^3$	$3.49 \cdot 10^3$	$3.49 \cdot 10^3$
Poisson ratio	0.27	0.262	0.5	0.5
Longitudinal tensile strength (MPa)	1546	609.2	42.9	396
Longitudinal compressive strength (MPa)	1047	474.7	70.7	448.9
Transverse tensile strength (MPa)	46.6	38.1	42.9	76.4
Transverse compressive strength (MPa)	158	112.6	70.7	174.7
Shear strength (MPa)	55	18.9	103.4	103.4
Puck constant I	0.35	0.3	0.3	0.3
Puck constant II	0.25	0.2	0.2	0.2

**Table 4.3:** Fiber reinforced materials properties.

The core material is used for its low weight and high shear modulus which is important for sandwich structures subjected to bending. The core material used is a medium density foam (PVC) and its characteristics are reported in Table 4.4.

Density (kg/m <sup>3</sup> )	E (MPa)	G (MPa)
130	129.2	48.95

**Table 4.4:** Core properties.



### 4.2.3 Layers

Carbon fiber is used in the *spar caps*, the regions of the blade cross section which covers the shear webs. Spar caps help to resist the flapwise load yielding a lower tip deflection, higher buckling resistance, and lighter weight than an all glass layup. Triaxial Glass fiber is used for shell skin, both outer and inner, while the Unidirectional Glass fiber is only used as leading and trailing edge reinforcement, helping to counteract the edgewise moment. Biaxial Glass fiber is used as shear webs skin. The core is used as a filler for the remaining shell panel and for the shear webs. In Figures 4.10 to 4.14 are shown five different blade cross sections and their relative material definition.

- Carbon UD
- Glass UNI
- Glass Biax
- Glass Triax
- Medium density foam

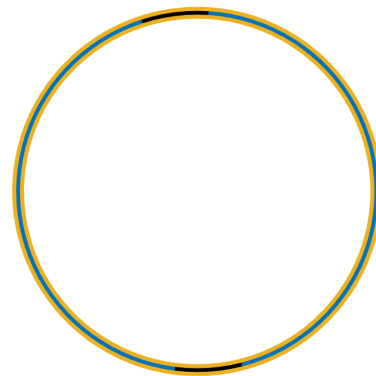


Figure 4.10: Section 0%

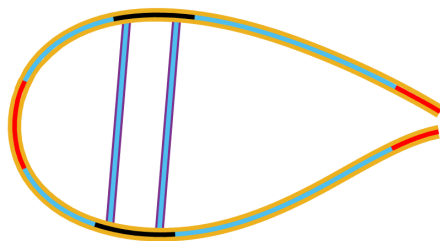


Figure 4.11: Section 25%

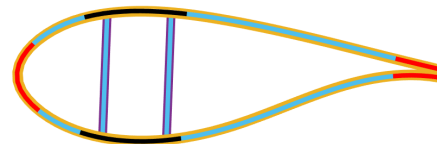


Figure 4.12: Section 50%

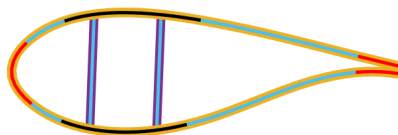
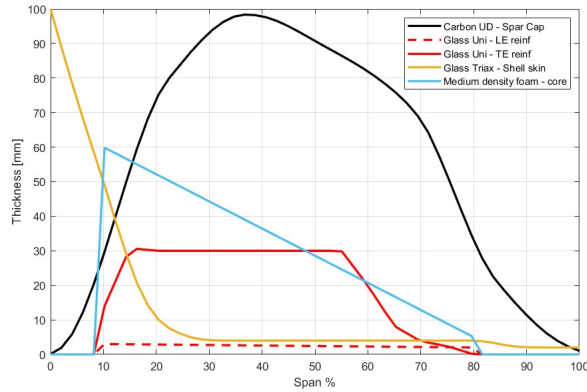


Figure 4.13: Section 75%



Figure 4.14: Section 100%

Once each regions of the blade is assigned to its specific laminate, the variable thickness along the blade span must be set. Figure 4.15 shows the thickness of each material along the blade span.



**Figure 4.15:** Material thickness along blade span (shell).

In the same way, Figure 4.16 shows the thickness of materials which compose both the shear webs along the blade span.

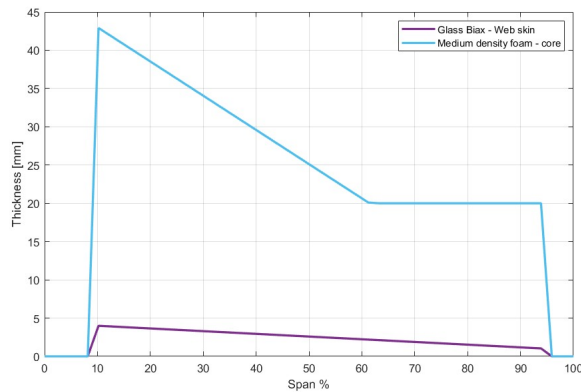


**Figure 4.16:** Material thickness along blade span (shear web).

In the FEM model, the layers are defined using the *Layered section* feature of Ansys Mechanical. It only allows to assign a discrete value of thickness, so it is not possible to assign a continuous distribution of thickness. To override this limit, the blade was discretized into 49 sections and each one was assigned a discrete value of thickness for each material. These discretized thickness values was extrapolated from files of the reference turbine available online on GitHub, and the results are

reported in Figures 4.17 to 4.21 for each region of the blade. Each regions is defined with the same thickness both in suction and pressure side so it is reported only once. Also the shear webs are identical so only one diagram is presented.

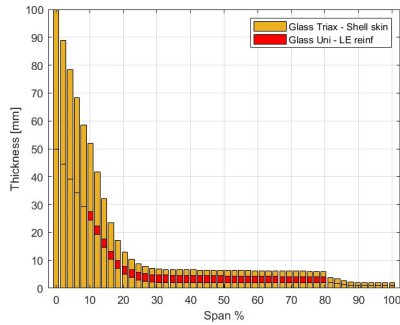


**Figure 4.17:** Leading edge reinforcement.

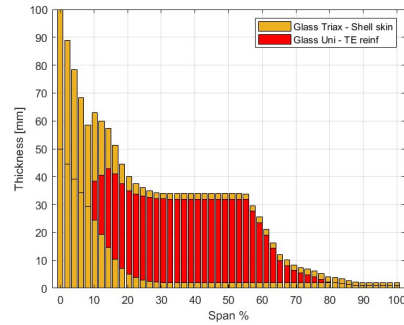


**Figure 4.18:** Trailing edge reinforcement.

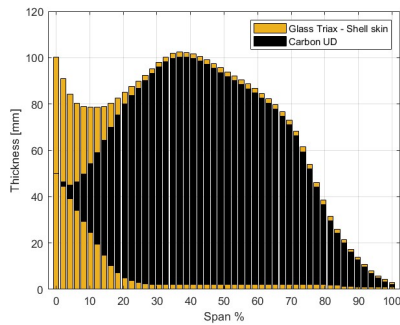


**Figure 4.19:** Spar cap.

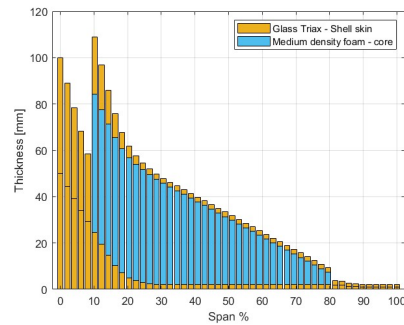


**Figure 4.20:** Panels.

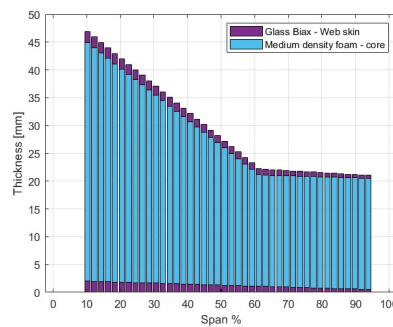


**Figure 4.21:** Shear web.

Figures 4.22 and 4.23 offer an overview of the thickness distribution of blade materials.

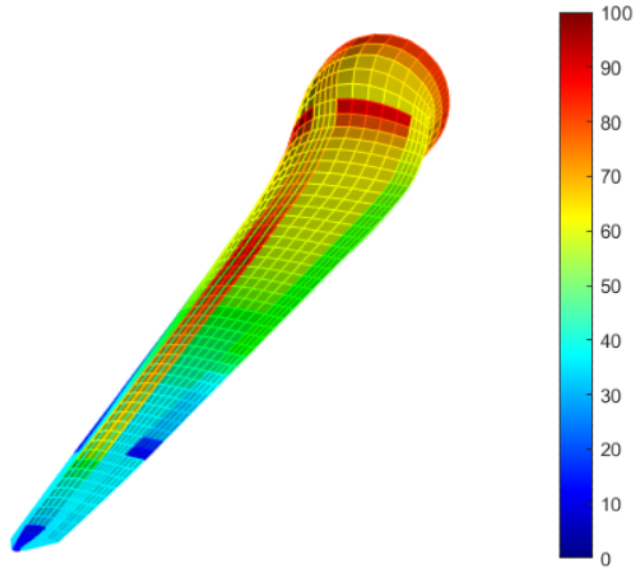


**Figure 4.22:** Thickness plot - trailing edge view (mm).

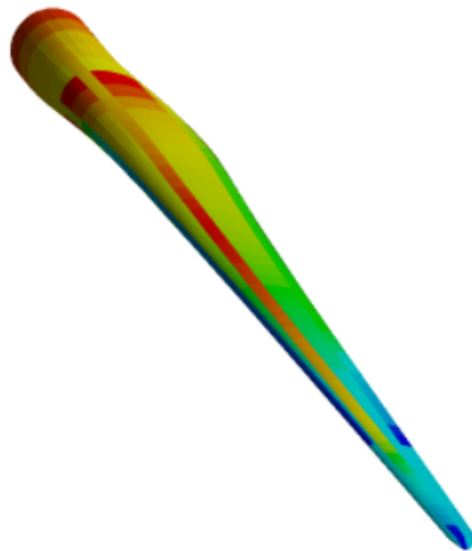


**Figure 4.23:** Thickness plot - leading edge view (mm).

#### 4.2.4 Puck failure criteria

In this paragraph, a brief overview of the Puck failure criteria is given, as it is used in this work for the strength analysis of the blade. The Puck failure criteria is one of the most widely used criteria to analyze the strength of laminate composites and it was first developed for unidirectional laminate composites materials [24]. It distinguishes two type of failures: **fiber failure (FF)** and **inter fiber failure (IFF)**. For fiber failure, Puck's criterion is expressed as follows:

$$f_{E(FF)}^T = \frac{\sigma_1}{X_T} = 1$$

$$f_{E(FF)}^C = \frac{\sigma_1}{X_C} = 1$$

where  $f_{E(FF)}^T$  and  $f_{E(FF)}^C$  are the *failure exposure*, in the case of tension and compression respectively, which indicate the initiation of failure once they reach the value of 1.  $\sigma_1$  is the stress value in the fiber direction and  $X_T$ ,  $X_C$  are tensile and compressive strengths in fiber direction, respectively.

For inter fiber failure, Puck criterion consider three failure mode:

- **IFF Mode A**, caused by tensile and shear stresses;
- **IFF Mode B**, caused by compressive and shear stresses;
- **IFF Mode C**, a dangerous failure mode in compressive shearing which may lead to ultimate failure.

Puck failure criteria for inter fiber failure are expressed as follows:

$$f_{E(IFF)}^A = \left[ \left( \frac{\sigma_6}{S} \right)^2 + \left( 1 - p_{\perp II}^{(+)} \frac{Y_T}{S} \right)^2 \left( \frac{\sigma_2}{Y_T} \right)^2 \right]^{1/2} + p_{\perp I}^{(+)} \frac{\sigma_2}{S} = 1$$

$$f_{E(IFF)}^B = \frac{1}{S} \left\{ \left[ (\sigma_6)^2 + (p_{\perp II}^{(-)} \sigma_2)^2 \right]^{1/2} + p_{\perp II}^{(-)} \sigma_2 \right\} = 1$$

$$f_{E(IFF)}^C = \left[ \left( \frac{\sigma_6}{2(1 + p_{\perp}^{(-)}) S} \right)^2 + \left( \frac{\sigma_2}{Y_C} \right)^2 \right] \frac{Y_C}{(-\sigma_2)} = 1$$

In the equations above  $p_{\perp I}^{(+)}$ ,  $p_{\perp II}^{(-)}$  and  $p_{\perp}^{(-)}$  are the *Puck constants* and represent inclination parameters that control the shape of the failure envelope.  $\sigma_2$  is the stress value in the transverse fiber direction,  $Y_T$  and  $Y_C$  are tensile and compressive strengths in the transverse fiber direction. Shear stress and shear strength are represented by  $\sigma_6$  and  $S$ , respectively.

### 4.3 Modal analysis

The blades of offshore wind turbines are exposed to significant wind forces throughout their operating life. The wind turbine blade is under a coupled process of forces, so when the natural frequency for the blade and the excitation forces are the same, resonance occurs. This makes the modal analysis of the blade of great importance, hence the scope of the present section, which deals with determining the natural mode shapes and frequencies of the reference blade.

Modal analysis allows to determine the natural frequencies and mode shapes of a system and it is based on the solution of an eigenvalue problem of a linear system of type

$$(K - \omega^2 M) \cdot \phi = 0$$

where  $K$  is the *stiffness matrix* and  $M$  is the *mass matrix* while  $\omega$  is the eigenvalue which represents the *natural frequency* and  $\phi$  is the eigenvector which represents the *mode shape*. The calculated natural frequencies are reported in Table 4.5.

Mode	Frequency (Hz)	Description
1	0.54	1st Flapwise
2	0.70	1st Edgewise
3	1.63	2nd Flapwise
4	2.30	2nd Edgewise

**Table 4.5:** Natural frequencies.

In Figures 4.24 to 4.27 are shown the first 4 mode shapes, in terms of displacements.

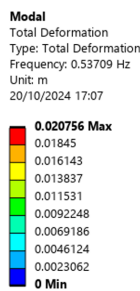


**Figure 4.24:** 1st Flapwise.

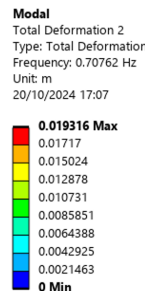


**Figure 4.25:** 1st Edgewise.

**Modal**  
 Total Deformation 3  
 Type: Total Deformation  
 Frequency: 1.6331 Hz  
 Unit: m  
 20/10/2024 17:08

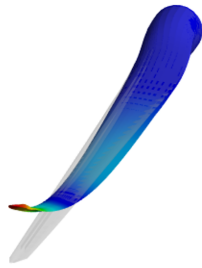
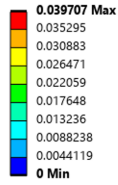


Figure 4.26: 2nd Flapwise.

**Modal**  
 Total Deformation 4  
 Type: Total Deformation  
 Frequency: 2.2946 Hz  
 Unit: m  
 20/10/2024 17:08

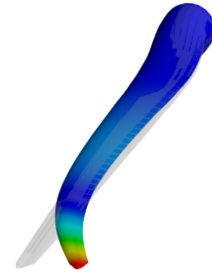
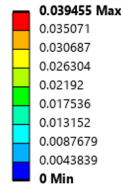


Figure 4.27: 2nd Edgewise.

These results are well in accordance with reference literature [25]. As shown in Figure 4.28 the first natural frequencies are well computed and the maximum error of 9% occurs only from the fourth natural frequency, probably due to some differences in the FEM model, such as the material definition, and the different solver.

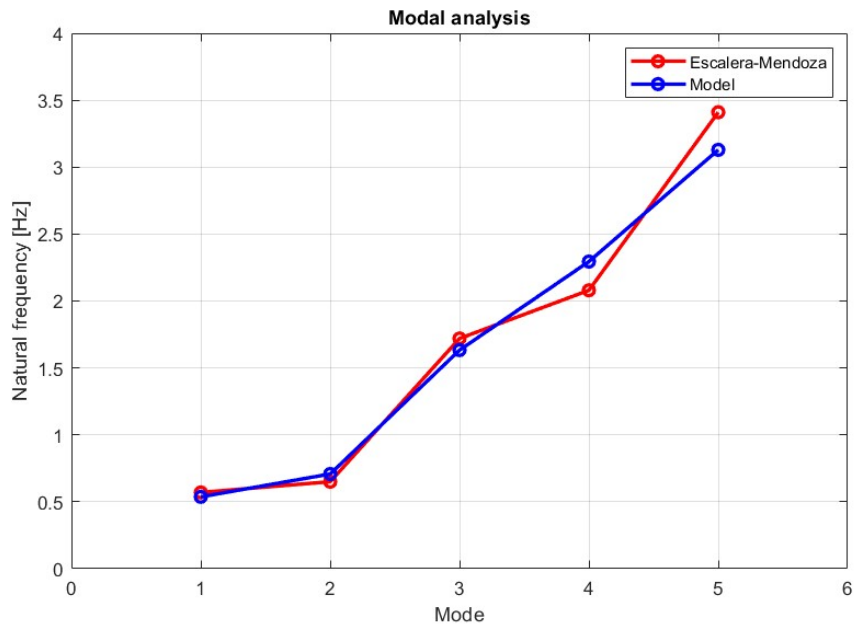


Figure 4.28: Modal analysis - comparison with literature.

## 4.4 Static structural analysis

This section presents the results of several static structural analysis conducted on the developed blade model. It begins with a brief description of the static loads applied to simulate the blade's structural behavior. The results of the analysis are then presented, focusing on maximum displacements to ensure compliance with tip clearance requirements. Subsequently, reaction forces at the blade root are calculated, along with a strength analysis using the Puck criteria. Finally, the results of the buckling analysis are included, along with the calculation of the buckling load multiplier.

### 4.4.1 Loads

Static loads include aerodynamic, gravitational and inertial forces due to the rotor's rotational velocity. Aerodynamic loads are calculated using a Matlab code that implements the *Blade Element Momentum theory (BEM)*. The Blade Element Momentum Theory (BEM) is a combination of the *Momentum Theory* and the *Blade Element Theory*. The momentum theory refers to a control conservation of momentum, while the blade element theory refers to a force analysis of a blade section as function of the incoming flow and the blade geometry. In the BEM theory, the forces of the blade element method are related to the momentum change of the momentum theory. This allows calculations of the performance characteristics per annular section of the rotor. The Matlab code computes, through an iterative process, the normal and the tangential pressure on a line [ $N/m$ ] (without considering the chordwise dimension of the blade) along the blade span, whose expressions are

$$p_n = \frac{1}{2} \cdot \rho \cdot C_n \cdot c \cdot V_{rel}^2$$

$$p_t = \frac{1}{2} \cdot \rho \cdot C_t \cdot c \cdot V_{rel}^2$$

where  $\rho$  is the air density [ $kg/m^3$ ],  $C_n$  and  $C_t$  are the normal and the tangential force coefficient derived from the lift and drag coefficient of the airfoil, following the expressions

$$C_n = C_l \cos(\phi) + C_d \sin(\phi)$$

$$C_t = C_l \sin(\phi) - C_d \cos(\phi)$$

where  $\phi$  is the angle between the vector of the velocity relative to the blades  $V_{rel}$  and the plane of the rotor rotation.  $V_{rel}$  is a combination of the wind speed axial and tangential components and the induction factor. Expressions of  $V_{rel}$  under



several hypothesis can be found in [15]. Giving the Matlab code the steady states working conditions of the 15 MW IEA wind turbine in input, namely the value nominal value of rotor speed and blade pitch for each value of wind speed, it is possible to compute the line normal and tangential pressure [ $N/m$ ], as shown in Figures 4.29 and 4.30.

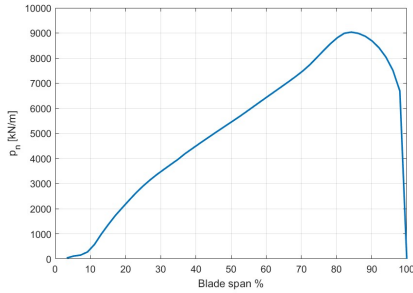


**Figure 4.29:** Normal pressure.

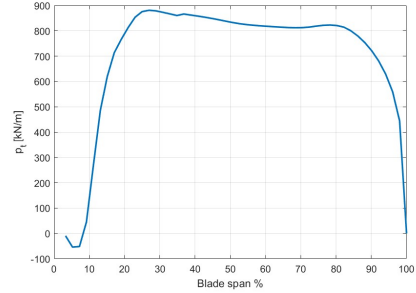


**Figure 4.30:** Tangential pressure.

By integrating normal and tangential pressure along the blade span it is possible to obtain the total thrust and the tangential force, responsible for the rotor torque. The load is implemented in the FEM model by applying remote forces at the 49 sections in which the CAD model is divided. Each remote force is obtained by dividing the pressure value at that point of the blade span and the width of the section on which the force is applied. The remote forces applied to the model (in the direction of thrust X and in the tangential direction Y) are shown as bar graphs in Figures 4.31 and 4.32.

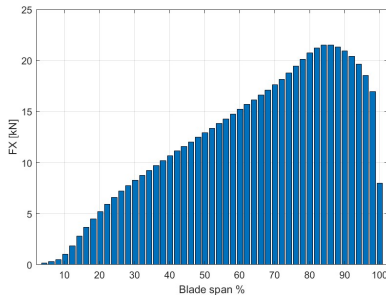


**Figure 4.31:** FX.

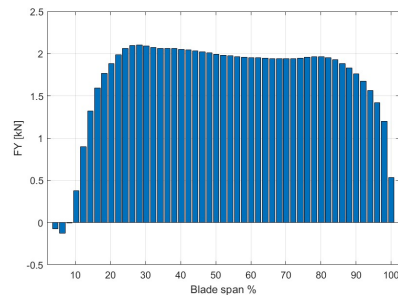


**Figure 4.32:** FY.

To simulate the gravitational load, an acceleration of  $g$  is applied to the model, and a rotational velocity is applied to introduce the centrifugal force. A fixed support is applied to the root of the blade to simulate the link to the hub of the wind turbine.

## Operating condition

In operating conditions, the turbine is expected to face wind speed between 3 to 25  $m/s$ . In this work, only static load are considered, and for the analysis, 7 load cases have been considered. The operating conditions of the load cases selected are reported in Table 4.6.

LC	Wind speed (m/s)	Rotor speed (rpm)	Blade pitch (deg)	Thrust (kN)	Power (MW)
1	3.00	5.00	3.71	230	0.08
2	7.00	5.10	0.024	1130	4.54
3	10.00	7.25	2.98	1840	12.06
4	11.50	7.25	5.10	1806	15
5	16.00	7.25	13.34	1171	15
6	20.50	7.25	18.36	924	15
7	25.00	7.25	23.63	790	15

**Table 4.6:** Operating condition of the 7 load cases selected.

The force distribution in the seven cases taken into consideration are reported in the following Figures.

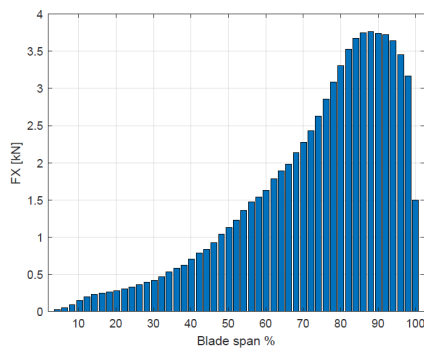


**Figure 4.33:** FX (case 1).

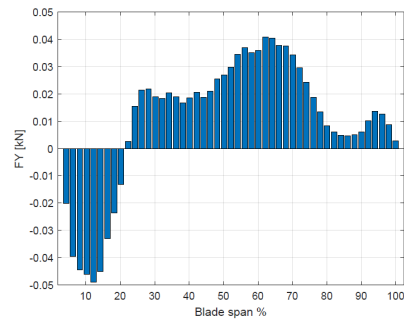


**Figure 4.34:** FY (case 1).

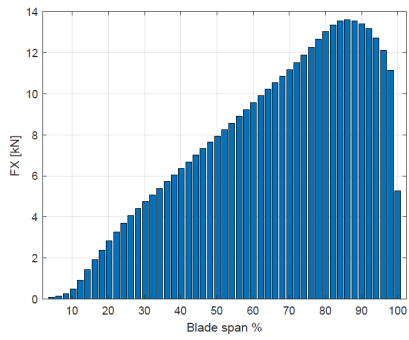


Figure 4.35: FX (case 2).

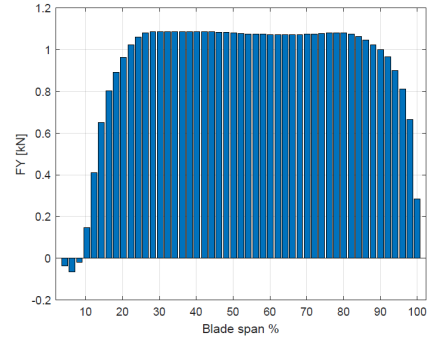


Figure 4.36: FY (case 2).

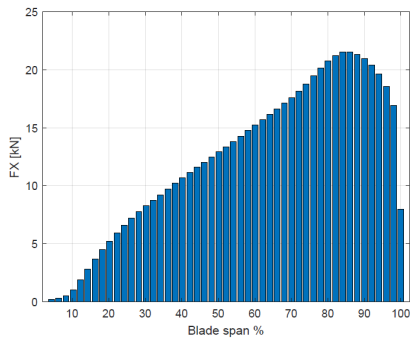


Figure 4.37: FX (case 3).

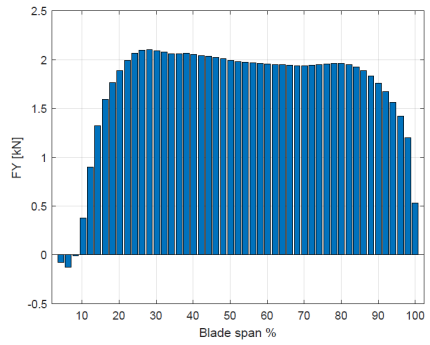


Figure 4.38: FY (case 3).

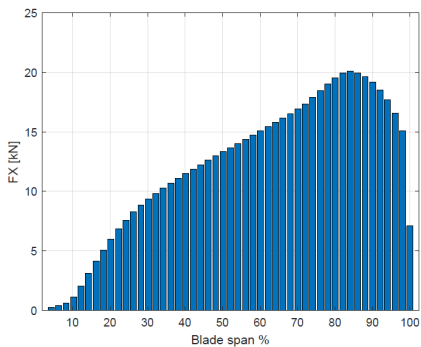


Figure 4.39: FX (case 4).

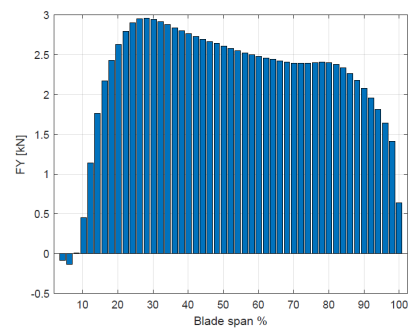


Figure 4.40: FY (case 4).

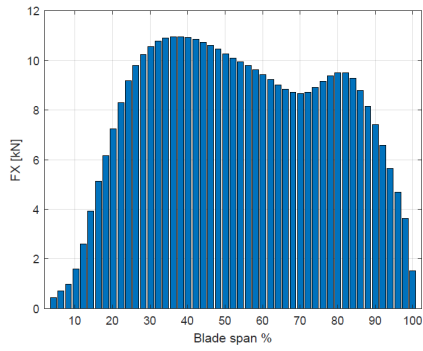


Figure 4.41: FX (case 5).

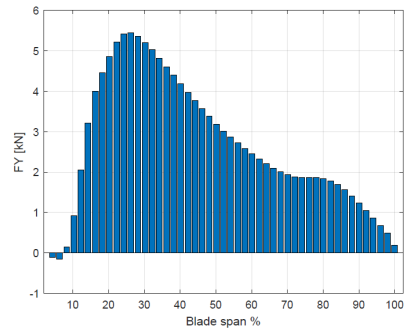


Figure 4.42: FY (case 5).

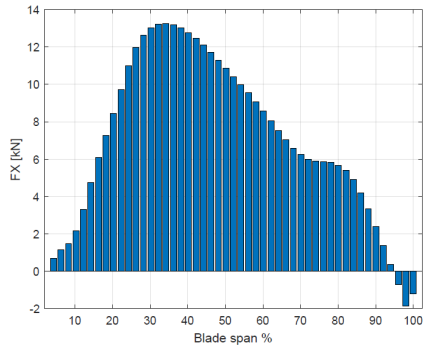


Figure 4.43: FX (case 6).

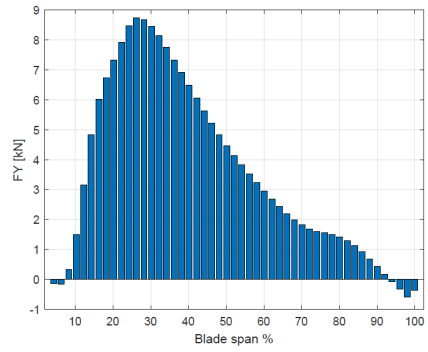


Figure 4.44: FY (case 6).

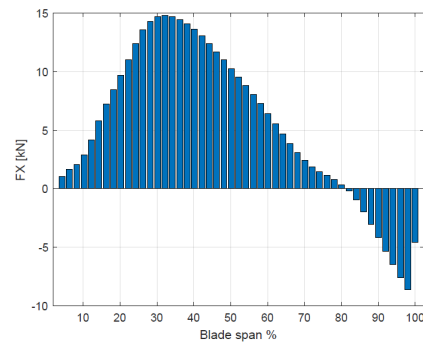


Figure 4.45: FX (case 7).

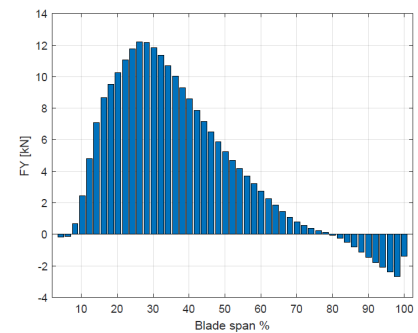
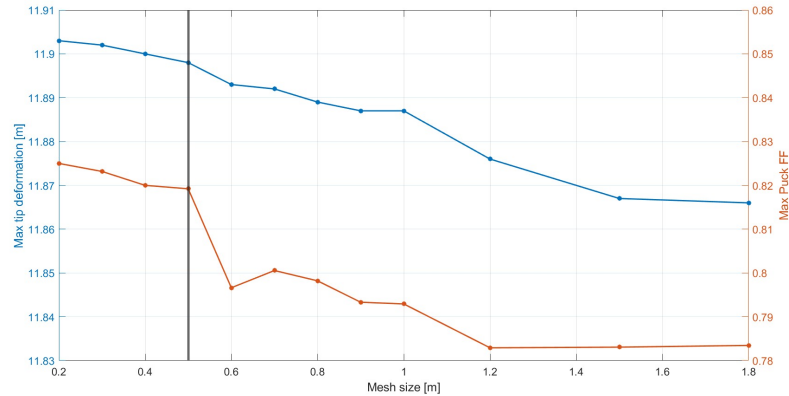


Figure 4.46: FY (case 7).

## Mesh convergence

The element size selected for the analysis is 0.4 m, the choice following a mesh convergence analysis considering maximum tip displacement and maximum Puck failure index. Evidence of the mesh convergence analysis are reported in Figure 4.47.



**Figure 4.47:** Mesh convergence.

The results show that the convergence occur also with larger element order but under 0.5 m the oscillations seem to stabilize.

## 4.4.2 Results

In this paragraph, the results of the static structural analysis are presented. Three main output are checked: tip deflection, root reaction forces and strength analysis. Buckling load multiplier are analyzed.

### Tip deflection

According to *IEC International Standards*, in normal operating conditions the tip deflection must to be checked in order to verify that it respects the 30% of tower clearance requirement. Once the tower clearance is calculated, the analysis must ensure that the maximum tip deflection guarantees a tower clearance of almost 30%. The calculation of tower clearance is taken from [25]. Useful data are listed in Table 4.7. Negative values indicate upwind distances.

Data	Symbol	Value
Hub height	$H_H$	150 m
Rotor radius	$R$	120 m
Blade precone	$C$	$-4^\circ$
Shaft uptilt	$U$	$-6^\circ$
Blade pre-bend	$A_{Pb}$	$-1.91^\circ$
Overhang	$O$	-11.08 m
Reference tower radius	$T_r$	4.99 m

**Table 4.7:** Data for tower clearance calculation.

Reference tower radius  $T_r$  is the tower radius at the *height of undeflected blade tip*  $H_{ubt}$ , which can be calculated as follows

$$H_{ubt} = H_H - R * \cos(C + U + A_{Pb}).$$

The *blade tip clearance from tower axis*  $TC_{axis}$  can be calculated as

$$TC_a = O * \cos(U) + R * \sin(C + U + A_{Pb})$$

and so, the *blade tip clearance from tower*  $TC$  is easily calculated as

$$TC = TC_{axis} + T_r.$$

Results of the calculations are reported in Table 4.8.

Height of undeflected blade tip	m	32.58
Blade tip clearance from tower axis	m	-35.78
Tower radius at height of undeflected blade tip	m	4.99
Blade tip clearance from tower	m	-30.79
Admissible deflection ( 30% tower clearance)	m	-21.56

**Table 4.8:** Tower clearance.

Figure 4.48 shows the maximum tip deflection in the direction of the axis rotor, obtained from the simulations of the 7 load cases.

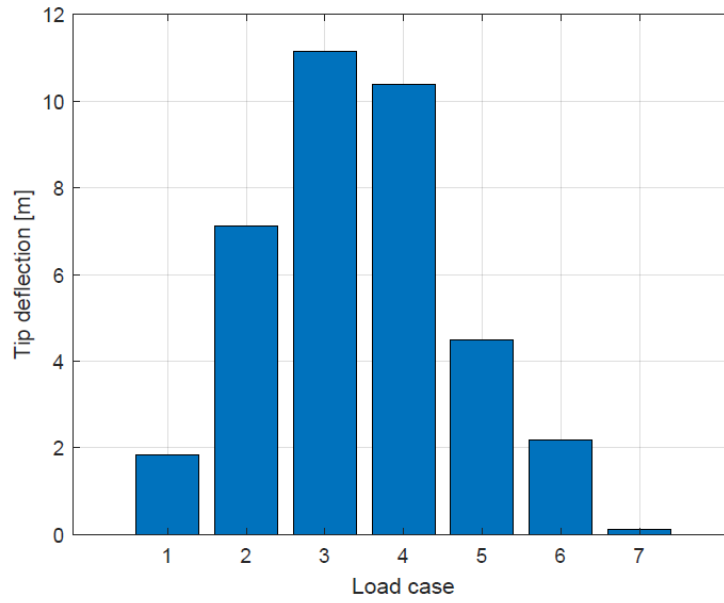


Figure 4.48: Tip deflection.

It is evident that the critical load case is the third, which coincides with the case of maximum thrust. The deformed shape in load case 3 is reported in Figure 4.49.

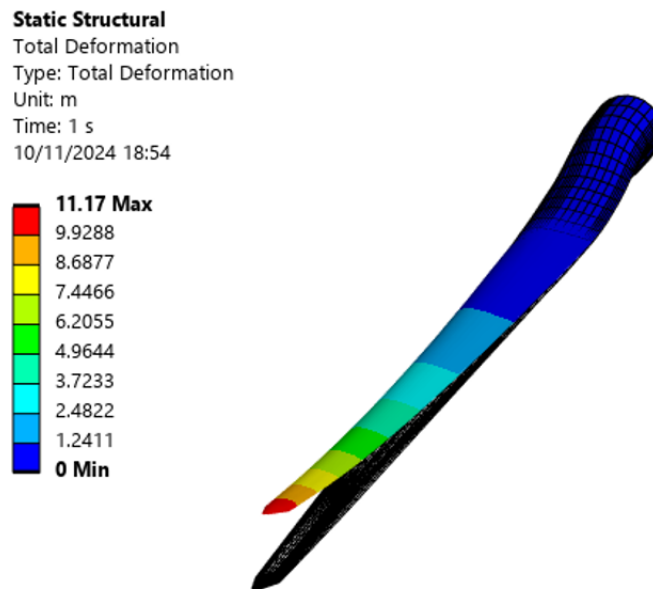
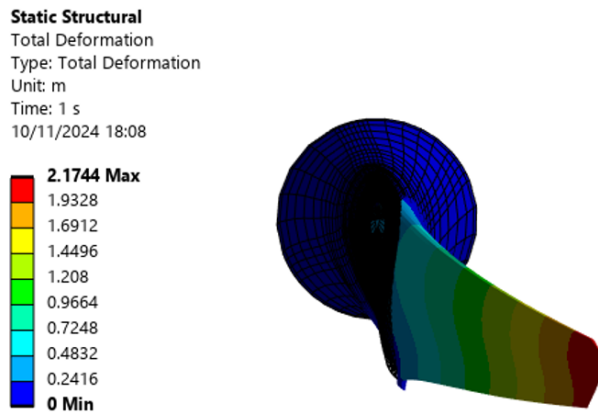
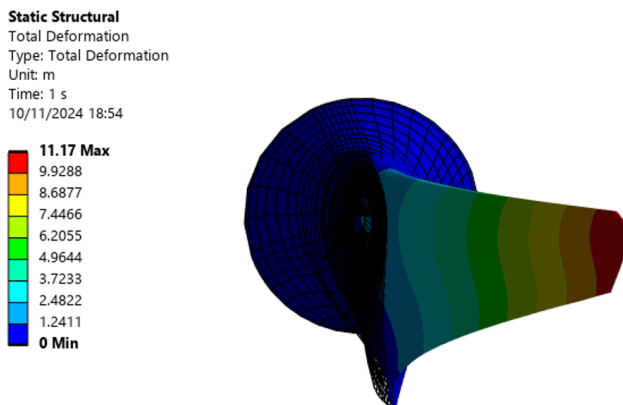


Figure 4.49: Deformed shape (load case 3).

Further from the critical case, thrust decreases and so the the maximum tip deflection in the direction of the tower. In load cases 1 and 7, aerodynamic forces are so small, due to the low wind speed and the high pitch angle respectively, that the maximum displacement is in the direction of the ground due to gravity. Figure 4.50 show the front view of the deformed shape in the load case 1, while 4.51 shows the front view of the deformed shape in load case 3.



**Figure 4.50:** Tip deflection load case 1 (front view).



**Figure 4.51:** Tip deflection load case 3 (front view).

In all the static load cases simulated, the maximum tip deflection respects the tower tip clearance requirement.



### Root reaction forces

In Figures 4.52 to 4.54 reaction forces at blade root are reported.

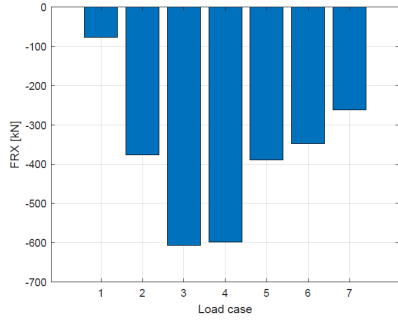


**Figure 4.52: FRX.**

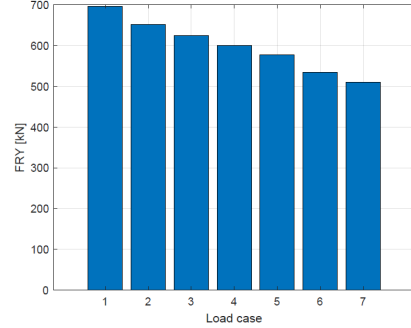


**Figure 4.53: FRY.**

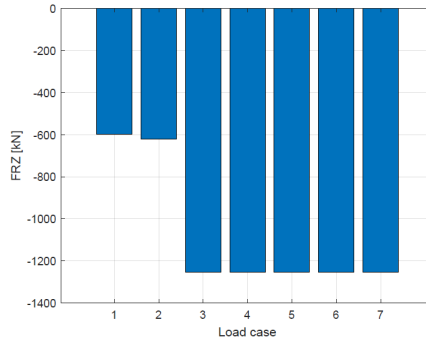


**Figure 4.54: FRZ**

Figures 4.55 and 4.56 show the reaction moments at the blade root.

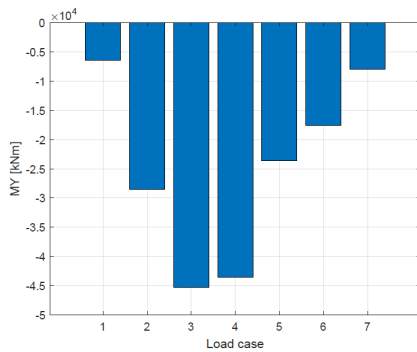


**Figure 4.55: Flapwise (MY).**

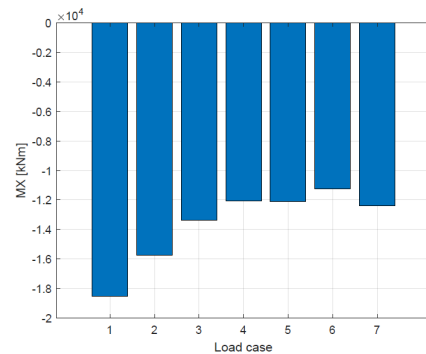


**Figure 4.56: Edgewise (MX).**

## Strength analysis

To verify the blade strength, Puck's criterion is used. As stated in the previous sections, the most critical load case is load case 3, so firstly Figure 4.57 shows an overview of the blade stress condition in load case 3, using an equivalent stress (Von Mises).

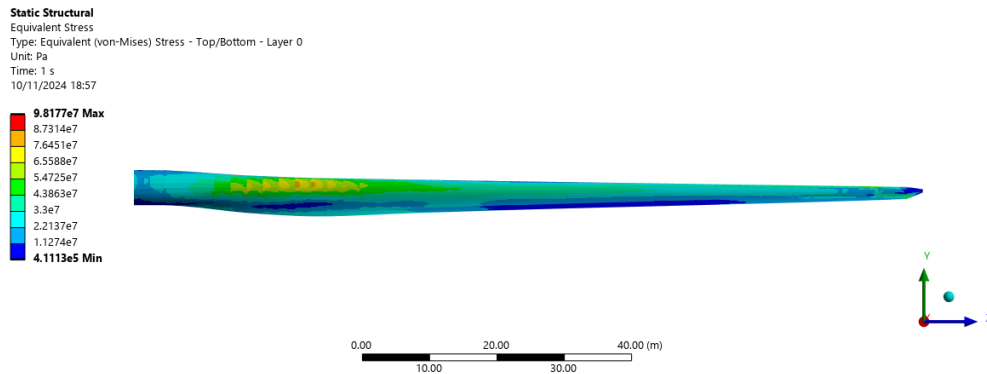


**Figure 4.57:** Equivalent (Von Mises) stress in load case 3.

The most stressed blade region is the leading edge corresponding to the maximum chord region. However, this zone of triaxial fiberglass reinforced with a middle layer of uniaxial fiberglass does not undergo significant damage, as stated by Puck failure indices in Figure 4.58, for tensile fiber failure.

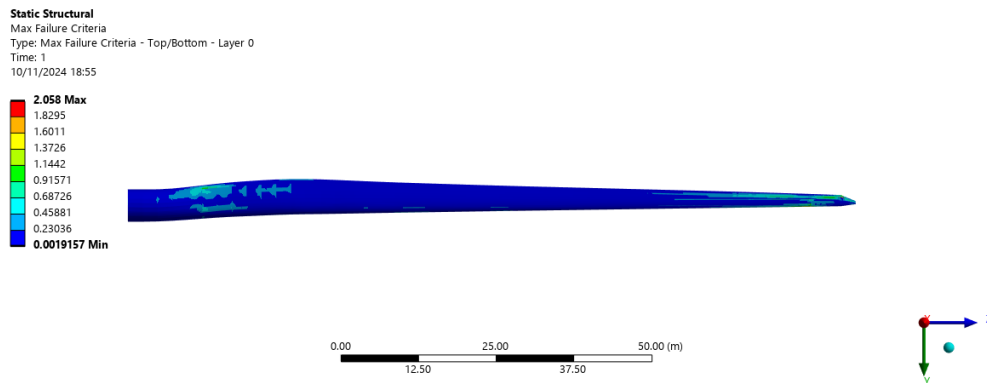


**Figure 4.58:** Puck's failure indices (tensile fiber failure).

In the most stressed region, the Puck failure index is less than 1, this indicating that damage is not occurring in the region. Puck's failure indexes plot show a globally acceptable structural behavior of the blade. However, in some load cases,

the maximum Puck failure index is greater than 1, as reported in Table 4.9.

Load case	Max Puck's Failure Index
1	0.36999
2	1.3358
3	2.058
4	1.8463
5	0.81721
6	0.5082
7	1.802

**Table 4.9:** Maximum Puck's failure index.

Results of Puck failure indices indicate that with this configuration, damage occur in the blade. For all load cases simulated, damage occurs at tip, as shown in Figure 4.59.

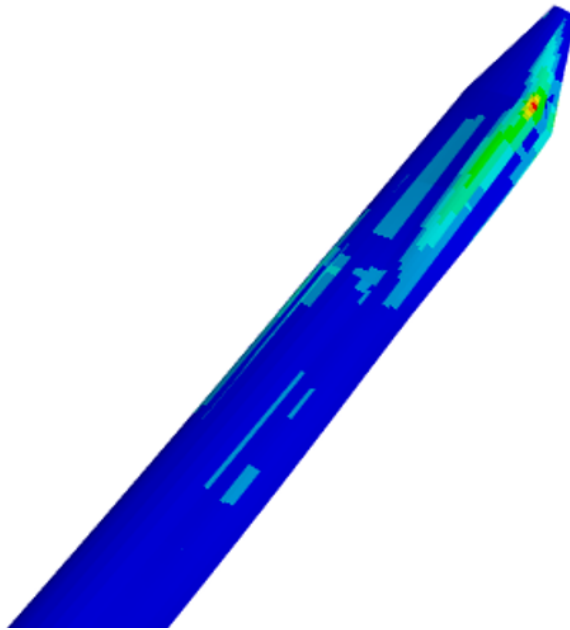


**Figure 4.59:** Tip damage (load case 3).

Puck criterion analysis showed that in several load cases, the tip region is subjected to structural damage. The damage is similar in each load case in which the maximum Puck failure index reaches the value of 1, this indicating a structural modify of the tip region is needed and it is reported in the next section.

## Buckling

The purpose of a buckling analysis is to predict the maximum load a structure can support prior to instability or collapse. Similarly to modal analysis, it is based on the solution of an eigenvalue problem of a linear system of type

$$(K - \omega^2 K_s) \cdot \phi = 0$$

where  $K$  is the *stiffness matrix* and  $K_s$  is the *tension matrix*, dependent from the load. The eigenvalue  $\omega$  represents the *load multiplier*, the ratio between the buckling load and the applied load. By multiplying the applied load and the load multiplier, the buckling load can be obtained. It is evident that if the load multiplier is less than 1, buckling has occurred with the current load. The eigenvectors  $\phi$  represent the *buckling mode shape*. With the original blade configuration, buckling occurs too soon in all the load cases, except for load case 1, as stated in Table 4.10.

Load case	Load Multiplier	Buckling occurs at
1	$10^{-3}$	Tip
2	$10^{-2}$	Tip
3	$10^{-2}$	Tip
4	$10^{-2}$	Tip
5	0.26	Tip
6	0.65	Tip
7	$10^{-4}$	Tip

**Table 4.10:** Buckling analysis results.

The buckling analysis confirms that the original blade structure configuration is not adapted to carry the static load cases. In fact, buckling occurs too soon at tip (Figure 4.60) which is confirmed to be structurally not adapted.

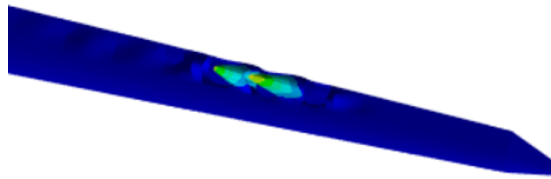


**Figure 4.60:** Buckling occurring at blade tip.

In the next section, a modified version of the blade is analyzed and verified.

## 4.5 Modified 15 MW IEA Wind Turbine

Results of the analysis on the original 15 MW IEA Wind Turbine, with the model built in this thesis, show that the structure is not adequate to support the static load cases simulated. In this section, a modified version of the same blade is built and the same analysis are repeated on the new blade version. With the update structure, the blade results adequate to support the loads. However, the changes made on the blade structure are conservative and thus lead too an unnecessary high increase in mass and cost of materials for the blade. Following this issue, an optimization process, aiming to minimize the blade mass, is presented in the next chapter.

### 4.5.1 Modified blade structure

Given the unsatisfactory results of analysis of the previous section and following the considerations taken in [26], a modified version of the reference wind turbine blade is built. Some of the key characteristics of the update model are:

- same geometry of the 15 MW IEA wind turbine;
- same geometry and location for shear webs;
- same material layup (same division in trailing edge, spar cap and leading edge);
- all layers thickness doubled except for unidirectional carbon fibers layers (spar caps);
- carbon layer width augmented in the tip region.

An optimization process is necessary to mitigate the mass increase following the structure updates.

### 4.5.2 Analysis results

Considering the update model, the analysis of the previous section are repeated. Reaction forces remain unchanged so only tip deflection, strength and buckling results are presented.

## Tip deflection

Figure 4.61 shows results for the tip displacement in the direction of the tower. They are in accordance with the original model but the maximum tip displacement is reduced of 10%, being well under the clearance limit.

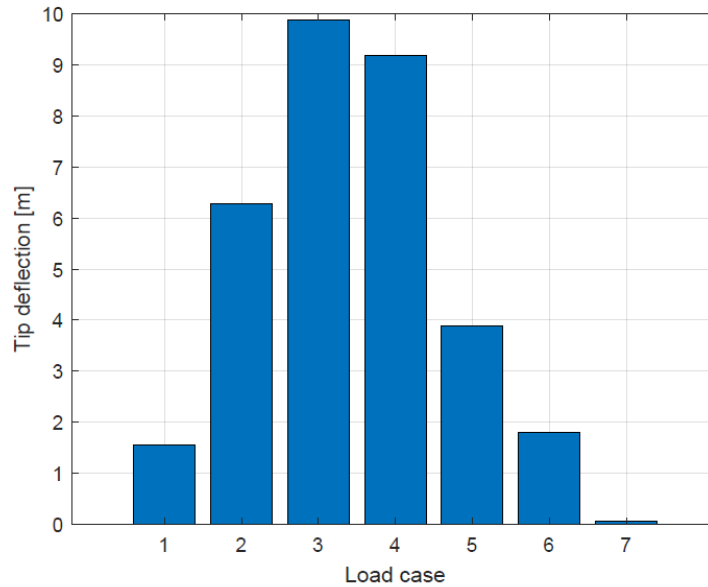


Figure 4.61: Tip deflection.

The deformed shape in the load case 3 is reported in Figure 4.62.

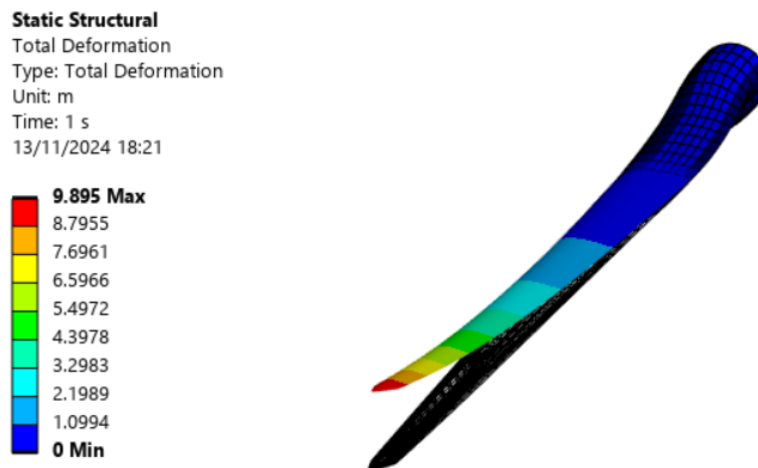


Figure 4.62: Deformed shape load case 3.

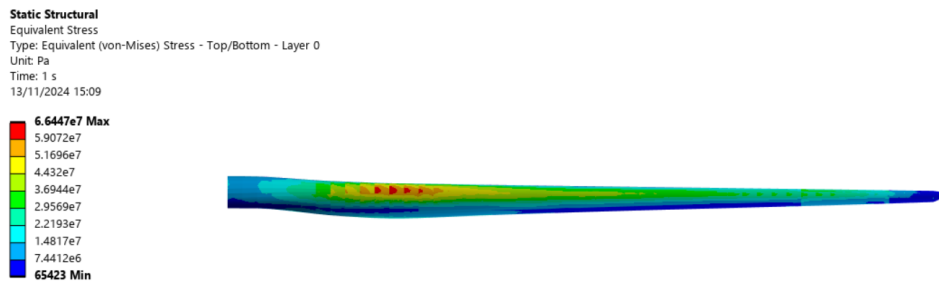
## Strength analysis

Table 4.11 shows the maximum Puck's failure indices for the 7 load cases, considering *Fiber Tensile (FT)*, *Fiber Compression (FC)*, *Matrix Tensile (MT)* and *Matrix Compression (MC)* as possible failure. Considering the modified version of the blade it is evident that the blade materials are not subjected to damage (all the failure indices are below 1).

LC	FT	FC	MT	MC
1	0.10765	0.04279	0.17620	0.09336
2	0.33664	0.14087	0.40287	0.20862
3	0.52075	0.22892	0.60007	0.21742
4	0.49254	0.21598	0.56523	0.29803
5	0.25732	0.09160	0.30086	0.14353
6	0.17492	0.04658	0.20551	0.10843
7	0.10769	0.05906	0.18578	0.13386

**Table 4.11:** Maximum Puck's Failure Index.

The most stressed load case remains load case 3, which is characterized by the highest thrust force. Figure 4.63 shows the equivalent Von Mises stress, which confirms that the most stressed region of the blade is near the leading edge in the region of the maximum chord.



**Figure 4.63:** Equivalent Stress (Von Mises): load case 3.

Figures 4.64 and 4.65 show the maximum Puck failure index plot on the blade.



Figure 4.64: Maximum Puck's failure index - left view.

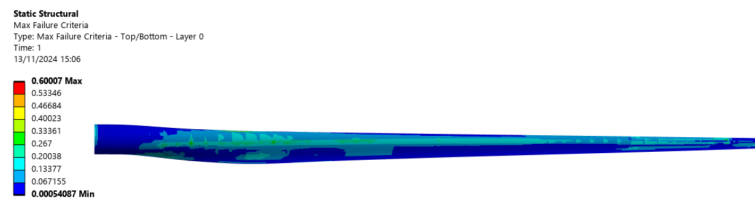


Figure 4.65: Maximum Puck's failure index - right view.

Table 4.11 shows that the most critical possible damage are fiber and tensile failure mechanisms. A plot of the failure indices on the blade referred to these possible damages are reported in Figures 4.66 and 4.67.

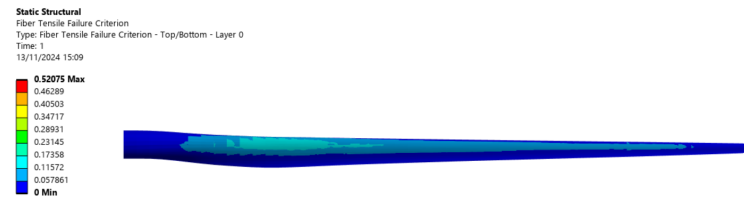


Figure 4.66: Maximum Puck's failure index - Fiber Tensile.

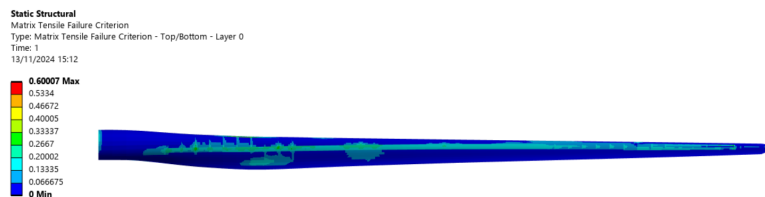
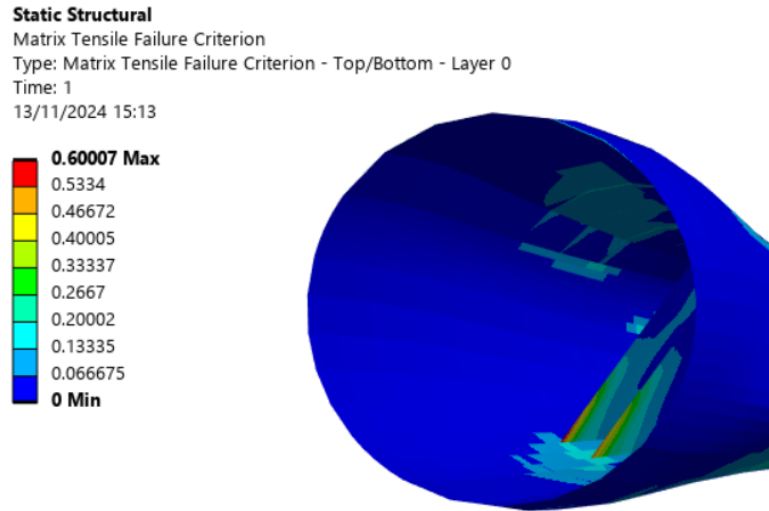


Figure 4.67: Maximum Puck's failure index - Matrix Tensile.

In the end, some details of the shear webs are shown. Figure 4.68 shows that the maximum Puck's failure index occurs at the shear web root, as a result of stress



concentration due to a rough geometry change. This suggests a possible geometry variation, which is not the objective of this study.



**Figure 4.68:** Maximum Puck's failure index - Shear Web.

Figures 4.69 and 4.70 show the shear web Puck's failure indices considering the fiber tensile and compression criterion, respectively.

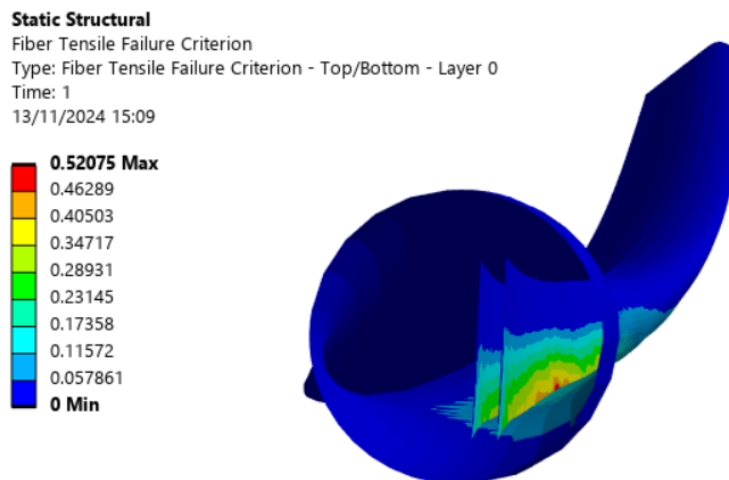


**Figure 4.69:** Maximum Puck's failure index - Shear Web tensile.

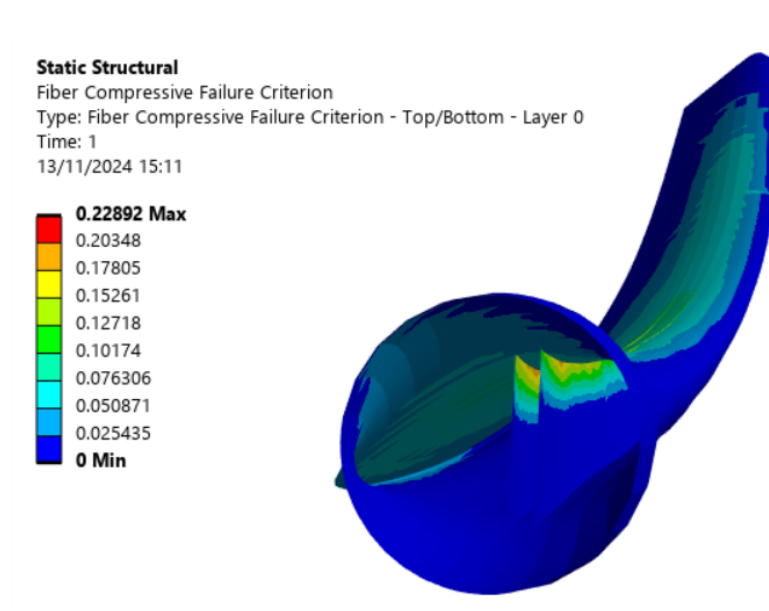


**Figure 4.70:** Maximum Puck's failure index - Shear Web compression.

### Buckling

Modifying the blade has also lead to a safe buckling analysis, as demonstrated by Table 4.12 which shows that all the load multiplier for the first buckling mode are higher than 1.

Load case	Load Multiplier
1	3.4231
2	2.1213
3	1.1591
4	1.4764
5	5.7854
6	4.7777
7	1.8478

**Table 4.12:** Buckling analysis results

## Chapter 5

# Structural optimization

Using the 15 MW IEA reference wind turbine PyMechanical model described in the previous chapter, it is possible to conduct further analysis. In particular, in this chapter, a first attempt of structural optimization is presented. Introducing some simplifying hypotheses, the mass of the blade is reduced, which involves a reduction in material needs and costs.

### 5.1 Literature review

Several works which aim to a structural optimization of a composite turbine blade are available in literature. According to [27], a wide range of optimization algorithms have been used for wind turbine structural optimization, from *linear* and *quadratic programming*, *Lagrangian relaxation* and *heuristic optimization*. The main differences is that the *genetic algorithms* are less sensitive to local minima but they are highly time consuming, the *gradient based methods* are easier to implement and faster but they are not as accurate as genetic algorithms. Several references can be found in [27], the most interesting are reported in the following lines.

[28] is an important example for this work, since authors utilize a similar approach in modeling the wind turbine blade. They conduct a coupled aerodynamic and structural optimization using the *Globally Convergent Method of Moving Asymptotes (GCMMA)*. Their reference wind turbine blade is a 122 meters long composite blade designed for a 20 MW offshore horizontal axis wind turbine.

In [29], authors perform a coupled aero-structural optimization of a 10 MW wind turbine blade dividing the optimization problem in several steps. For the structural optimization they use an algorithm base on the *Sequential Quadratic Programming* method.

In [30] authors report a structural optimization process of a composite horizontal axis wind turbine blade. Even though the reference turbine is a 2 MW, with a

40 meters blade, the paper is interesting because presents an optimized blade in terms of mass reduction, and authors compare several optimization algorithms. In particular, results of the optimization process are presented using *deterministic* (gradient and pattern search) and *stochastic* (particle swarms) algorithms.

[31] describes a structural optimization in which authors utilizes the Matlab's *Fmincon* function. Their objective is to maximize the turbine performances and the variables used are only geometric parameters. Their reference turbine is a 20 kW turbine with a rotor diameter of 20 meters.

In [32] an interesting work on a 7.2 meters long horizontal axis wind turbine blade is reported. Authors conduct a structural optimization with the objective to reduce the mass of the blade and the maximum displacement by optimizing the composite materials layup definition. They use Ansys as finite element solver and Matlab to implement a *Genetic Algorithm (GA)* for the optimization process.

[33] presents a structural optimization process with the objective to minimize the mass of a composite vertical axis wind turbine blade. They use a *Genetic Algorithm (GA)* to explore the solutions domain in order to select the best parameters in terms of blade design and material selection.

## 5.2 Objective

The primary objective of the present structural optimization is a cost reduction. Figure 5.1, taken from the *2022 Cost of Wind Energy Review* published by *NREL*, shows the components cost breakdown of a floating offshore wind turbine.

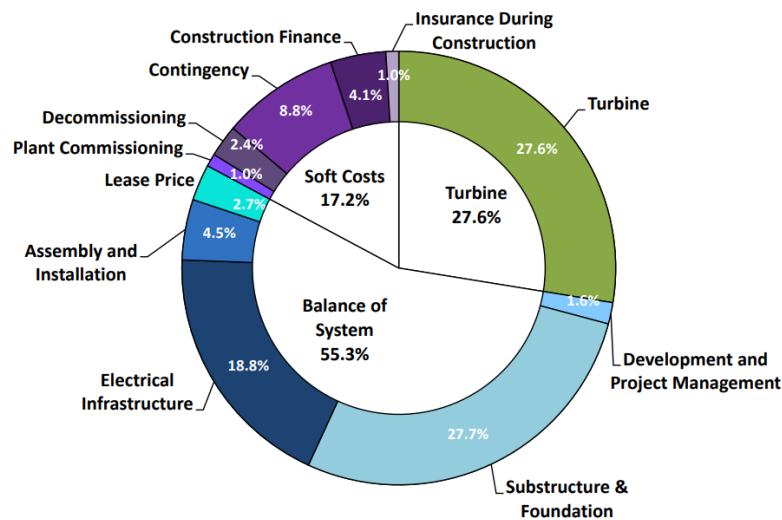


**Figure 5.1:** Floating offshore wind turbine component cost breakdown [34].

It is evident that the turbine costs are only 27.6% of the entire costs, and blade costs are part of them. The aim of this thesis is to reduce the blade costs, by optimizing material usage for the blade structure. In previous chapters, a conservative model of the blade has been developed, in order to respect the structural requirements. The conservative model, however, is not optimal and it has excess of material in blade regions in which it is not structurally necessary. Reducing the material usage, obviously, involves a total mass reduction of the blade and a cost reduction. The reference unit costs used for blade structure materials are taken from the reference wind turbine ontology and are listed in Table 5.1.

Material	Unit cost
Glass Uni	1.87
Glass Biax	3
Glass Triax	2.86
Carbon UD	30
Foam	13

**Table 5.1:** Materials unit costs.

## 5.3 Optimization process

The optimization process presented in this work is based on Finite Element Analysis, and the FEM model used is the PyMechanical model developed in previous chapters.

### 5.3.1 Model definition

To reduce the time needed for the optimization, some adjustments are made to the model. In particular, the number of sections in which the blade is divided is reduced from 49 to 10 (see Figure 5.2), this allowing a way faster definition of material layers in Ansys Mechanical.

The material thickness is set at 6 key points along the blade span (see Figure 5.3), which means that the thickness is assigned to 6 sections. To assign the thickness to the other 4 sections, an interpolation is used. The *"PChipInterpolator"* of the Python *"scipy.interpolate"* library is used. The optimization algorithm will change the material thickness at key points in order to minimize the objective function respecting the constraints. The interpolator changes the material thickness in the other sections by interpolating the new thickness at key points.

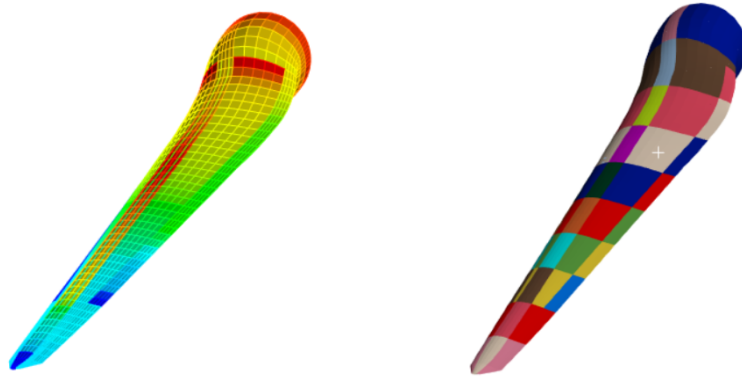


**Figure 5.2:** Simplification from 49 to 10 sections.

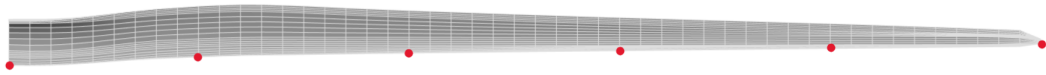


**Figure 5.3:** Key points.

As first material definition to start the optimization process, an initial thickness must be given. This is set to be, for each of the ten section, the maximum thickness of the other 5 sections that it groups, given by the blade ontology. This is a conservative choice to set the initial thickness, just to be sure that the blade respects all the structural requirements (as stated from analysis of the previous chapter). Figures 5.4 to 5.10 show the initial thickness set for the optimization process for each material.

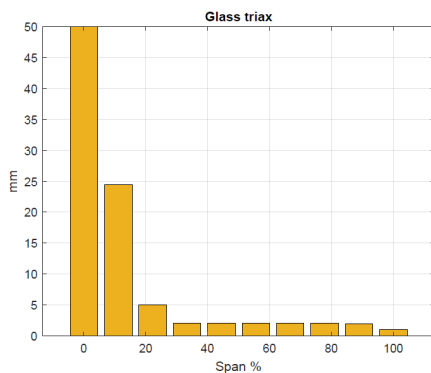


**Figure 5.4:** Glass Triax - first set.

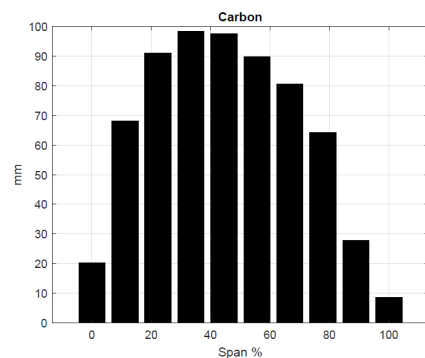


**Figure 5.5:** Carbon - first set.

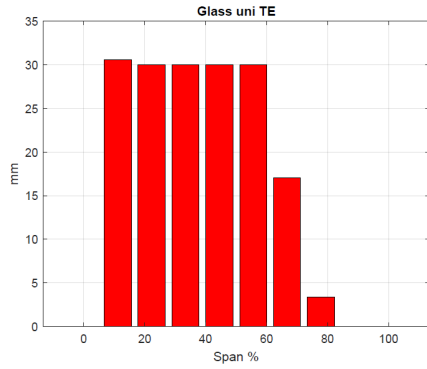


Figure 5.6: Glass uni te - first set.

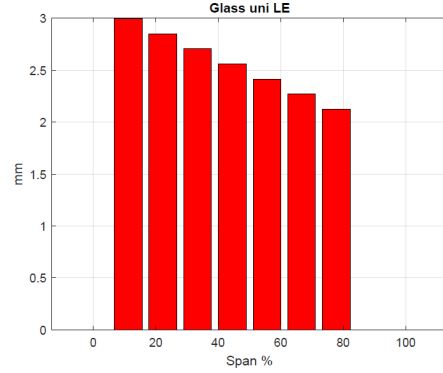


Figure 5.7: Glass uni te - first set.

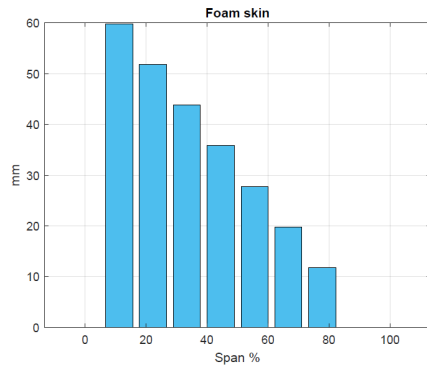


Figure 5.8: Foam skin - first set.

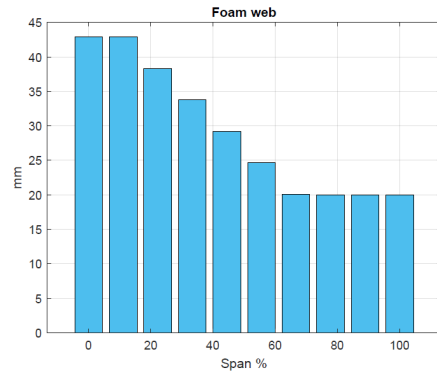


Figure 5.9: Foam web - first set.

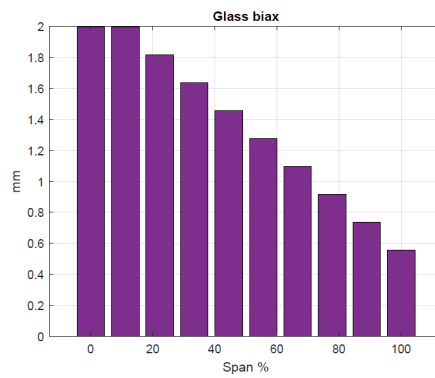


Figure 5.10: Glass Biax - first set.

### 5.3.2 Objective function

The optimisation process utilized in this study employs the “scipy.optimize.fmin” function from the SciPy library (“Fmin Function” 2024) [35]. This function implements the *COBYLA algorithm*. The choice of this algorithm was driven by its straightforward implementation and its ability to rapidly converge to a solution. The optimization algorithm is set to minimize the objective function by changing the material thickness. For optimization purposes, the geometry of the blade doesn’t change, this allowing a significant reduction of optimization variables. As aforementioned, the objective of the current optimization attempt is to minimize the material cost of the blade. Several structural constraints must be taken into account while minimizing the material mass, such as maximum tip deflection, strength requirements, frequency decoupling and buckling. However, for this first optimization attempt, only maximum tip deflection and strength resistance are implemented in order to avoid computational time necessary to add a modal and a buckling analysis at each iteration. In addition, modal analysis and buckling analysis showed, in the previous chapter, that the blade has natural frequencies safely far from the exciting frequencies due to rotor rotation and buckling load multiplier safely higher than 1. As a result, the objective function is written as

$$OBJ = COST_{blade} + OBJ_{Tip} + OBJ_{Puck}$$

where the penalties are formulated as

$$OBJ_{Tip} = \begin{cases} c_{Tip} \cdot (U^{Tip} - U_{allowed}^{Tip})^\delta & \text{if } U^{Tip} > U_{allowed}^{Tip}, \\ 0 & \text{if } U^{Tip} < U_{allowed}^{Tip}. \end{cases}$$

$$OBJ_{Puck} = \begin{cases} c_{Puck} \cdot (FI - FI_{allowed})^\delta & \text{if } FI > FI_{allowed}, \\ 0 & \text{if } FI < FI_{allowed}. \end{cases}$$

in which the coefficients are defined as

$$c_{Tip} = \frac{Val}{(U_{allowed}^{Tip} \cdot K_{Tip} - U_{allowed}^{Tip})^\delta}$$

$$c_{Puck} = \frac{Val}{(FI_{allowed} \cdot K_{Puck} - FI_{allowed})^\delta}$$

Table 5.2 reports all the coefficients needed for the objective function formulation.  $U_{allowable}^{Tip}$  and  $FI_{allowable}$  are the structural limits discussed in the previous chapter (the last considering a safety factor of 1.5).  $Val$ ,  $K_{Tip}$ ,  $K_{Puck}$  and  $\delta$  are coefficients which have the function to make the penalties real effective to penalize the objective function.



Type	Value
$U_{allowable}^{Tip}$	21.76 m
$FI_{allowable}$	0.68
$Val$	300000
$K_{Tip}$	1.5
$K_{Puck}$	1.5
$\delta$	1.5
$c_{Tip}$	7312.65
$c_{Puck}$	1558845.73

Table 5.2: Optimization data.

## 5.4 Case 1: Carbon optimization

The first case analyze a simplified optimization attempt in order to test the functioning of the script and the algorithm. In this first case, only carbon layer are effectively optimized, since it is the most expensive between the materials involved. As a result, this optimization case has 6 variables, which are the carbon thickness at the 6 key points. Figure 5.11 shows the minimization and the reach of a stable value for the objective function in about 40 iterations. The same occurs for penalties: in particular the penalty regarding the maximum tip deflection is not activated during the optimization process, this showing that the Puck penalty is more critical.

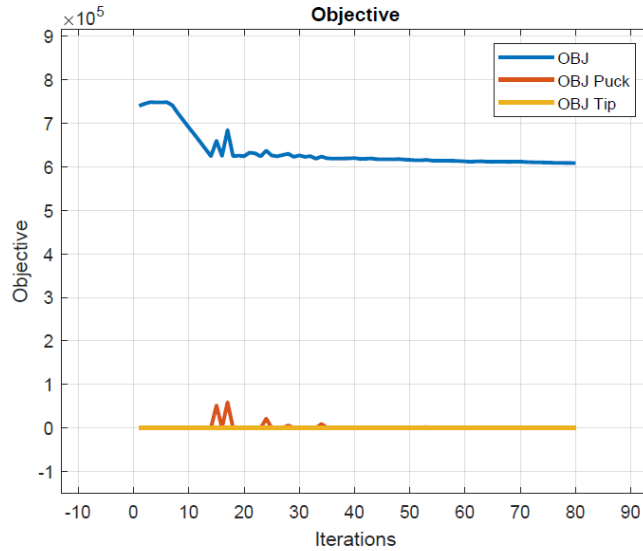


Figure 5.11: Objective function: case 1.

The trend is confirmed by Figures 5.12 and 5.13. It is evident that while the maximum Puck failure index reaches asymptotically the ultimate value, the maximum tip deflection is safely far from the maximum allowable tip deflection to avoid a tower impact.

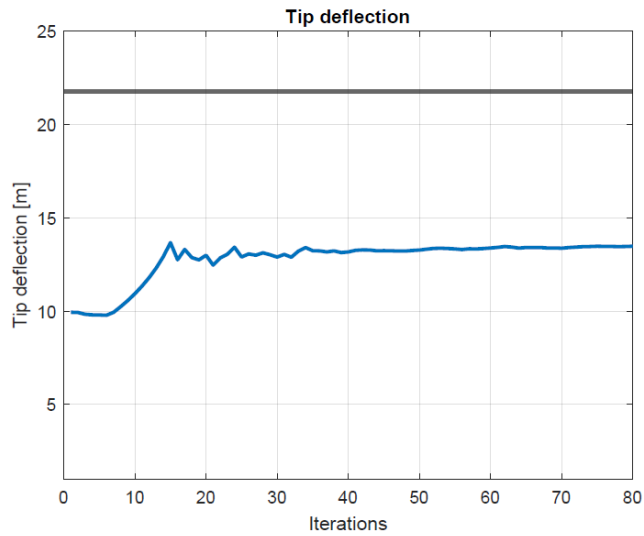


Figure 5.12: Tip deflection: case 1.

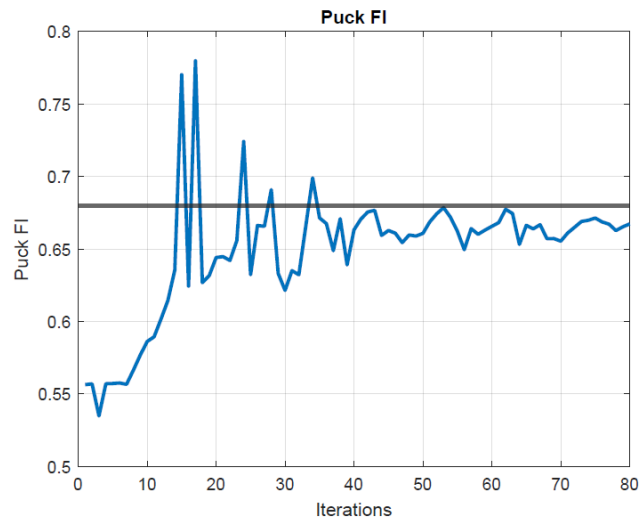


Figure 5.13: Maximum Puck Failure Index: case 1.

Figure 5.14 shows the evolution of the blade mass by differentiating each material. Only carbon mass changes, due to initial hypothesis, while other materials have a constant mass value. Glass triax mass is not reported in the chart since it is constant out of scale due to the fact that each laminates has a double glass triax layer, so it would have hidden the carbon mass evolution. The carbon mass is reduced by around 4 tons and this leads to an obvious reduction in the total blade cost, as reported in Figure 5.15.

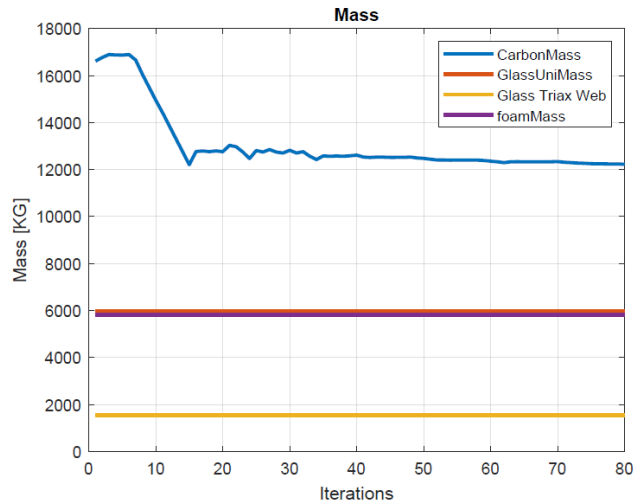


Figure 5.14: Mass evolution: case 1.

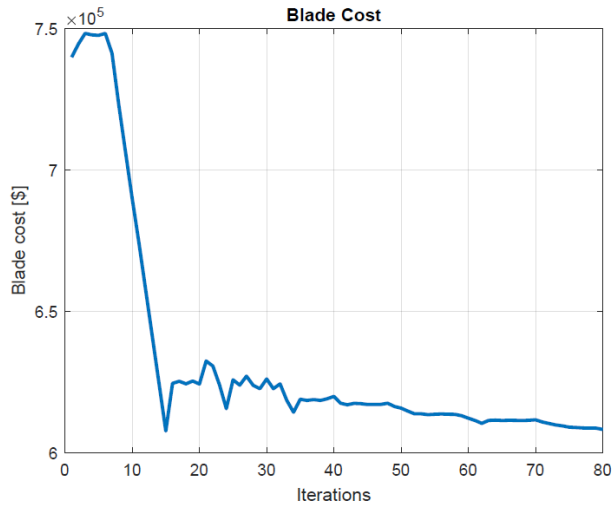
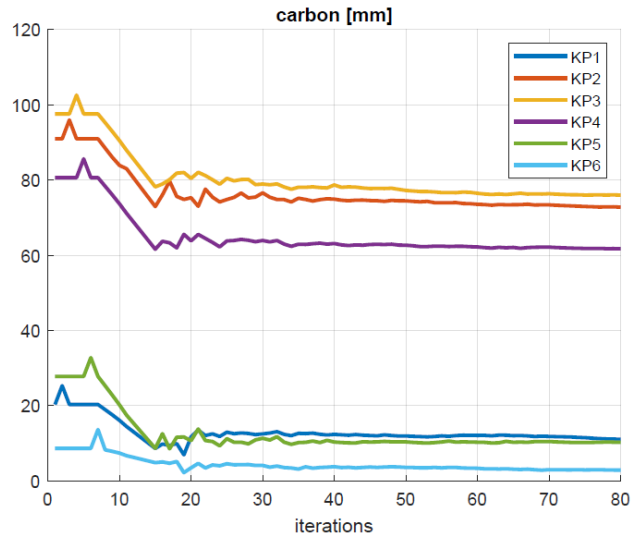


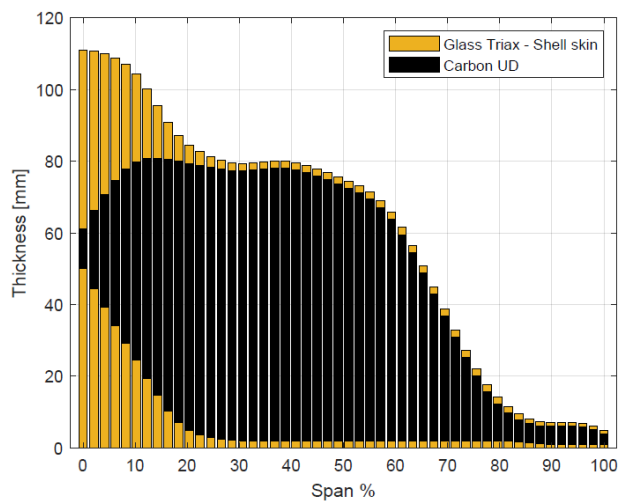
Figure 5.15: Blade cost: case 1.

Figure 5.16 shows a detail of the evolution of the optimization variables, namely the carbon thickness at the key points. Key points 1 is the nearest to the blade hub, increasing towards the blade tip.



**Figure 5.16:** Carbon thickness: case 1.

In the end, once the carbon thickness at the 10 sections are known, they are interpolated to have an idea of the thickness distribution along the blade span using the original blade model with 49 sections. It is reported in Figure 5.17



**Figure 5.17:** Spar cap optimized (case 1).

## 5.5 Case 2: Blade optimization

The second optimization performed try to fully optimize the blade cost considering all the materials involved. Taking into account *Glass triax*, *Glass biax*, *Glass uni (trailing edge)*, *Glass uni (trailing edge)*, *Carbon*, *foam (blade skin)* and *foam (shear web skin)* at the 6 key points, it results in a total of 42 optimization variables. This increases noticeably the computational time and the iterations required to find a minimum. Figure 5.18 shows the minimization of the objective function, confirming the dominance of the Puck penalty as in case 1.

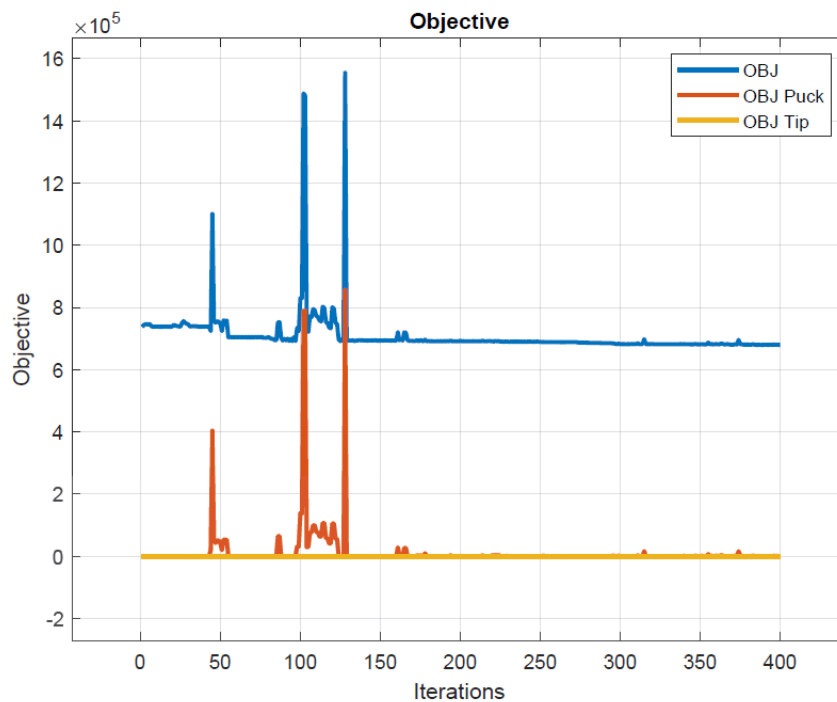


Figure 5.18: Objective function: case 2.

Figures 5.19 and 5.20 show the evolution of maximum tip deflection and maximum Puck failure index with the optimization. Puck failure index reaches the limit value while the maximum tip deflection is safely under the limit value and it is less than the maximum tip deflection reported in case 1, this suggesting a smoother carbon mass reduction which is further investigated in next lines.

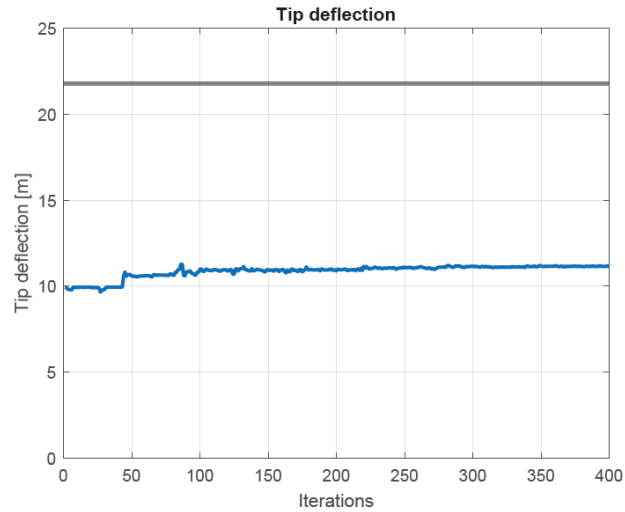


Figure 5.19: Tip deflection: case 2.

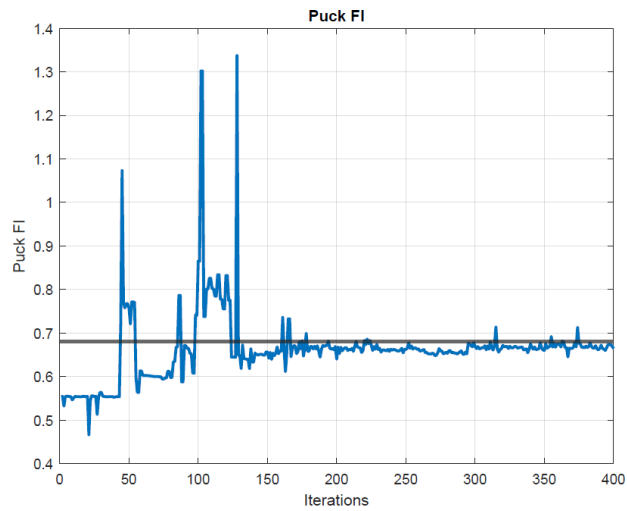


Figure 5.20: Maximum Puck Failure Index: case 2.

Figures 5.21 and 5.22 show the mass reduction of all materials involved in the blade design. The material with the highest mass reduction is glass triax, which is used for the blade skin, while carbon has a lower mass reduction than that seen in case 1, this suggesting some optimization algorithm issues.

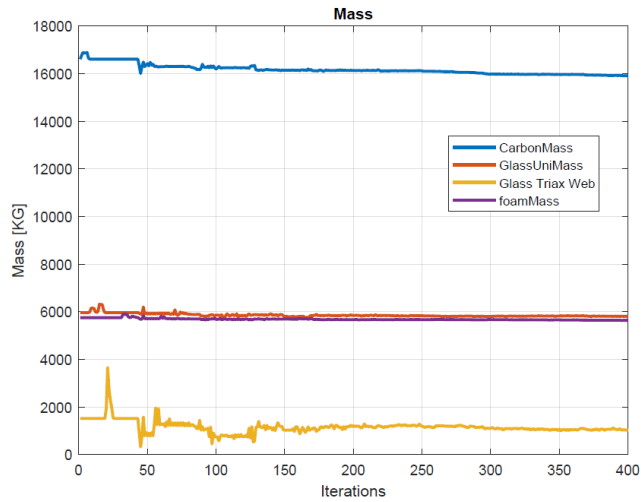


Figure 5.21: Mass evolution: case 2.

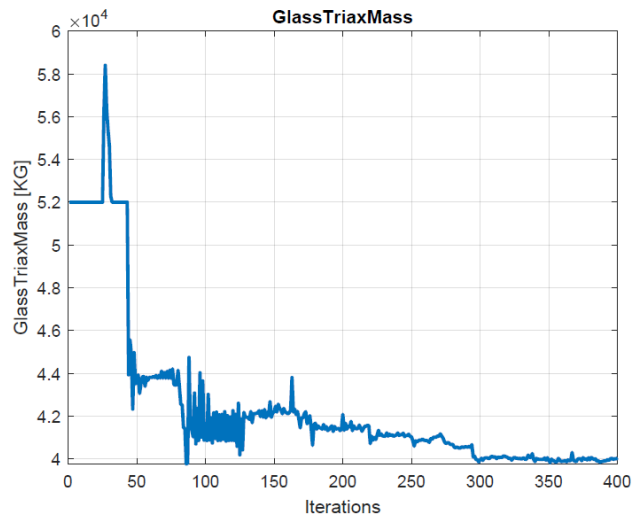


Figure 5.22: Glass Triax Mass evolution: case 2.

The blade cost reduction in the optimization process is shown in Figure 5.23.

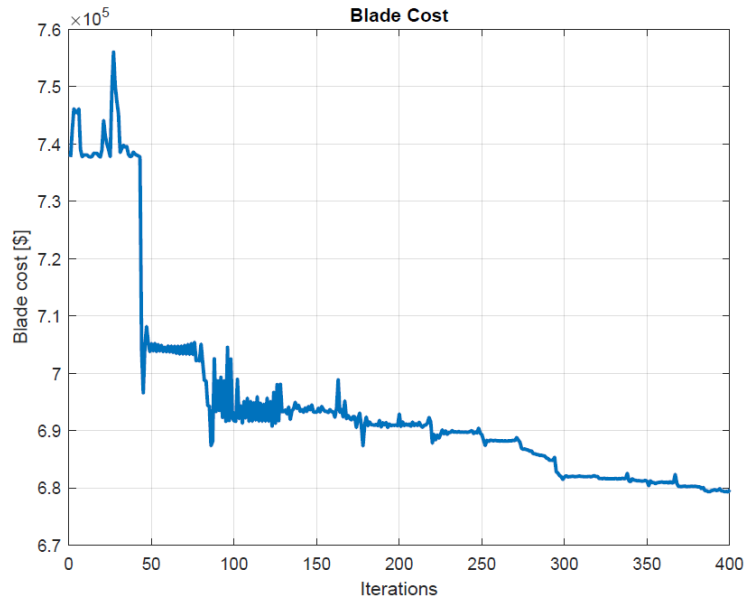


Figure 5.23: Blade cost: case 2.

The details of the evolution of material thickness at the 6 key points are reported in Figures 5.24 to 5.30.

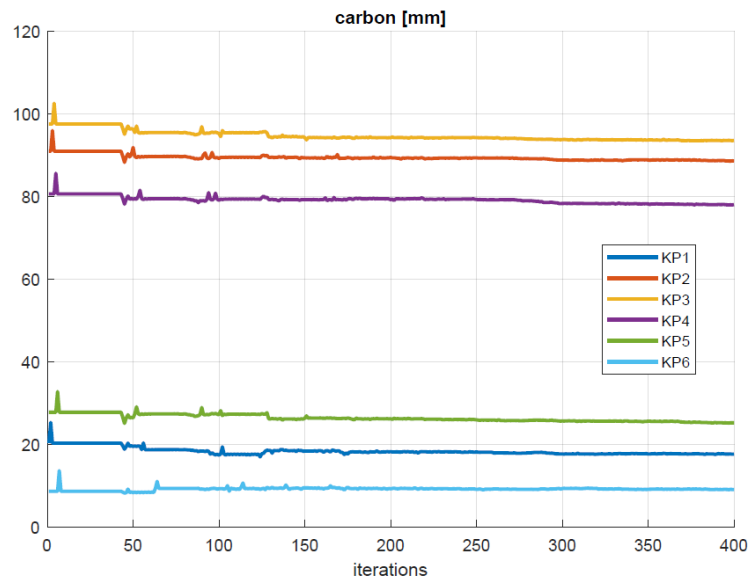


Figure 5.24: Carbon thickness: case 2.



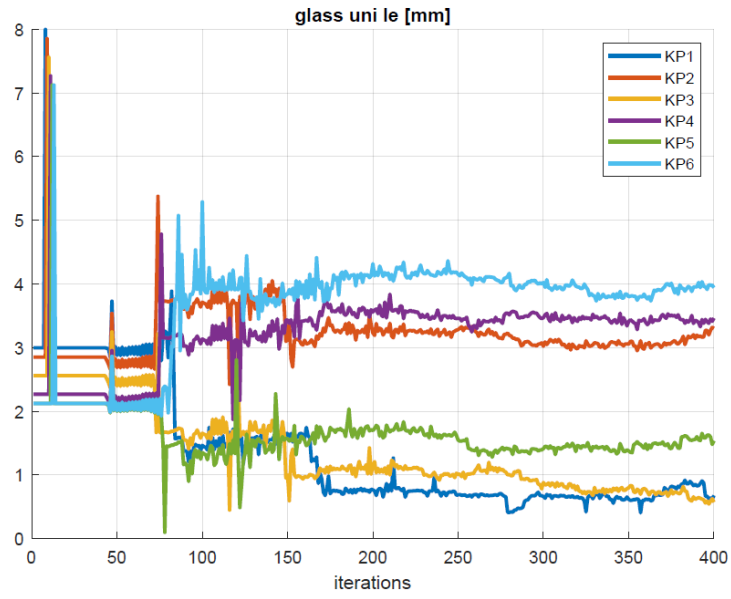


Figure 5.25: Glass UNI (LE) thickness: case 2.

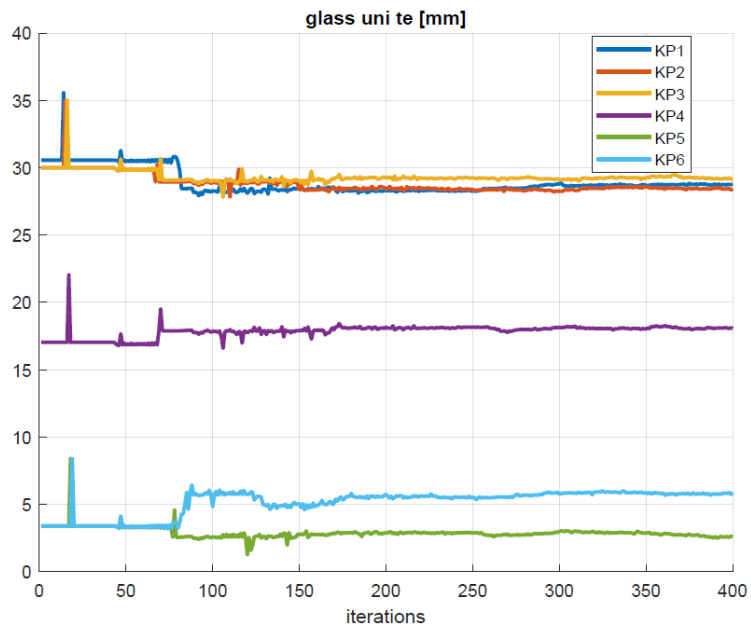


Figure 5.26: Glass UNI (TE) thickness: case 2.

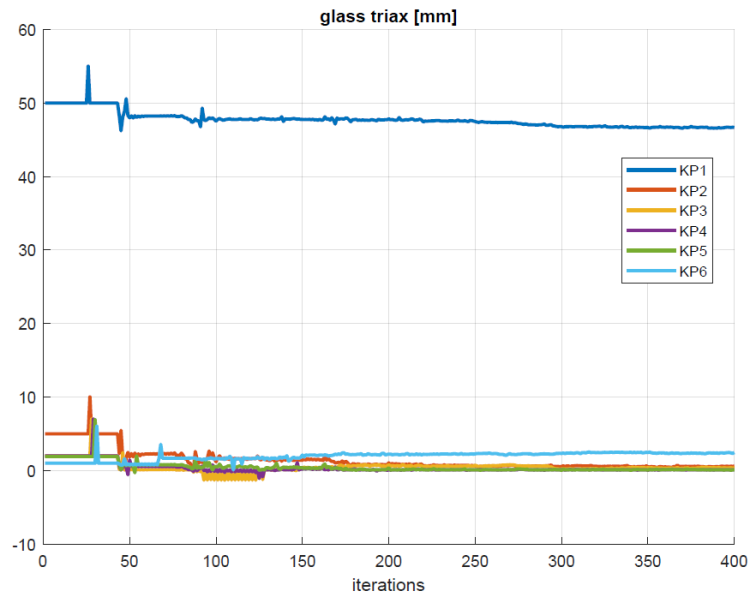


Figure 5.27: Glass TRIAX (skin) thickness: case 2.

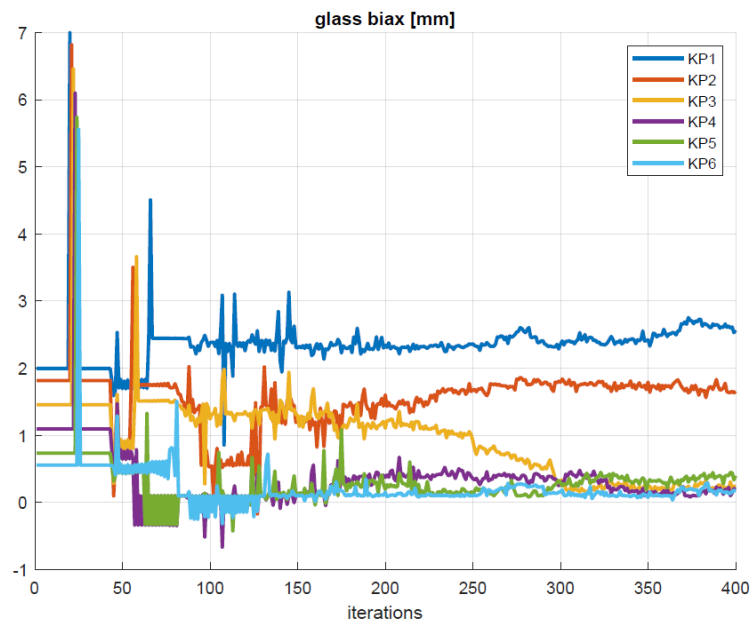


Figure 5.28: Glass Biax (web) thickness: case 2.

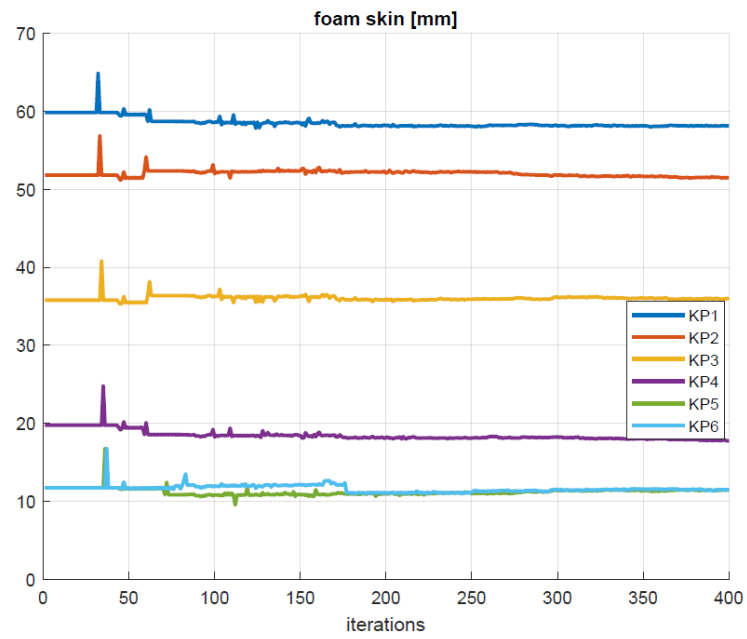


Figure 5.29: Foam (skin) thickness: case 2.

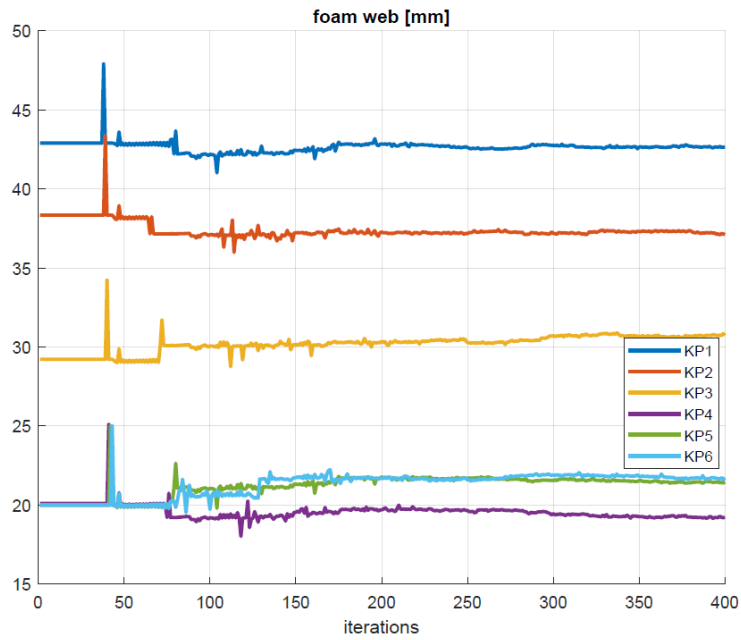
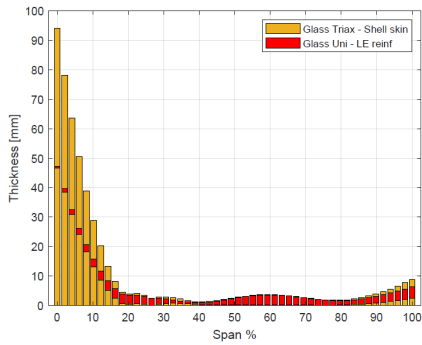
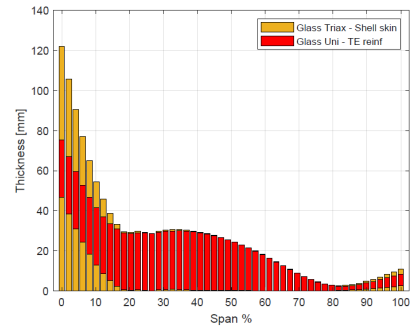


Figure 5.30: Foam (web) thickness: case 2.

Finally, following the process used in case 1, the known material thicknesses at the 10 sections are interpolated to obtain the optimized material thickness distribution along the blade span for each laminates, which are presented in Figures 5.31 to 5.35.



**Figure 5.31:** Leading edge reinforcement optimized.



**Figure 5.32:** Trailing edge reinforcement optimized.

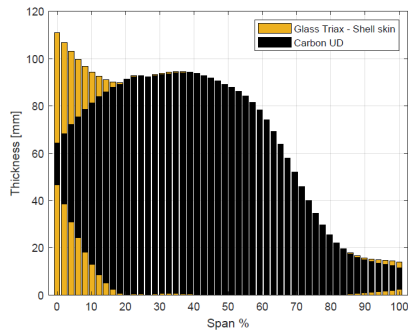


**Figure 5.33:** Spar cap optimized.

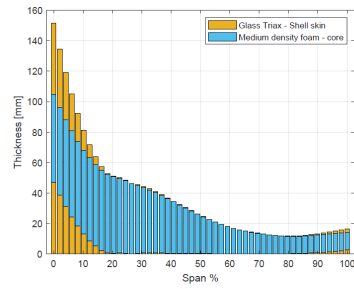


**Figure 5.34:** Panels optimized.

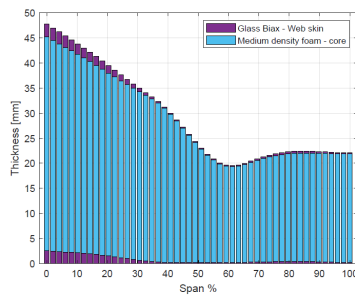


**Figure 5.35:** Shear web optimized.

For a better visualization, Figures 5.36 to 5.39 show a zoom of the laminates starting from 20% of the blade span, excluding the representation of the thick root which hides some details of the blade.

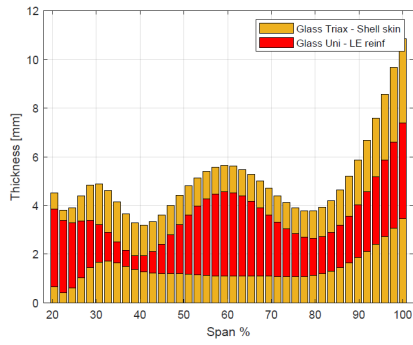


**Figure 5.36:** Leading edge reinforcement optimized (zoom).

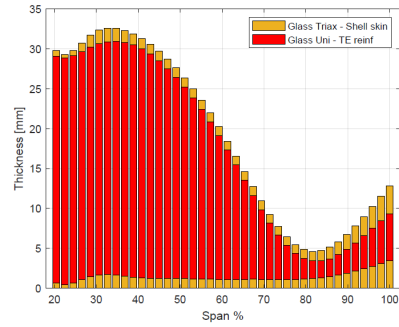


**Figure 5.37:** Trailing edge reinforcement optimized (zoom).

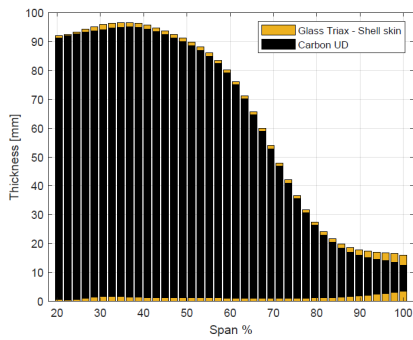


**Figure 5.38:** Spar cap optimized (zoom).

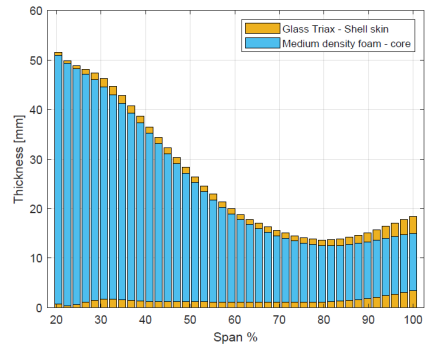


**Figure 5.39:** Panels optimized (zoom).

Figures 5.40 and 5.41 show the static structural outputs on the optimized blade.

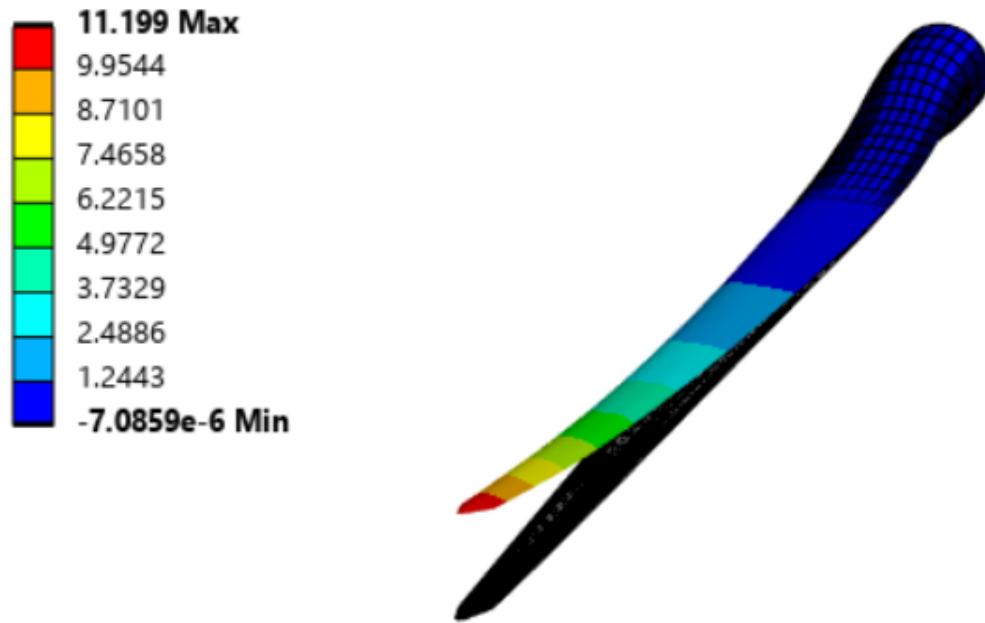


Figure 5.40: Maximum displacement (optimized blade).

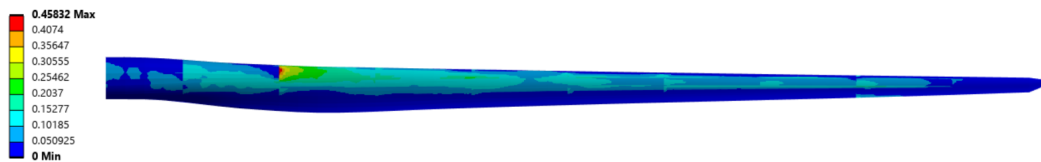


Figure 5.41: Maximum Puck failure index (optimized blade).

# Chapter 6

## Conclusions

In this thesis, a Python code has been developed in order to generate an automated Finite Element Model using Ansys Mechanical. The interaction between Python code and Ansys Mechanical is achieved through PyMechanical, a Python application programming interface. The main function of the Python code is to import and process a generic blade geometry and define the material layups. Modern wind turbine blades are built using composite materials, so the model is built considering variable thickness of the materials and the several laminates typology at different blade regions. The material definition is fully automated accessing each surface of the shell CAD model through the defined name.

Once the Python code has been completed to run Ansys Mechanical simulations, some FEM analysis are performed on a 15 MW reference wind turbine blade in order to verify the code functioning.

A modal analysis is performed to calculate the natural frequencies of the blade which is an essential data to avoid vibrations and resonance phenomena. The natural frequencies calculated with the developed model agree with a small error with some data found in literature, in particular the first natural frequency is calculated with an error smaller than 2%, which is a good result since the first natural frequency is essential to be compared to the exciting frequency of the rotor rotation to avoid resonance. With the modal analysis is also possible to calculate and represent the deformed shape of each mode.

Static structural analysis have been performed on the blade considering only static loads due to aerodynamics, gravity and inertia. 7 load cases have been simulated in 7 different steady states condition which differed from each other in wind speed, rotor angular velocity and blade pitch. The analysis showed that the original reference blade structural definition is not able to respect the essential structural design requirements such as maximum blade deflection to avoid tower collisions, strength resistance using Puck's criterion for composite materials and buckling resistance. To achieve a structural integrity, some changes to the original

blade structure are made and successfully analyzed.

However, the static loads considered in this work are only a little part of the load conditions to which an offshore wind turbine blades of such dimensions is subjected. To fully validate a blade model, in a future work many other load sources and typologies must be taken into account. Even under normal wind conditions, a wind turbine blade is continuously subjected to alternating loads so the fatigue life must be studied. The increasing blade dimensions represent an additional challenge in the study of the material fatigue. In addition, large structures have always an elastic behavior so, under changing loads, dynamic loads are expected, so vibrations and resonances must be studied. Also, especially for offshore wind turbine blades, extreme load endurance must be studied to guarantee the stability of the turbine in the presence of heavy storms and hurricanes.

In the last chapter of this thesis, a first optimization attempt is performed on the reference blade. The objective of the optimization performed is to reduce the blade material cost. However, in defining the budget of a wind turbine many actors must be considered and the material cost of the blade is only a part of the total budget. The optimization is performed using the *COBYLA* algorithm inserted in a minimization Python function. The objective function is built to minimize the blade material costs by considering some structural constraints as penalties. In particular, maximum tip deflection and maximum Puck failure index are considered in this work. Two cases were performed, the first optimizing only the carbon layer thickness, the second optimizing the thickness of all materials involved. Table 6.1 shows the results of the optimization process. Results show that in both cases a significant reduction of blade mass is obtained, inducing a significant reduction in blade materials costs. However, in the first case the cost reduction is higher than in the second case. This result highlights some possible optimization algorithm problem. In fact, *COBYLA* algorithm solves a constrained optimization by approximating the problem with a linear programming problem at each iterations. This method is fast but, in the case of optimization problem with a high number of optimization variables could be too sensitive to the problem of local minima.

In a future work, considering higher computational time and higher computer performances, the optimization problem can be complicated and improved. Some other constraints can be added such as natural frequencies to avoid frequency coupling and resonances and buckling load multipliers. Adding these constraints requires to add a modal and buckling analysis at each iterations which will significantly augment the computational time required for the optimization. Also, other kind of optimization algorithm can be explored to find the best solution. Following the literature trend, *Genetic Algorithms* seem a good choice when a high number of optimization variables are involved. However, this kind of optimization algorithm is the less sensitive to local minima but it requires higher computational time.



Value	Initial value	Case 1	Case 2	Variation
Blade cost [\$]	748038	618465	679666	-17.3% (case 1) -9.14% (case 2)
Blade mass [kg]	82730	77984	68474	-5.7% (case 1) -17.2% (case 2)
Carbon cost [\$]	506510	364110	477764	-28.1% (case 1) -5.6% (case 2)
Carbon mass [kg]	16883	12137	15925	-28.1% (case 1) -5.6% (case 2)
Foam cost [\$]	75508	75508	73355	-0% (case 1) -2.85% (case 2)
Foam mass [kg]	5808	5808	5642	-0% (case 1) -2.85% (case 2)
Glass Uni cost [\$]	11151	11151	10863	-0% (case 1) -2.58% (case 2)
Glass Uni mass [kg]	5963	5963	5809	-0% (case 1) -2.58% (case 2)
Glass Biax cost [\$]	4601	4601	3136	-0% (case 1) -31.8% (case 2)
Glass Biax mass [kg]	1533	1533	1045	-0% (case 1) -31.8% (case 2)
Glass Triax cost [\$]	150267	150267	114545	-0% (case 1) -23.77% (case 2)
Glass Triax mass [kg]	52541	52541	40050	-0% (case 1) -23.77% (case 2)

**Table 6.1:** Optimization results.

# Bibliography

- [1] Fleming PD and Probert SD. «The evolution of wind-turbines: an historical review». In: *Appl Energy*, 18 (1984), pp. 163–177 (cit. on p. 2).
- [2] Pasqualetti MJ and Gipe P. Righter R. «Wind energy, History of». In: *Encyclopedia Energ* (2004), pp. 419–433 (cit. on p. 2).
- [3] John K. Kaldellis and D. Zafirakis. «The wind energy (r)evolution: A short review of a long history». In: (Feb. 2011) (cit. on p. 2).
- [4] United Nations. *What is climate change?* 2022. URL: <https://www.un.org/en/climatechange/what-is-climate-change> (cit. on p. 3).
- [5] D. Adu, D. Jianguo, S.N. Asomani, and A. Abbey. «Energy generation and carbon dioxide emission - The role of renewable energy for green development». In: *Energy Reports*, 12 (2024) (cit. on p. 4).
- [6] Q. Hassana, S. Algburi, A.Z. Sameenc, T.J. Al-Musawi, A.K. Al-Jiboorya, H.M. Salmane, B.M. Ali, and M. Jaszczur. «A comprehensive review of international renewable energy growth». In: *Energy and Built Environments*, 12 (2024) (cit. on pp. 4, 6, 7).
- [7] M. Tutak and J. Brodny. «Renewable energy consumption in economic sectors in the EU-27. The impact on economics, environment and conventional energy sources. A 20-year perspective». In: *J. Clean. Prod.*, 345 (2022) (cit. on p. 5).
- [8] *Eurostat - energy consumption and production*. 2023. URL: <https://ec.europa.eu/eurostat/data/database> (cit. on p. 6).
- [9] Q. Hassan, A.M. Abdulateef, S.A. Hafedh, A. Al-samari, J. Abdulateef, A.Z. Sameen, and M. Jaszczur. «Renewable energy-to-green hydrogen: a review of main resources routes, processes and evaluation». In: *Int. J. Hydrogen Energy* (2023) (cit. on p. 6).
- [10] Q. Hassan, M. Al-Hitmi, V.S. Tabar, A.Z. Sameen, H.M. Salman, and M. Jaszczur. «Middle East energy consumption and potential renewable sources: an overview». In: *Clean. Eng. Technol.* (2023) (cit. on p. 6).

- [11] R. McKenna, S. Pfenninger, H. Heinrichs, J. Schmidt, I. Staffell, C. Bauer, and J. Wohland. «High-resolution large-scale onshore wind energy assessments: a review of potential definitions, methodologies and future research needs». In: *Renew. Energy*, 182 (2022) (cit. on p. 8).
- [12] J.M. Weinand, E. Naber, R. McKenna, P. Lehmann, L. Kotzur, and D. Stolten. «Historic drivers of onshore wind power siting and inevitable future trade-offs». In: *Environ. Res. Lett.*, 17 (2022) (cit. on p. 8).
- [13] X. Sun, D. Huang, and G. Wu. «The current state of offshore wind energy technology development». In: *Energy*, 17 (2012) (cit. on p. 8).
- [14] M. Dolores Esteban, J. Javier Diez, Jose S. López, and Vicente Negro. «Why offshore wind energy?». In: *Renewable Energy*, 36 (2011) (cit. on p. 10).
- [15] Erich Hau. *Wind Turbines*. Third. Munich, Germany: Springer-Verlag, 2013 (cit. on pp. 14–16, 19–21, 23–28, 31, 32, 61).
- [16] S. Eriksson, H. Bernhoff, and M. Leijon. «Evaluation of different turbine concepts for wind power». In: *Renewable and Sustainable Energy Reviews*, 12 (2008) (cit. on p. 16).
- [17] G. Ertek and L. Kailas. «Analyzing a Decade of Wind Turbine Accident News with Topic Modeling». In: *Sustainability*, 13 (2021) (cit. on p. 17).
- [18] G. Schmitz. *Theorie und Entwurf von Windradern optimaler Leistung*. 5th ed. Rostock: Wiss. Zeitschrift der Univ, 1956 (cit. on p. 24).
- [19] P.J. Schubel and R.J. Crossley. «Wind Turbine Blade Design». In: *Energies*, 5 (2012) (cit. on pp. 35–40).
- [20] R. Gasch and J. Twele. *Wind Power Plants*. Berlin: Solarpraxis, 2002 (cit. on pp. 35, 37).
- [21] D.A. Griffin and M.D. Zuteck. «Scaling of composite wind turbine blades for rotors of 80 to 120 meter diameter». In: *J. Sol. Energy Eng. Trans. ASME*, 123 (2001) (cit. on p. 37).
- [22] L. Mishnaevsky, K. Branner, H.N. Petersen, J. Beauson, M. McGugan, and B.E. Sorensen. «Materials for Wind Turbine Blades: An Overview». In: *Materials*, 10 (2017) (cit. on p. 40).
- [23] E. Gaertner et al. «Definition of the IEA 15 Megawatt Offshore Reference Wind». In: *Technical Report NREL/TP-5000-75698*, National Renewable Energy Laboratory (NREL), Golden, Colorado (2020) (cit. on pp. 45–49).
- [24] M. Ozyildiz, C. Muyan, and D. Coker. «Strength Analysis of a Composite Turbine Blade using Puck Failure Criteria». In: *Journal of Physics, Conf. Ser.* 1037 (2018) (cit. on p. 57).

- [25] A.S.E. Mendoza, I. Mishra, and D.T. Griffith. «An Open-Source NuMAD Model for the IEA 15 MW Blade with Baseline Structural Analysis». In: University of Texas at Dallas, Richardson, Texas (2023) (cit. on pp. 59, 65).
- [26] S. Scott, P. Greaves, T. Macquart, and A. Pirrera. «Comparison of blade optimisation strategies for the IEA 15MW reference turbine». In: *Journal of Physics, Conf. Ser.* 2265 (2022) (cit. on p. 73).
- [27] A. Chehouri, R. Younes, A. Ilinca, and J. Perron. «Review of performance optimization techniques applied to wind turbines». In: *Applied Energy* 142 (2015) (cit. on p. 79).
- [28] S. Scott, P. Greaves, P.M. Weaver, A. Pirrera, and T. Macquart. «Efficient structural optimisation of a 20MW wind turbine blade». In: *Journal of Physics, Conf. Ser.* 1618 (2020) (cit. on p. 79).
- [29] C.L. Bottasso, P. Bortolotti, A. Croce, and F. Gualdoni. «Integrated aero-structural optimization of wind turbines». In: *Multibody Syst Dyn* 38 (2016) (cit. on p. 79).
- [30] T. Bagherpoora and L. Xueminb. «Structural Optimization Design of 2MW Composite wind turbine blade». In: *Energy Procedia* 105 (2017) (cit. on p. 79).
- [31] Fangfang Song, Yihua Ni, and Zhiqiang Tan. «Optimization design, modeling and dynamic analysis for composite wind turbine blade». In: *Procedia Engineering* 16 (2011) (cit. on p. 80).
- [32] A.D. Monte, M.R. Castelli, and E. Benini. «Multiobjective structural optimization of a HAWT composite blade». In: *Composite Structures* 106 (2013) (cit. on p. 80).
- [33] P. Xue, Y. Wan, J. Takahashi, and H. Akimoto. «Structural optimization using a genetic algorithm aiming for the minimum mass of vertical axis wind turbines using composite materials». In: *Helyion* 10 (2024) (cit. on p. 80).
- [34] T. Stehly, P. Duffy, and D.M. Hernando. «2022 Cost of Wind Energy Review». In: National Renewable Energy Laboratory (2023) (cit. on p. 80).
- [35] M. Sirigu, A. Ghigo, G. Giorgi, and G. Bracco. «A novel optimisation process for static structural finite element analysis of offshore wind turbine floating foundations». In: Politecnico di Torino (2020) (cit. on p. 84).